THE EFFECT OF NOZZLE NONLINEARITIES ON THE NONLINEAR STABILITY OF LIQUID ROCKET MOTORS

A THESIS

Presented to

The Faculty of the Division

of Graduate Studies

By

M. S. Padmanabhan

In Partial Fulfillment

of the Requirements for the Degree

Doctor of Philosophy

in the School of Aerospace Engineering

Georgia Institute of Technology

November 1975

THE EFFECT OF NOZZLE NONLINEARITIES ON THE NONLINEAR STABILITY OF LIQUID ROCKET MOTORS

Approved:

Ben T. Zinn, Chairman

Warren C. Strahle

Eugene A. Powell

Date Approved by Chairman: 11/3/75

ACKNOWLEDGEMENTS

It is a pleasure to record here my gratitude to people who helped me in my research.

I wish to thank Dr. Ben T. Zinn for his suggestion of the thesis topic and for his constant guidance and encouragement. I have benefited greatly by my association with Dr. Zinn and I am very grateful to him.

Along with Dr. Zinn, Dr. Eugene A. Powell was associated with this research program from its inception. The frequent discussions that I had with Dr. Powell were of great help to me and I am very thankful to him. The vast experience gained by Dr. Zinn and Dr. Powell was an invaluable asset in my work. I thank Dr. Warren C. Strahle for his careful review of my thesis and for his useful suggestions.

I am indebted to Dr. Francis J. Klemm for all the help that I received from him. Particularly useful to this thesis were the many discussions that we had about numerical analysis and computer programming. I extend my deep gratitude to Dr. Klemm for everything he has done for me.

I thank Dr. William A. Bell for some useful discussions about the nozzle analysis. Several others have helped me with useful suggestions about computer programming and my thanks are extended to all of them. My appreciation goes to Mrs. Elise Ashley for an excellent job done in typing this thesis.

The financial support of the Georgia Institute of Technology and the National Aeronautics and Space Administration (under NASA Grant NGR 11-002-179) is gratefully acknowledged.

TABLE OF CONTENTS

LIST OF ILLUSTRATIONS

Figure Page

LIST OF SYMBOLS

A	dimensionless, φ-dependent amplitude in the approximating series for the velocity potential in the nozzle analysis
b	axial acoustic eigenvalue
B	dimensionless, time-dependent amplitude in the approximating series for the velocity potential in the combustion chamber analysis
c	dimensionless speed of sound, c^*/c_o^*
C	coefficients of linear terms in the amplitude equation for the combustion chamber
D	coefficients of nonlinear terms in the amplitude equation for the combustion chamber
$\underline{e}_\theta$	unit vector in the θ direction
$E(\tilde{\Phi}')$	differential equation residual
i	imaginary unit, $\sqrt{-1}$
I_p	inhomogeneous term in the amplitude equation in the nozzle analysis
J_m	Bessel function of the first kind of order m
K_p	ratio of the frequency of oscillation of the p^{th} mode to the frequency of oscillation of the fundamental mode
m	tangential mode number
M_e	steady-state Mach number at the nozzle entrance
n	radial mode number; also, pressure interaction index
N	total number of modes used to approximate the velocity potential
p	dimensionless pressure, p^*/p_o^*
P	pressure amplitude
r	dimensionless radial coordinate, r^*/R_c^*

r_{cc} dimensionless radius of curvature of the nozzle at the nozzle entrance, r_{cc}^*/R_c^*

r_{ct} dimensionless radius of curvature of the nozzle at the nozzle throat, r_{ct}^*/R_c^*

r_{th} dimensionless radius of the nozzle throat, r_{th}^*/R_c^*

R radial acoustic eigenfunction

R_c^* chamber radius

S_{mn} the n^{th} root of the equation $dJ_m(x)/dx = 0$

S_p dimensionless transverse mode frequency for the p^{th} mode

t dimensionless time, $t^*c_o^*/R_c^*$

u dimensionless axial velocity component, u^*/c_o^*

$\underrightarrow{V}$ dimensionless velocity vector, $\underrightarrow{V}^*/c_o^*$

W_m' unsteady combustion mass source

Y linear admittance coefficient

z dimensionless axial coordinate, Z^*/R_c^*

Z axial acoustic eigenfunction

α an integral involving trigonometric functions in Appendix B

β an integral involving Bessel functions in Appendix B

γ ratio of specific heats

Γ nonlinear admittance coefficient

θ azimuthal coordinate

θ_1 nozzle half-angle

Θ tangential acoustic eigenfunction

ρ dimensionless density, ρ^*/ρ_o^*

τ dimensionless pressure sensitive time lag, $\tau^*c_o^*/R_c^*$

φ steady-state velocity potential in the nozzle

Φ velocity potential

ψ steady state stream function in the nozzle

Ψ radial acoustic eigenfunction

ω frequency of the fundamental mode

Subscripts

e evaluated at the nozzle entrance

i imaginary part of a complex quantity

j the quantity evaluated for the j^{th} mode

o stagnation quantity

p the quantity evaluated for the p^{th} mode

r real part of a complex quantity, partial differentiation with respect to r

t partial differentiation with respect to t

w evaluated at the nozzle wall

z partial differentiation with respect to z

θ partial differentiation with respect to θ

φ partial differentiation with respect to φ

ψ partial differentiation with respect to ψ

Superscripts

$( )'$ perturbation quantity; also, differentiation with respect to the argument

$(\bar{})$ steady-state value

$( )^*$ dimensional quantity; also, complex conjugate

$(\tilde{})$ approximate solution

SUMMARY

In this dissertation, the behavior of finite-amplitude waves inside the subsonic portion of a choked, axisymmetric nozzle has been investigated with the objective of determining the nonlinear admittance at the nozzle entrance. The nonlinear conservation equations describing the wave motion inside the nozzle are solved using the Galerkin method and the resulting solutions are used to obtain a nonlinear nozzle admittance relation. This nonlinear nozzle admittance relation is used to analyze the nonlinear combustion instability in a cylindrical combustor with uniform injection of propellants at one end and a slowly converging nozzle at the other end. The Galerkin method is also used to determine the behavior of pressure perturbations in the rocket combustor. In these computations, a three-mode series expansion consisting of the first tangential, the second tangential and the first radial modes is used. Computations have been performed for different values of the following parameters: (1) the combustion process time lag, (2) the interaction index, (3) the steady-state Mach number at the nozzle entrance and (4) the chamber length-to-diameter ratio. In each case, limit-cycle pressure amplitudes and wave forms have been obtained with both the linear and the nonlinear nozzle admittance conditions. These results show that the inclusion of nozzle nonlinearities has no significant effect on the limiting amplitude and pressure wave forms. This result can be attributed to the fact that

the amplitudes of the second tangential and the first radial modes are considerably smaller than the amplitude of the first tangential mode. Hence, in nonlinear stability calculations of liquid rocket motors, the effect of nozzle nonlinearities can be safely neglected.

CHAPTER I

INTRODUCTION

Background

Various aerospace propulsion devices, such as liquid and solid propellant rocket motors and air breathing jet engines, are often subject to combustion instabilities which are detrimental to their performance and safety of operation. Observation of the behavior of unstable rocket motors indicates that these combustion instabilities can be divided into two categories: (1) linear instability and (2) nonlinear instability. Linear instabilities are spontaneous in nature and are usually an outgrowth of the random combustion and flow fluctuations present in the system. On the other hand, nonlinear or triggered instability results from the introduction of a sufficiently large disturbance in a motor, which is stable with respect to small amplitude disturbances. In either case, the instability, after passing through a transient period, reaches a limiting amplitude (or limit-cycle amplitude) at which it oscillates with a frequency that is close to the frequency of one of the chamber's acoustic modes. These limit-cycle oscillations are often characterized by nonsinusoidal pressure waveforms with sharp peaks and flattened minima. The limit-cycles, triggered instability and nonsinusoidal waveforms are all caused by the nonlinearities of the system. A dynamically stable motor is stable with respect to disturbance of any amplitude. In order to design

stable engines, capabilities for a priori determination of the linear and nonlinear characteristics of the instability and the range of operating conditions for which these engines are dynamically stable must be acquired.

The stability characteristics of a rocket motor can be significantly affected by the interaction between pressure oscillations inside a rocket combustion chamber and wave motion in the exhaust nozzle. Hence, it is necessary to understand the behavior of the exhaust nozzle under oscillatory flow conditions. In particular, it is important to know how a wave generated in the combustion chamber is partially transmitted and partially reflected at the nozzle entrance. Since the flow is supersonic downstream of the nozzle throat, disturbances in this region cannot propagate upstream and affect the chamber conditions. It is therefore sufficient in combustion instability analyses to consider the behavior of the oscillations in the convergent section of the nozzle only.

In practice, it is convenient to analyze the oscillations in the combustion chamber and nozzle separately. For such an analysis, the combustion chamber extends from the injector plate to the nozzle entrance as shown in Figure 1. All combustion is assumed to take place in this region, and, as is reasonable in many practical systems, the mean flow Mach number is assumed to be relatively low. In contrast, it is assumed that no combustion takes place in the nozzle and the magnitude of the mean flow Mach number is allowed to vary from a low value at the nozzle entrance to unity at the throat. The consequence of this separate analysis of chamber and nozzle flows is to move the

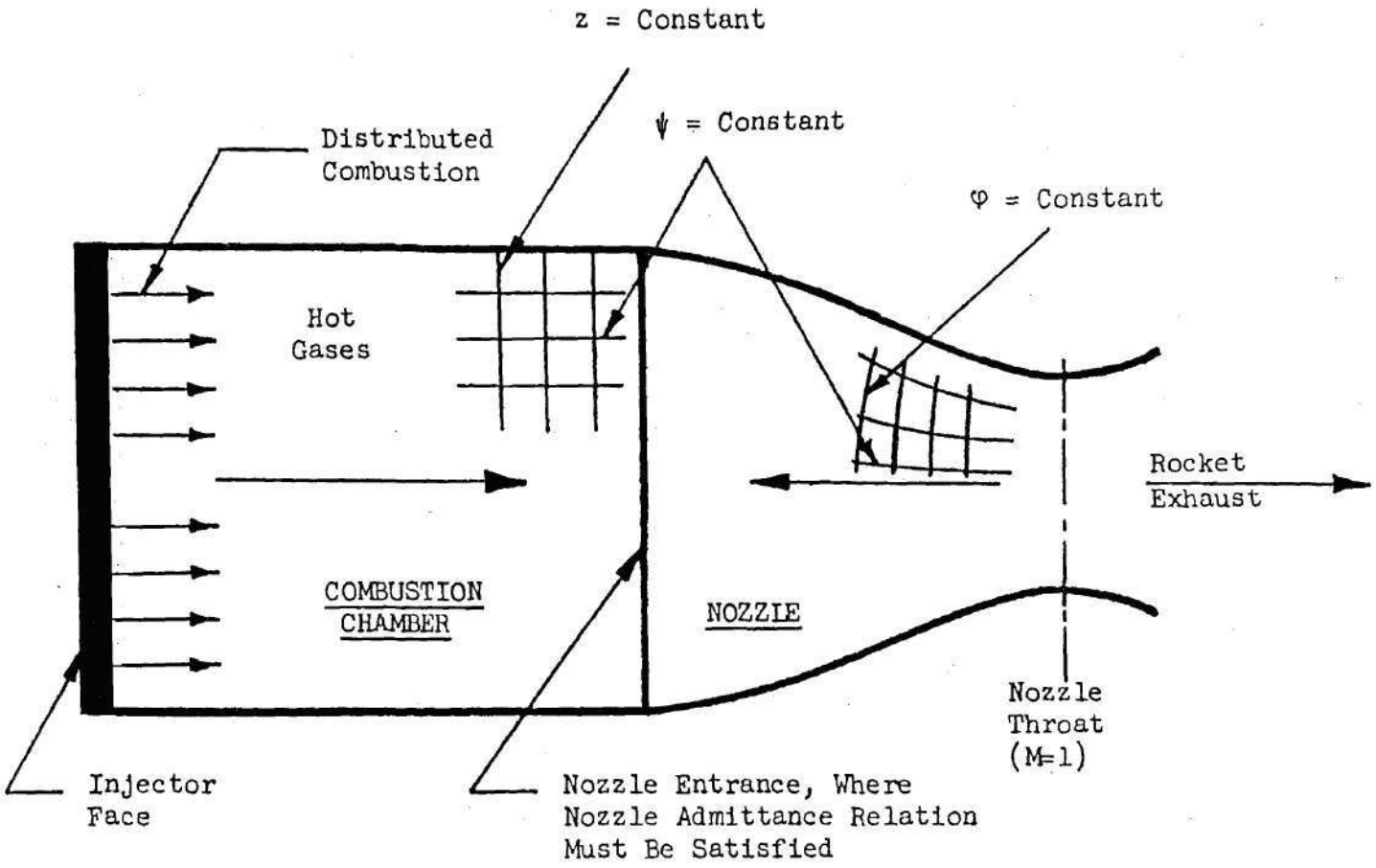

Figure 1. Typical Mathematical Model of a Liquid Rocket Engine

boundary of the combustion chamber from the throat up to the nozzle entrance, where the information derived from the nozzle analysis is expressed as a boundary condition that must be satisfied by the solutions provided by the combustion chamber analysis. This boundary condition is usually referred to as the Nozzle Admittance Relation. The presence of the nozzle is effectively replaced by this nozzle admittance relation. Once this relation has been established, combustion instability analysis can be performed by limiting attention to the combustion chamber alone. Knowledge of the nozzle admittance relation is of great importance in most combustion instability studies.

Calculation of the nozzle admittance has been the subject of several investigations. The behavior of oscillations in a converging-diverging supercritical nozzle was first treated by Tsien[1] who considered the case in which the oscillation of the incoming flow was one-dimensional and isothermal. Tsien accounted for the effect of the nozzle by introducing a "transfer function", defined as the ratio of the mass flow oscillations to the chamber pressure oscillation at the nozzle entrance. This study was restricted to the limiting cases of very high and very low frequency oscillations. Crocco[2,3] extended Tsien's work to include the entire frequency range and to cover the more general cases of non-isothermal one-dimensional and three-dimensional oscillations. It was Crocco that introduced the concept of admittance to study the influence of the nozzle on the combustor flow oscillations. The analyses of Tsien and Crocco are both restricted to small-amplitude (i.e., linear) oscillations. More recently, a nonlinear nozzle theory has been developed by Zinn and Crocco[4,5,6] who extended the previous

linear theories to the investigation of the behavior of finite-amplitude waves. In this investigation, the conservation equations describing the unsteady flow in a slowly converging nozzle were solved by a perturbation technique. While the first order solutions were obtained by the method of separation of variables, the method of eigenfunction expansions was used to obtain the higher-order solutions.

In recent studies conducted by Zinn, Powell, and Lores, theories were developed to describe the nonlinear behavior of longitudinal[7,8] and transverse[9,10] instabilities in liquid-propellant rocket chambers with quasi-steady nozzles. These theories have now been extended to situations in which the instabilities are three-dimensional and the rocket combustors are attached to conventional nozzles[11]. All these studies used, however, a linear nozzle admittance relation due to the non-availability of an appropriate nonlinear nozzle admittance relation.

Objectives of the Present Investigation

The objective of this research program is to develop a three-dimensional, nonlinear nozzle admittance relation to be used as a boundary condition in the above nonlinear combustion instability theories and determine the relative importance of nozzle nonlinearities in these combustion instability studies.

A new nonlinear nozzle theory is needed for the following reasons. While the above-mentioned nonlinear combustion instability theories (see References 7 through 11) used the Galerkin method to obtain both the transient and limit-cycle solutions, the nonlinear analysis of Zinn[5,6] used a perturbation analysis to study the periodic behavior of the flow

in the combustion chamber. The nonlinear nozzle admittance relation developed by Zinn using the perturbation analysis was not easily applicable in the nonlinear combustion theories developed in References 7 through 11. Consequently, a linear nozzle boundary condition or a short nozzle (quasi-steady) assumption had to be used in all of the combustion instability theories developed to date. Unless it is shown that the linear nozzle boundary condition adequately describes the flow conditions at the nozzle entrance in the presence of large amplitude instabilities, the use of a linear nozzle admittance relation in a non-linear stability is obviously inconsistent.

The objectives stated above are accomplished by performing the following three tasks:

Task I. Development of a theoretical approach for the calculation of the nonlinear nozzle admittance.

Task II. Calculation of the nonlinear nozzle response.

Task III. Application of the nonlinear nozzle theory to the liquid-rocket combustion instability problem.

Chapters II, III and IV describe how these three tasks are carried out. The results of the combustion chamber analysis are presented and discussed in Chapter V. Concluding remarks follow in Chapter VI.

CHAPTER II

DEVELOPMENT OF THE NOZZLE ADMITTANCE THEORY

Derivation of the Nozzle Wave Equation

As in the Zinn-Crocco analysis[5,6], finite-amplitude, periodic oscillations inside the slowly convergent, subsonic portion of an axisymmetric nozzle operating in the supercritical range are investigated. The flow in the nozzle is assumed to be adiabatic and inviscid and to have no body forces or chemical reactions. The fluid is also assumed to be calorically perfect.

The flow field is described in terms of the following dimensionless variables:

$$\underset{\rightarrow}{V} = \underset{\rightarrow}{V}^{*}/\bar{c}_{o}^{*} \text{ , velocity}$$

$$P = P^{*}/\bar{P}_{o}^{*} \text{ , pressure}$$

$$\rho = \rho^{*}/\bar{\rho}_{o}^{*} \text{ , density}$$

$$S = S^{*}/C_{p}^{*} \text{ , entropy}$$

where the "barred" quantities refer to steady state flow, the subscript o refers to stagnation conditions and the superscript * denotes a dimensional quantity.

The nondimensional equations describing the gas motion in the

nozzle can be written in the following form:

$$\frac{\partial \rho}{\partial t} + \nabla \cdot (\rho \underset{\rightarrow}{V}) = 0 \tag{2-1}$$

$$\frac{\partial \underset{\rightarrow}{V}}{\partial t} + \frac{1}{2} \nabla(\underset{\rightarrow}{V} \cdot \underset{\rightarrow}{V}) + (\nabla \times \underset{\rightarrow}{V}) \times \underset{\rightarrow}{V} + \frac{1}{\gamma \rho} \nabla p = 0 \tag{2-2}$$

$$\frac{\partial S}{\partial t} + \underset{\rightarrow}{V} \cdot \nabla S = 0 \tag{2-3}$$

$$S = \frac{1}{\gamma} \ln p - \ln \rho + \text{constant} \tag{2-4}$$

In the above equations, the dimensionless time is given by

$$t = \frac{\bar{c}_o^{\,*} \, t^*}{R^*}$$

and the dimensionless gradient operator is given by

$$\nabla = r_c^{\,*} \, \nabla^*$$

where $r_c^{\,*}$ is the radius of the chamber to which the nozzle is attached.

It is further assumed that the nozzle flow is isentropic and irrotational. Under these conditions, Eq. (2-3) is no longer needed and Eq. (2-4) reduces to the isentropic flow relation, $p = \rho^{\gamma}$. Furthermore, a velocity potential Φ exists such that

$$\nabla \Phi = \underset{\rightarrow}{V} \tag{2-5}$$

The continuity and momentum equations can now be combined with the aid of the isentropic relation to yield the following equation, which

describes the behavior of the velocity potential (see Appendix A):

$$\nabla^2\Phi - \Phi_{tt} = 2\,\nabla\Phi \cdot \nabla\Phi_t + (\gamma-1)\,\Phi_t\nabla^2\Phi$$

$$+ \frac{\gamma - 1}{2}\,(\nabla\Phi \cdot \nabla\Phi)\,\nabla^2\Phi + \tfrac{1}{2}\,\nabla\Phi \cdot \nabla(\nabla\Phi \cdot \nabla\Phi) \qquad (2\text{-}6)$$

This equation is consistent with the wave equation used in the second-order nonlinear combustion instability theory developed by Powell, Zinn and Lores (see References 7 and 10).

In the nonlinear combustion instability theories developed by Powell and Zinn[10,11], each variable was expressed as the sum of a space-dependent steady state quantity and a perturbation quantity dependent on both space and time. In order to obtain a nozzle admittance relation compatible with these theories, the velocity potential is expressed as follows:

$$\Phi = \bar{\Phi} + \Phi' \qquad (2\text{-}7)$$

where the prime denotes the perturbation quantity and the bar denotes the steady-state quantity. Substituting Eq. (2-7) into Eq. (2-6), and subtracting the steady-state equation from the resulting equation gives the following wave equation for the nozzle:

$$\left[1 - \frac{\gamma - 1}{2}\,\bar{V}^2\right]\nabla^2\Phi' - \Phi'_{tt} = 2\,\vec{\bar{V}} \cdot \left[\nabla\Phi'_t + \tfrac{1}{2}\,\nabla(\vec{\bar{V}} \cdot \nabla\Phi')\right]$$

$$+ (\gamma - 1)(\nabla \cdot \vec{\bar{V}})\left[\Phi'_t + \vec{\bar{V}} \cdot \nabla\Phi'\right] + \tfrac{1}{2}\,\nabla(\bar{V}^2) \cdot \nabla\Phi'$$

$$+ 2\nabla\Phi' \cdot \left[\nabla\Phi'_t + \tfrac{1}{2}\,\nabla(\vec{\bar{V}} \cdot \nabla\Phi')\right] + \tfrac{1}{2}\,\vec{\bar{V}} \cdot \nabla(\nabla\Phi' \cdot \nabla\Phi')$$

$$+ (\gamma - 1)\,\nabla^2\Phi' \left[\, \Phi'_t + \bar{\underset{\rightarrow}{V}} \cdot \nabla\Phi' \,\right] + \frac{\gamma - 1}{2}\,(\nabla \cdot \bar{\underset{\rightarrow}{V}})(\nabla\Phi' \cdot \nabla\Phi')$$

$$+ \left\{ \frac{\gamma - 1}{2}\,\nabla^2\Phi'(\nabla\Phi' \cdot \nabla\Phi') + \tfrac{1}{2}\,\nabla\Phi' \cdot \nabla(\nabla\Phi' \cdot \nabla\Phi') \right\} \qquad (2\text{-}8)$$

where

$$\bar{\underset{\rightarrow}{V}} = \nabla\bar{\Phi} \qquad (2\text{-}5a)$$

In order to solve the above wave equation, a coordinate system appropriate for the introduction of the boundary condition at the nozzle walls must be chosen. Following the approach used by Zinn and Crocco[5,6] for an axisymmetric nozzle, the axial variable z is replaced by the steady-state potential function φ, and the radial variable r is replaced by the steady-state stream function ψ. The potential and stream functions are defined by

$$\bar{u} = \frac{d\varphi}{\delta s} \qquad (2\text{-}9)$$

and

$$r\bar{\rho}\bar{u} = \frac{d\psi}{\delta n}$$

where δs and δn respectively represent elementary (non-dimensional) lengths in the directions of the unperturbed streamlines and of their normals on the meridianal planes (see Figure 2) and $\bar{u}$ is the steady-state velocity. A third independent variable, θ, measures the azimuthal variation. In the new coordinate system, the perturbation velocity is expressed in terms of its components along the coordinate directions as:

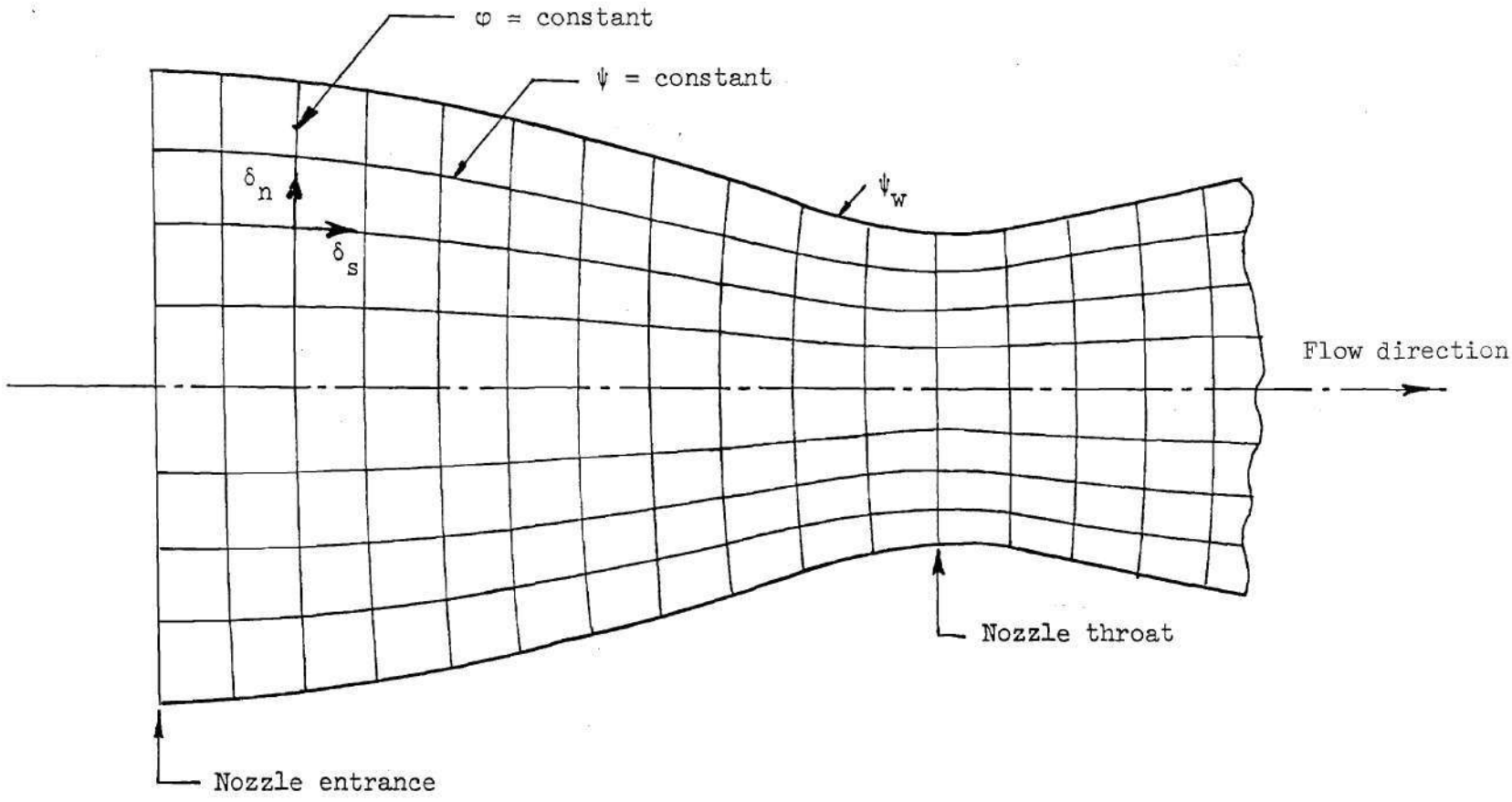

Figure 2. Coordinate System used for the Solution of the Oscillatory Nozzle Flow.

$$V' = u'\underset{\rightarrow}{e}_{\varphi} + v'\underset{\rightarrow}{e}_{\psi} + w'\underset{\rightarrow}{e}_{\theta} \qquad (2\text{-}10)$$

where the e's are unit vectors.

The transformation of Eq. (2-8) to (φ, ψ, θ) coordinates was carried out after assuming that the steady-state flow is one-dimensional, which is a reasonable approximation for slowly-convergent nozzles. Under this assumption, the dependence of $\bar{\rho}$ and $\bar{u}$ on ψ is neglected; i.e., $\bar{\rho}$ and $\bar{u}$ are considered to be practically uniform on each surface φ = constant. Also, the angle of obliquity of the streamlines with respect to the axis of symmetry is sufficiently small so that its cosine is practically unity and the normal δn along the surface φ = constant can be identified with dr. Hence, the first of Eqs. (2-9) can be integrated to give

$$r^2 = \frac{2}{\bar{\rho}\bar{u}}\,\psi \qquad (2\text{-}11)$$

In addition, the mean flow velocity vector appearing in Eq. (2-8) is given by

$$\underset{\rightarrow}{\bar{V}} = \bar{u}(\varphi)\,\underset{\rightarrow}{e}_{\varphi} \qquad (2\text{-}12)$$

Using Eqs. (2-11) and (2-12) and the expressions for the Laplacian, divergence and gradient in the (φ, ψ, θ) coordinate system (see Appendix D of Reference 4), Eq. (2-8) is written in (φ, ψ, θ) coordinate system as follows:

$$f_1(\varphi)\Phi'_{\varphi\varphi} - f_2(\varphi)\,\Phi'_{\varphi} + f_3(\varphi)\left[2(\psi\Phi'_{\psi\psi} + \Phi'_{\psi}) + \frac{1}{2\psi}\,\Phi'_{\theta\theta}\right]$$

$$- 2\Phi'_{\varphi t} + f_4(\varphi)\,\Phi'_t - \frac{1}{\bar{u}^2}\,\Phi'_{tt}$$

$$= 2\,\Phi'_{\varphi}\,\Phi'_{\varphi t} + \frac{4\bar{\rho}}{\bar{u}}\,\psi\Phi'_{\psi}\Phi'_{\psi t} + \frac{\bar{\rho}}{\bar{u}\psi}\,\Phi'_{\theta}\,\Phi'_{\theta t}$$

$$+ (\gamma + 1)\,\bar{u}^2\,\Phi'_{\varphi}\Phi'_{\varphi\varphi} + 2\,\bar{\rho}\bar{u}\,\psi\Phi'_{\psi}\Phi'_{\psi\varphi}$$

$$+ \frac{\bar{\rho}\bar{u}}{2\psi}\,\Phi'_{\theta}\Phi'_{\theta\varphi} + f_5(\varphi)(\Phi'_{\varphi})^2$$

$$+ f_6(\varphi)\,\psi(\Phi'_{\psi})^2 + f_6(\varphi)\,\frac{1}{4\psi}\,(\Phi'_{\theta})^2 + (\gamma - 1)\,\Phi'_{\varphi\varphi}\Phi'_t$$

$$- f_4(\varphi)\,\Phi'_{\varphi}\Phi'_t + (\gamma - 1)\,\frac{\bar{\rho}}{\bar{u}}\left[2\left(\psi\Phi'_{\psi\psi} + \Phi'_{\psi}\right)\right.$$

$$\left. + \frac{1}{2\psi}\,\Phi'_{\theta\theta}\right]\Phi'_t + (\gamma - 1)\,\bar{\rho}\bar{u}\left[2\left(\psi\Phi'_{\psi\psi} + \Phi'_{\psi}\right) + \frac{1}{2\psi}\,\Phi'_{\theta\theta}\right]\Phi'_{\varphi} \qquad (2\text{-}13)$$

where

$$f_1(\varphi) = \bar{c}^2 - \bar{u}^2$$

$$f_2(\varphi) = \frac{1}{\bar{c}^2}\,\frac{d\bar{u}^2}{d\varphi}$$

$$f_3(\varphi) = \frac{\bar{\rho}\bar{c}^2}{\bar{u}}$$

$$f_4(\rho) = \frac{-(\gamma - 1)}{2\bar{c}^2}\,\frac{d\bar{u}^2}{d\varphi}$$

$$f_5(\varphi) = \frac{3}{2}\left[1 + \frac{\gamma - 1}{2}\frac{\bar{u}^2}{\bar{c}^2}\right]\frac{d\bar{u}^2}{d\varphi}$$

$$f_6(\varphi) = \frac{\rho}{2\bar{u}}\left[1 - (2 - \gamma)\frac{\bar{u}^2}{\bar{c}^2}\right]\frac{d\bar{u}^2}{d\varphi} \qquad (2\text{-}14)$$

In Eq. (2-14), $\bar{c}$ is the steady-state sonic velocity given by

$$\bar{c}^2 = 1 - \frac{\gamma - 1}{2}\bar{u}^2 \qquad (2\text{-}15)$$

In deriving Eq. (2-13), the third-order terms (i.e., the last two terms on the right-hand side of Eq. (2-8)) have been neglected; thus, it is correct to second order.

Application of the Galerkin Method

Since the equations obtained by the above procedure have no known closed-form mathematical solutions, it is necessary to resort to either numerical solution techniques or approximate analytical techniques. The numerical solution techniques generally require excessive computer time; hence, the latter approach will be used here. In the nonlinear combustion instability theories developed by Powell and Zinn (see References 7-11), the governing equations were solved by means of an approximate solution technique known as the Galerkin method, which is a special case of the Method of Weighted Residuals[12,13]. In these investigations, it was shown that the Galerkin method could be successfully applied in the solution of nonlinear combustion instability problems; its application was straightforward and it required relatively little computation time. Hence, the Galerkin method was also used in

the present investigation to calculate the nonlinear nozzle admittance relation.

In order to employ the Galerkin method in the solution of Eq. (2-13), it was first necessary to express the velocity potential, Φ', as an approximating series expansion. The structure of the chosen series expansion was guided by the nonlinear nozzle admittance studies performed by Zinn and Crocco[5] as well as the nonlinear combustion instability analyses of Powell and Zinn[10]. Based on these studies, the velocity potential Φ' is expressed in the following form:

$$\Phi' = \sum_{m=0}^{M_1} \sum_{n=1}^{N_1} A_{mn}(\varphi) \cos(m\theta)\, J_m\left[S_{mn}\left(\frac{\psi}{\psi_w}\right)^{\frac{1}{2}}\right] e^{iK_{mn}\omega t} \qquad (2\text{-}16)$$

In Eq. (2-16), the coefficients $A_{mn}(\varphi)$ are unknown, complex functions of the axial variable φ. The θ- and ψ-dependent eigenfunctions are determined from the first-order solutions obtained in the analysis of the linear nozzle response functions[5]. In these functions, m is the tangential mode number, n is the radial mode number, J_m is the Bessel function of the first kind and of order m, ψ_w is the value of the steady-state stream function evaluated at the nozzle wall and S_{mn} is the n^{th} root of the equation $dJ_m(x)/dx = 0$. The expansion given above describes standing wave motion; it can be modified to describe spinning wave motion, In describing the time-dependence, ω is the fundamental frequency which must be specified and the integers K_{mn} describe the frequencies of the higher harmonics. The values of K_{mn} for the various modes appearing in Eq. (2-16) must be determined from the results of the nonlinear combustion instability analysis of Powell and Zinn.[10]

For example it was found that due to nonlinear coupling between modes, the second tangential (i.e., m = 2, n = 1) and the first radial (i.e., m = 0, n = 1) modes oscillated with twice the frequency of the first tangential (i.e., m = 1, n = 1) mode. Hence, in Eq. (2-16), $K_{11} = 1$ for the first tangential mode and $K_{mn} = 2$ for the second tangential and the first radial modes. The amplitudes and phases of the various modes depend on the axial location in the nozzle through the unknown functions $A_{mn}(\varphi)$.

In order to simplify the algebra involved in the application of the Galerkin method, the approximating series expansion for Φ' is written as the following single summation:

$$\tilde{\Phi}' = \sum_{p=1}^{N} A_p(\varphi)\, \Theta_p(\theta)\, \Psi_p(\psi)\, e^{iK_p \omega t} \tag{2-17}$$

where to each value of the index p there correspond the mode numbers m(p) and n(p), which determine the value of K_p. This correspondence is illustrated in Table 1 for a three-term expansion consisting of the first tangential (1T), second tangential (2T) and first radial (1R) modes. While in this investigation the three-term expansion described in Table 1 was used in all of the numerical computations, the theory developed herein is applicable to any number of modes. In Eq. (2-17), N is the number of terms used in the series expansion while $\Theta_p(\theta)$ and $\Psi_p(\psi)$ represent the θ- and ψ-dependent functions whose form can be obtained from Eq. (2-16).

In order to obtain the desired solution, the unknown φ-dependent functions, $A_p(\varphi)$, are determined by the Galerkin method as follows.

Table 1. Description of the Terms in the Series Expansion Used in the Present Computations

p	Mode	m(p)	n(p)	K_p
1	1T	1	1	1
2	2T	2	1	2
3	1R	0	1	2

The assumed series expansion for the velocity potential given by Eq. (2-17) is substituted into the wave equation to form the residual, $E(\tilde{\Phi}')$. In the event that this residual is identically zero, the assumed solution is the exact solution. The residual therefore represents the error incurred by using the approximate series given by Eq. (2-17). The Galerkin method determines the amplitudes $A_p(\varphi)$ that minimize the residual $E(\tilde{\Phi}')$.

Applying the Galerkin method[13], the residual $E(\tilde{\Phi}')$ is required to satisfy the following Galerkin orthogonality conditions:

$$\int_0^T \int_s E(\tilde{\Phi}')\, T_j(t)\, \Theta_j(\theta)\, \Psi_j(\psi)\, ds dt = 0, \quad j = 1, 2, \ldots N \qquad (2\text{-}18)$$

The weighting functions $T_j(t)$, $\Theta_j(\theta)$ and $\Psi_j(\psi)$ correspond to the terms that appear in the assumed series expansion. The temporal weighting function, $T_j(t)$, is the complex conjugate of the assumed time dependence; that is

$$T_j(t) = e^{-iK_j\omega t} \qquad (2\text{-}19)$$

The azimuthal weighting functions, $\Theta_j(\theta)$, are given by

$$\Theta_j(\theta) = \cos m\theta \tag{2-20}$$

while the radial weighting functions, $\Psi_j(\psi)$, are given by

$$\Psi_j(\psi) = J_m[A_j(\psi/\psi_w)^{\frac{1}{2}}] \tag{2-21}$$

The time integration is performed over one period of oscillation, $T = 2\pi/\omega$, while the spatial integration is performed over any surface of φ = constant in the nozzle (in Eq. (2-18), ds indicates an incremental area on this surface).

Evaluating the spatial and temporal integrals in Eq. (2-18) yields the following system of N nonlinear, second order, coupled, complex ordinary differential equations to be solved for the complex amplitude functions, $A_p(\varphi)$:

$$\sum_{p=1}^{N} \left\{ C_1(\varphi, p, j) \frac{d^2A_p}{d\varphi^2} + C_2(\varphi, p, j) \frac{dA_p}{d\varphi} + C_3(\varphi, p, j) A_p \right\}$$

$$+ \sum_{p=1}^{N} \sum_{q=1}^{N} \left\{ D_1(\varphi, p, q, j) \frac{d^2A_p}{d\varphi^2} A_q + D_2(\varphi, p, q, j) \frac{d^2A_p}{d\varphi^2} \frac{dA_q}{d\varphi} \right.$$

$$+ D_3(\varphi, p, q, j) \frac{dA_p}{d\varphi} \frac{dA_q}{d\varphi} + D_4(\varphi, p, q, j) A_p \frac{dA_q}{d\varphi}$$

$$\left. + D_5(\varphi, p, q, j) A_p A_q \right\} + Q = 0 ,$$

$$j = 1, 2, \ldots N \tag{2-20}$$

In the above equations, the term Q represents the additional

nonlinear terms that arise when a complex solution (i.e., Eq. (2-17)) is used to solve the nonlinear wave equation (i.e., Eq. (2-13)). These terms are similar in form to the nonlinear terms shown, but they involve the complex conjugates of the amplitude functions. The procedure for deriving these terms is given in Appendix B of Reference 11. The coefficients C_k and D_k are functions of the axial variable φ as well as the indices j, p and q. The analytical expressions for these coefficients contain integrals involving trigonometric and Bessel functions, and are given in Appendix B. In the absence of closed-form expressions for the integrals of Bessel functions, these integrals must be computed numerically.

As a check on the above analysis, Eq. (2-22) is derived with a single mode series consisting of the first tangential mode; that is,

$$\tilde{\Phi}' = A(\varphi) \cos \theta \, J_1[S_{11}(\psi/\psi_w)^{\frac{1}{2}}] \, e^{i\omega t} \qquad (2\text{-}23)$$

For this case, all the coefficients of the nonlinear terms vanish and the coefficients of the linear terms can be evaluated analytically. The resulting linear equation is

$$\bar{u}^{-2}(\bar{c}^{-2} - \bar{u}^{-2}) \frac{d^2A}{d\varphi^2} - \bar{u}^{-2}\left[\frac{1}{\bar{c}^{-2}} \frac{d\bar{u}^{-2}}{d\varphi} + 2i\omega\right] \frac{dA}{d\varphi} \qquad (2\text{-}24)$$

$$+ \left[-\frac{S_{11}^2}{2\psi_w} \frac{\bar{\rho}\bar{u}^{-2}}{\bar{\rho}\bar{c}^{-2}} - \frac{\gamma-1}{2} i\omega \frac{\bar{u}^{-2}}{\bar{c}^{-2}} \frac{d\bar{u}^{-2}}{d\varphi} + \omega^2\right] A(\varphi) = 0 \qquad (2\text{-}24)$$

which is identical to the equation derived by Crocco and Sirignano[3] in their linear nozzle admittance analysis.

Dominance of the 1T Mode

Equation (2-22) can be further simplified using the well known fact that most transverse instabilities behave like the first tangential (1T mode) mode. Based on the results of recent combustion instability studies[11], it is assumed that the amplitude of the 1T mode is considerably larger than the amplitudes of the remaining modes in the series solution. Through an order of magnitude analysis, correct to second order in mode amplitude, Eq. (2-22) reduces to the following system of equations:

$$\bar{u}^2(\bar{c}^2 - \bar{u}^2)\frac{d^2A_1}{d\varphi^2} - \bar{u}^2\left[\frac{1}{\bar{c}^2}\frac{d\bar{u}^2}{d\varphi} + 2i\omega\right]\frac{dA_1}{d\varphi}$$

$$+\left(-\frac{S_1^2}{2\psi_w}\frac{}{\rho u c^2} - \frac{\gamma-1}{2}\, i\omega\,\frac{\bar{u}^2}{\bar{c}^2}\frac{d\bar{u}^2}{d\varphi} + \omega^2\right)A_1(\varphi) = 0 \qquad (2\text{-}25a)$$

$$\bar{u}^2(\bar{c}^2 - \bar{u}^2)\frac{d^2A_p}{d\varphi^2} - \bar{u}^2\left(\frac{1}{\bar{c}^2}\frac{d\bar{u}^2}{d\varphi} + 2iK_p\omega\right)\frac{dA_p}{d\varphi}$$

$$+\left(-\frac{S_p^2}{2\psi_w}\frac{}{\rho u c^2} - \frac{\gamma-1}{2}\, iK_p\omega\,\frac{\bar{u}^2}{d\varphi} + K_p^2\,\omega^2\right)A_p(\varphi)$$

$$= I_p\left\{A_1, \frac{dA_1}{d\varphi}, \frac{d^2A_1}{d\varphi^2}\right\}, \qquad (2\text{-}25b)$$

$$p = 2, 3, \ldots N$$

In the above system of equations, the inhomogeneous terms I_p are functions of φ and they contain products of the amplitude of the 1T

mode, $A_1(\varphi)$, and its first and second order derivatives.

It can be seen that as a result of the order of magnitude assumption, the above equations are decoupled with respect to the 1T mode; that is, the solution for A_1 can be obtained independently of the amplitudes of the other modes. Thus, to second order, the nonlinearities of the problem do not affect the 1T mode. On the other hand the nonlinearities influence the amplitudes of the higher modes (i.e., A_2, A_3 . . .) by means of the inhomogeneous terms in the equations for the other modes.

The above equations can be written concisely as

$$H_p(\varphi) \frac{d^2 A_p(\varphi)}{d\varphi^2} + M_p(\varphi) \frac{dA_p(\varphi)}{d\varphi} + N_p(\varphi) A_p(\varphi) = I_p(\varphi) ,$$

$$p = 1, 2, \ldots N \qquad (2\text{-}26)$$

where

$$H_p(\varphi) = \bar{u}^2(\bar{c}^2 - \bar{u}^2) \qquad (2\text{-}27a)$$

$$M_p(\varphi) = -\bar{u}^2 \left[\frac{1}{\bar{c}^2} \frac{d\bar{u}^2}{d\varphi} + 2iK_p\omega \right] \qquad (2\text{-}27b)$$

$$N_p(\varphi) = \left[-\frac{S_p^2}{2\psi_w} \frac{}{\rho u c^2} - \frac{\gamma-1}{2} iK_p\omega \frac{\bar{u}^2}{\bar{c}^2} \frac{d\bar{u}^2}{d\varphi} + K_p^2\omega^2 \right] \qquad (2\text{-}27c)$$

with

$$I_1(\varphi) = 0$$

Homogeneous and Particular Solutions

Equation (2-26) is a second order, linear ordinary differential

equation and its general solution is a combination of the homogeneous solution that satisfies the homogeneous part of Eq. (2-26), i.e.,

$$L\left\{ A_p^{(h)} \right\} = H_p \frac{d^2 A_p^{(h)}}{d\varphi^2} + M_p \frac{dA_p^{(h)}}{d\varphi} + N_p A_k^{(h)} = 0 \qquad (2\text{-}28)$$

and the particular solution that satisfies Eq. (2-26). The general solution can be written in the following form:

$$A_p(\varphi) = \sigma_1 A_p^{(h)} + \sigma_2 \tilde{A}_p^{(h)} + A_p^{(i)}$$

where $A_p^{(h)}$ and $\tilde{A}_p^{(h)}$ are two independent solutions of Eq. (2-27), σ_1 and σ_2 are arbitrary constants, and $A_p^{(i)}$ is a particular solution of the inhomogeneous equation.

Examination of the coefficients of Eq. (2-26) shows that this equation has the following singular points:

$$\bar{u} = 0$$

$$\bar{u} = \bar{c} = (2/\gamma + 1)^{\frac{1}{2}} = \bar{c}_{throat}$$

For a supercritical nozzle with a finite area entrance, only the singularity at the throat is of concern. Assuming that the singularity of the solution appears in $\tilde{A}_p^{(h)}$, the condition requiring the regularity of the solution at the throat can be expressed[3] by requiring $\sigma_2 = 0$. Consequently, the required solution of Eq. (2-26) is of the form

$$A_p(\varphi) = \sigma_1 A_p^{(h)}(\varphi) + A_p^{(i)}(\varphi) \qquad (2\text{-}29)$$

Admittance Relation

Using the above result, a nonlinear admittance relation to be used as a boundary condition in the nonlinear combustion instability analyses can be derived. Noting that the velocity potential Φ' given by Eq. (2-17) is a summation of mode-potentials Φ_p' where

$$\Phi_p' = A_p(\varphi)\ \Theta_p(\theta)\ \Psi_p(\psi)\ e^{iK_p\omega t} \tag{2-30}$$

a nozzle admittance relation can be written for each of the mode-potentials. Substituting Eq. (2-29) into Eq. (2-30), and taking partial derivatives with respect to z and t gives

$$\frac{\partial \Phi_p'}{\partial z} - \bar{u}\ \Theta_p(\theta)\ \Psi_p(\psi)\ e^{iK_p\omega t}\ \frac{dA_p^{(i)}}{d\varphi}$$

$$= \sigma_1\ \bar{u}\ \Theta_p(\theta)\ \Psi_p(\psi)\ e^{iK_p\omega t}\ \frac{dA_p^{(h)}}{d\varphi} \tag{2-31}$$

$$\frac{\partial \Phi_p'}{\partial t} - iK_p\omega\ \Theta_p(\theta)\ \Psi_p(\psi)\ e^{iK_p\omega t}\ A_p^{(i)}$$

$$= \sigma_1\ iK_p\omega\ \Theta_p(\theta)\ \Psi_p(\psi)\ e^{iK_p\omega t}\ A_p^{(h)} \tag{2-32}$$

Eliminating σ_1 between Eqs. (28) and (29) and defining

$$\zeta_p = \frac{dA_p^{(h)}/d\varphi}{A_p^{(h)}} \tag{2-33}$$

$$\Gamma_p = \frac{1}{\bar{c}^2 A_p^{(h)}} \left[A_p^{(i)}\ \frac{dA_p^{(h)}}{d\varphi} - A_p^{(h)}\ \frac{dA_p^{(i)}}{d\varphi} \right] \tag{2-34}$$

$$Y_p = \frac{i\bar{u}\zeta_p}{\gamma K_p \omega} \tag{2-35}$$

yields

$$\frac{\partial \Phi_p'}{\partial z} + \gamma Y_p \frac{\partial \Phi_p'}{\partial t} = -\bar{u}\bar{c}^2 \Theta_p(\theta)\, \Psi_p(\psi)\, e^{iK_p \omega t}\, \Gamma_p$$

$$p = 1, 2, \ldots N \tag{2-36}$$

Equation (2-36) is the nonlinear nozzle admittance relation, to be used as the boundary condition at the nozzle entrance in nonlinear combustion instability analyses. The right-hand side of this equation arises from the nonlinear terms in the nozzle wave equation. The quantities Y_p and Γ_p are respectively the linear and nonlinear admittance coefficients for the p^{th} mode. The nonlinear admittance, Γ_p, represents the effect of nozzle nonlinearities upon the nozzle admittance and it is identically zero when nonlinearities are not present.

It can be shown that Eq. (2-36) can be written in terms of the pressure and axial velocity perturbations as:

$$U_p - Y_p P_p = -\bar{u}\bar{c}^2 \Gamma_p, \qquad p = 1, 2, \ldots N \tag{2-37}$$

where U_p and P_p are the amplitudes of the axial velocity and pressure perturbations respectively as given by:

$$p' = \sum_{p=1}^{N} P_p(\varphi)\, \Theta_p(\theta)\, \Psi_p(\psi)\, e^{iK_p \omega t} \tag{2-38}$$

$$u' = \sum_{p=1}^{N} U_p(\varphi)\, \Theta_p(\theta)\, \Psi_p(\psi)\, e^{iK_p \omega t} \tag{2-39}$$

In order to use the admittance relation (Eq. (2-36) or (2-37)) in the combustion instability theories, the admittance coefficients Y_p (or ζ_p) and Γ_p must be determined for the given nozzle. The equations governing these quantities are readily derived from Eq. (2-26) using the definitions for ζ_p and Γ_p (i.e., Eqs. (2-33) and (2-35)). The resulting equations are:

$$H_p \frac{d\zeta_p}{d\varphi} = - M_p \zeta_p - N_p - H_p \zeta_p^2 \tag{2-40}$$

$$H_p \frac{d\Gamma_p}{d\varphi} = \left(- H_p \zeta_p + H_p \frac{\gamma - 1}{2\bar{c}^2} \frac{d\bar{u}^2}{d\varphi} - M_p \right) \Gamma_p - \frac{I_p}{\bar{c}^2}$$

$$p = 1, 2, \ldots N \tag{2-41}$$

The method of solution of these equations, needed to obtain the nonlinear nozzle response, is described in the next chapter.

CHAPTER III

CALCULATION OF THE NOZZLE RESPONSE

Calculation Procedure

Equations (2-40) and (2-41) form a system of 2N complex, ordinary differential equations for the N linear admittance coefficients, ζ_p, and the N nonlinear admittance coefficients, Γ_p; N is the number of terms in the series expansion for the velocity potential. Equation (2-40) can be solved independently to obtain ζ_p for every mode. Since for the 1T mode, the nonlinear admittance coefficient is identically zero, it is only necessary to solve Eq. (2-41) for the remaining modes to obtain the required nonlinear coefficients, Γ_p. However, since Eq. (2-41) involves both ζ_p and I_p, these quantities must be evaluated before solving Eq. (2-41). The solution of Eq. (2-40) readily determines ζ_p, but the determination of I_p requires knowledge of the amplitude of the 1T mode, $A_1(\varphi)$, and its first and second order derivatives. The amplitude $A_1(\varphi)$ is obtained by numerically integrating Eq. (2-33). To obtain the constant of integration, it is necessary to specify the value of P_1 (i.e., the pressure amplitude of the 1T mode) at the nozzle entrance.

It may be observed that Eqs. (2-40) and (2-41) have singularities at the same points as Eq. (2-26). As before, the only singularity of interest is the throat. Since Eqs. (2-40) and (2-41) are first order ordinary differential equations, the numerical integration of these

equations must start at some initial point where the initial conditions are known, and terminate at the nozzle entrance where the admittance coefficients Y_p and Γ_p are needed. Since the equations are singular at the throat, the integration is initiated at a point that is located a short distance upstream of the throat. The needed initial conditions are obtained by expanding the dependent variables in a Taylor series about the throat ($\varphi = 0$); thus,

$$\zeta_p(\varphi) = \zeta_p(0) + \varphi\zeta_p'(0) + \ldots \tag{3-1}$$

$$\Gamma_p(\varphi) = \Gamma_p(0) + \varphi\Gamma_p'(0) + \ldots \tag{3-2}$$

The coefficients $\zeta_p(0)$ and $\zeta_p'(0)$ can be determined by substituting Eq. (3-1) in Eq. (2-40) and taking the limit as $\varphi \to 0$. The results are

$$\zeta_p(0) = -\frac{N_p(0)}{M_p(0)} \tag{3-3}$$

$$\zeta_p'(0) = \frac{-M_p'(0)\,\zeta_p(0) - H_p'(0)\,\zeta_p^2(0) - N_k'(0)}{h_p'(0) + M_p(0)} \tag{3-4}$$

$$p = 1, 2, \ldots N$$

Similarly, $\Gamma_k(0)$ and $\Gamma_k'(0)$ can be determined by substituting Eq. (3-2) in Eq. (2-41), and taking the limit as $\varphi \to 0$. The results are:

$$\Gamma_p(0) = -\frac{I_p(0)}{\bar{c}^2(0)\,M_p(0)} \tag{3-5}$$

$$\Gamma_p'(0) = \Big\{ - \bar{c}^{-2}(0)\, H_p'(0)\, \zeta_p(0)\, \Gamma_p(0) + \frac{\gamma - 1}{2} \frac{d\bar{u}^{-2}}{d\varphi}(0)\, H_p'(0)\, \Gamma_p(0)$$

$$- \bar{c}^{-2}(0)\, M_p'(0)\, \Gamma_p(0) + \frac{\gamma - 1}{2} \frac{d\bar{u}^{-2}}{d\varphi}(0)\, M_p(0)\, \Gamma_p(0)$$

$$- I_p'(0) \Big\} \Big/ \Big\{ \bar{c}^{-2}(0)\, H_p'(0) + \bar{c}^{-2}(0)\, M_p(0) \Big\}$$

In Eqs. (2-40) and (2-41), the quantities H_p, M_p, N_p and I_p are functions of the steady-state flow variables in the nozzle and these must be computed before performing the numerical integration to obtain ζ_p and Γ_p. For a specified nozzle geometry, the steady-state quantities are computed by solving the quasi-one-dimensional isentropic steady-state equations for nozzle flow. The variation of the steady state velocity in the subsonic portion of the nozzle is given by[14]

$$\frac{d\bar{u}^{-2}}{d\varphi} = \frac{1}{\bar{u}} \frac{d\bar{u}^{-2}}{dr} \frac{dr}{dz} \tag{3-7}$$

where

$$\frac{d\bar{u}^{-2}}{dr} = - \frac{4}{r_{th}} \left(\frac{2}{\gamma+1} \right)^{\frac{-\gamma - 1}{4(\gamma-1)}} (\bar{u}^{-2})^{5/4} \left[\frac{\left(1 - \frac{\gamma-1}{2} \bar{u}^{-2} \right)^{\frac{2\gamma - 1}{2(\gamma-1)}}}{1 - \frac{\gamma + 1}{2} \bar{u}^{-2}} \right] \tag{3-8}$$

and r_{th} is the radius of the nozzle throat. The quantity dr/dz must be evaluated for the specified nozzle geometry.

Figure 3 shows the nozzle geometry used in the present study. Starting at the combustion chamber, the contour is generated by a circular arc of radius r_{cc} turned through an angle θ_1, the nozzle half-

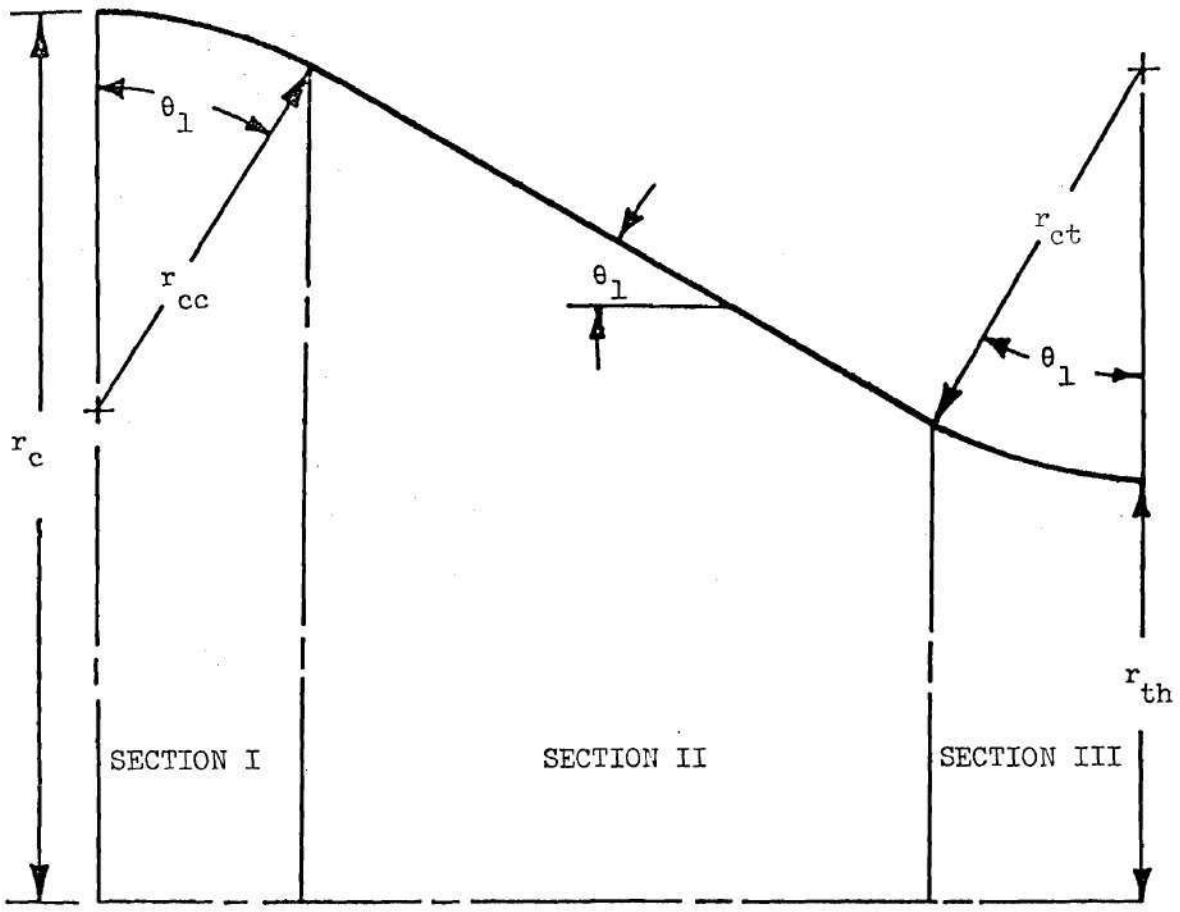

Figure 3. Nozzle Profile Used in Calculating Admittances

angle. This arc connects smoothly to a straight line which is inclined at an angle θ_1 to the nozzle axis. This straight line then joins with another circular arc of radius r_{ct} which turns through an angle θ_1 and ends at the throat. Thus the nozzle is considered to be composed of three separate regions as shown in Figure 3. All of the length variables have been non-dimensionalized with respect to the radius of the combustion chamber, to which the nozzle is attached; hence, $r_c = 1$. The throat radius r_{th} is fixed by the Mach number at the nozzle entrance plane. The nozzle profile is smooth and it is completely specified by r_{cc}, r_{ct} and θ_1, which are respectively the radius of curvature at the nozzle entrance, radius of curvature at the nozzle throat and the slope of the central conical section. A good degree of flexibility is allowed within the limits of this overall geometric description. However, should this class of nozzles prove to be too restrictive, the range of allowable nozzle geometries can be easily extended.

To obtain the steady-state velocity, Eq. (3-7) is integrated using equal steps in the steady-state potention φ, beginning at the throat ($\varphi = 0$) where the nondimensional steady-state velocity is known; that is,

$$\bar{u}(0) = \sqrt{\frac{2}{\gamma+1}} \tag{3-9}$$

The Adams-Moulton predictor-corrector scheme[15] was used to perform the numerical integration, with the starting values for this scheme being obtained by using a fourth order Runge-Kutta integration scheme. The computation is continued to the nozzle entrance where the radius of

the wall equals unity.

Once $\bar{u}$ is known, the corresponding value of $\bar{c}$ can be computed using the steady-state relationship

$$\bar{c}^2 = 1 - \frac{\gamma-1}{2} \bar{u}^2 \tag{3-10}$$

Once the steady-state flow variables are evaluated, they can be used in the computation of the quantities H_p, M_p, N_p and I_p that appear in Eqs. (2-40) and (2-41). As stated earlier, these coefficients involve some integrals of the Bessel functions for which there are no closed-form expressions. These integrals are evaluated numerically using Simpson's rule. The numerical values for S_{mn} are taken from Reference 16 and the specific heat ratio, γ, is assumed to equal 1.2.

After the steady-state flow variables and the above coefficients are evaluated, Eqs. (2-40) and (2-41) can be solved for the admittance coefficients ζ_p and Γ_p, and the linear admittance Y_p can be readily computed from ζ_p using Eq. (2-35). Computations of the admittance coefficients have been performed using the three-mode series expansion consisting of the first tangential, the second tangential and the first radial modes, as described in Chapter II. The same numerical scheme as was used for the evaluation of steady-state equation is also used in the determination of ζ_p and Γ_p. Computations have been performed for several nozzle geometries at different frequencies and different pressure amplitudes. Some of the results are discussed in the next section.

Results and Discussion

Figures 4 and 5 show the frequency dependence of the linear admittance coefficients for the 1T, 2T, and 1R modes for a typical nozzle ($\theta_1 = 20^\circ$, $r_{cc} - 1.0$, $r_{ct} = 0.9234$; $M = 0.2$). Here, ω is the frequency of the 1T mode, while the frequency of the 2T and 1R modes is 2ω due to nonlinear coupling. Hence, the real parts of the linear admittance coefficients for the 2T and 1R modes actually attain their peak values at a higher frequency than that for the 1T mode. The linear admittance coefficients for the 1T mode are in complete agreement with those calculated previously by Bell and Zinn[14]. This is not surprising since the governing equation for the 1T mode in Reference 14 is identical with Eq. (2-24) that was used in the present study.

The frequency dependence of the nonlinear admittance coefficient for the 2T mode is shown in Figures 6 and 7 with pressure amplitude of the 1T mode as a parameter. While the behavior of the linear admittance coefficient depends only upon the frequency of oscillations, the behavior of the nonlinear admittance coefficient is seen to depend on the amplitude of the 1T mode. This result is expected, since in Eq. (2-41), I_p is a function of the amplitude of the 1T mode. As expected, the absolute values of both Γ_r and Γ_i increase with increasing pressure amplitude of the 1T mode, which acts as a driving force. It is also observed that the absolute values of Γ_r and Γ_i vary similarly with frequency as the absolute values of Y_r and Y_i. The frequency dependence of the nonlinear admittance coefficient for the 1R mode is shown in Figures 8 and 9 with pressure amplitude of 1T mode as a parameter.

Figures 10 and 11 show the effect of pressure amplitude upon

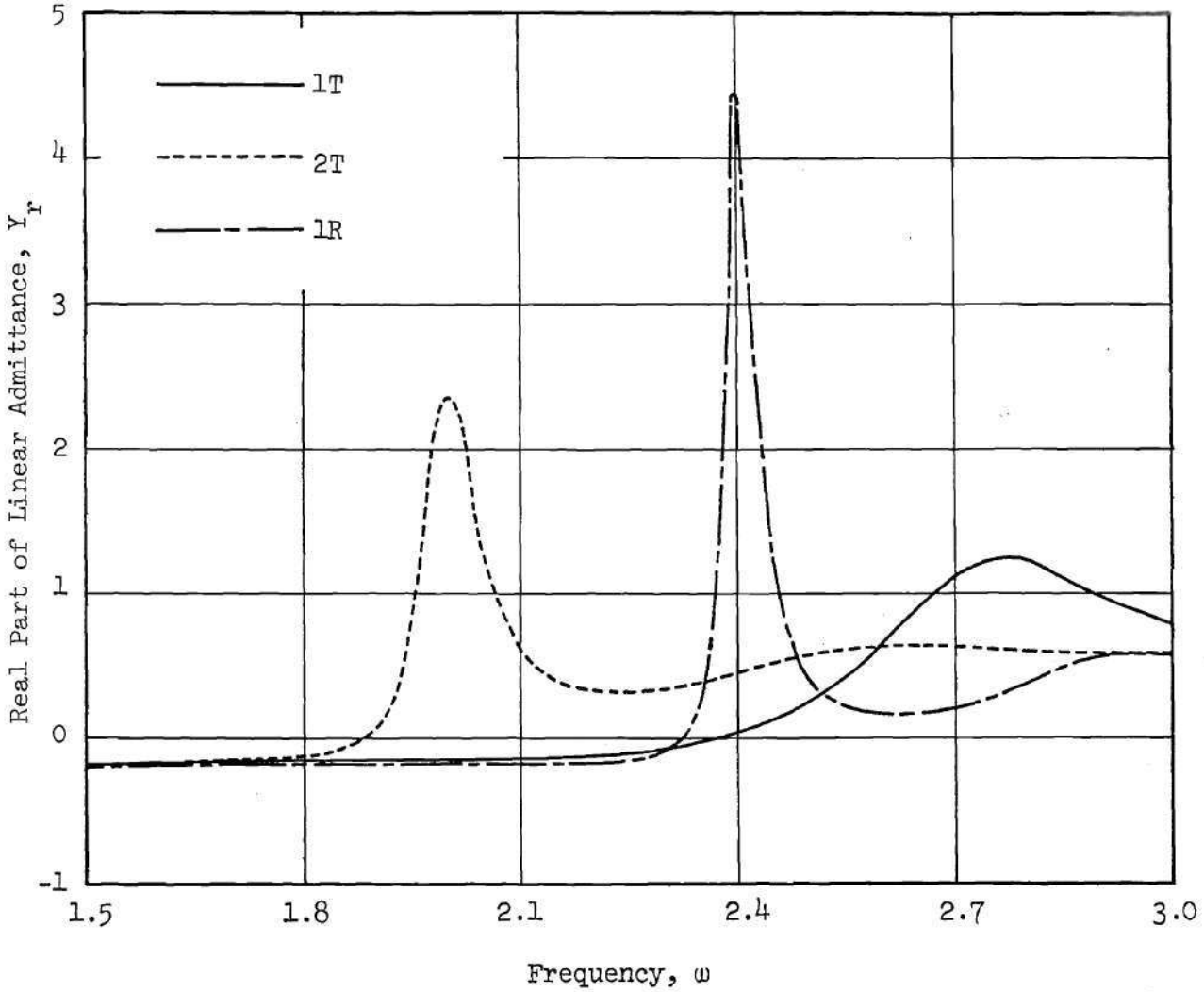

Figure 4. Linear Admittances for the 1T, 2T, and 1R Modes (Y_r)

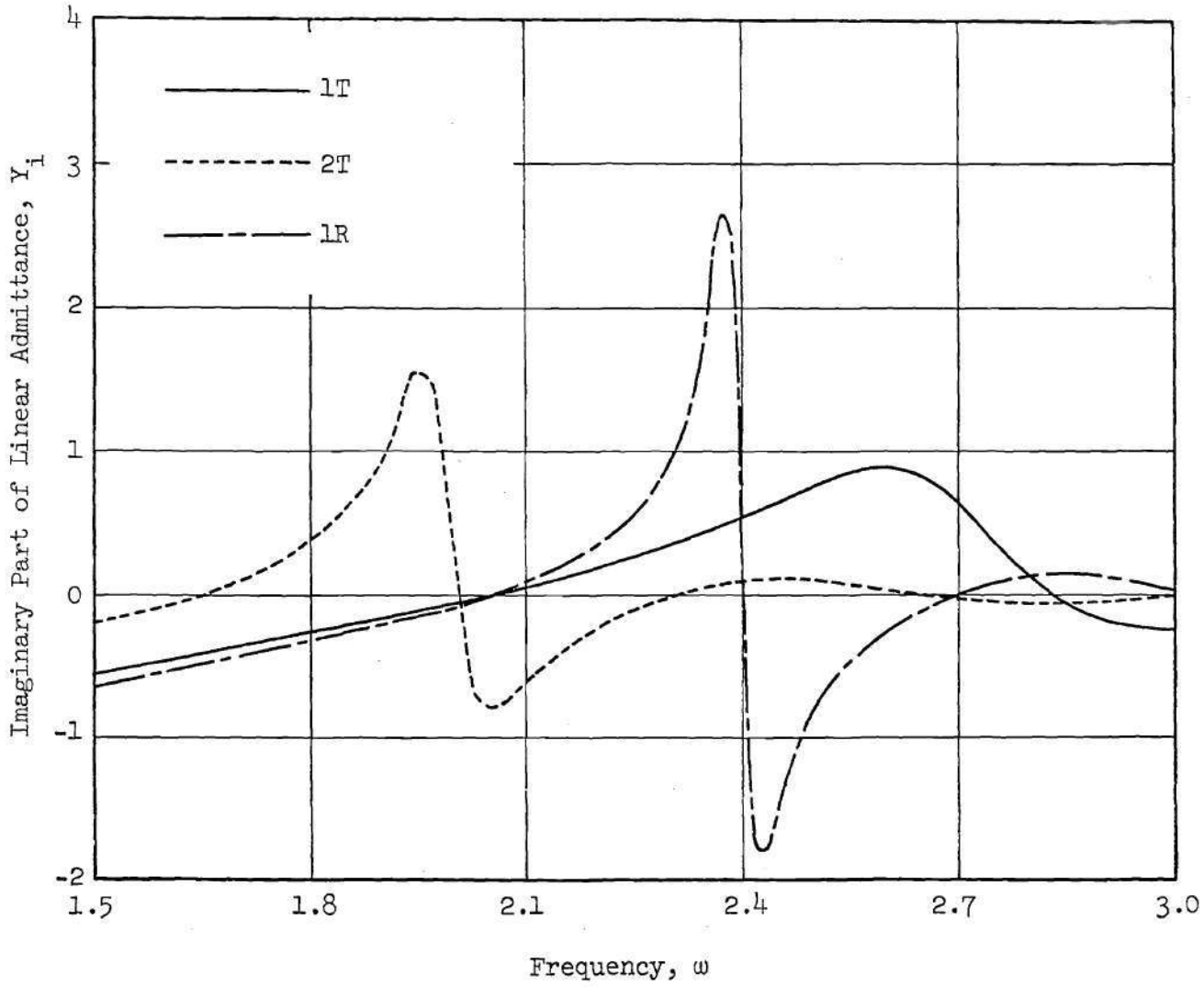

Figure 5. Linear Admittances for the 1T, 2T, and 1R Modes (Y_i)

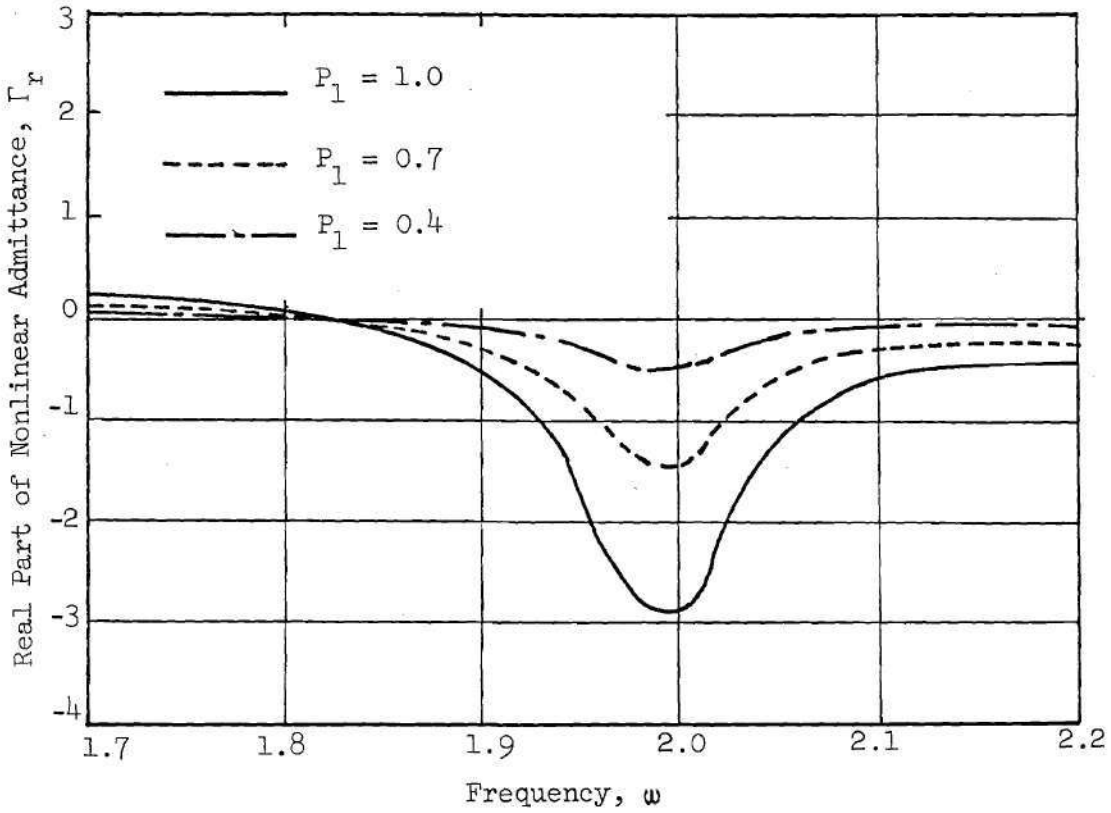

Figure 6. Real Part of the Nonlinear Admittance for the 2T Mode ($\theta_1 = 20^\circ$, $r_{cc} = 1.0$, $r_{ct} = 0.9234$, $M_e = 0.2$)

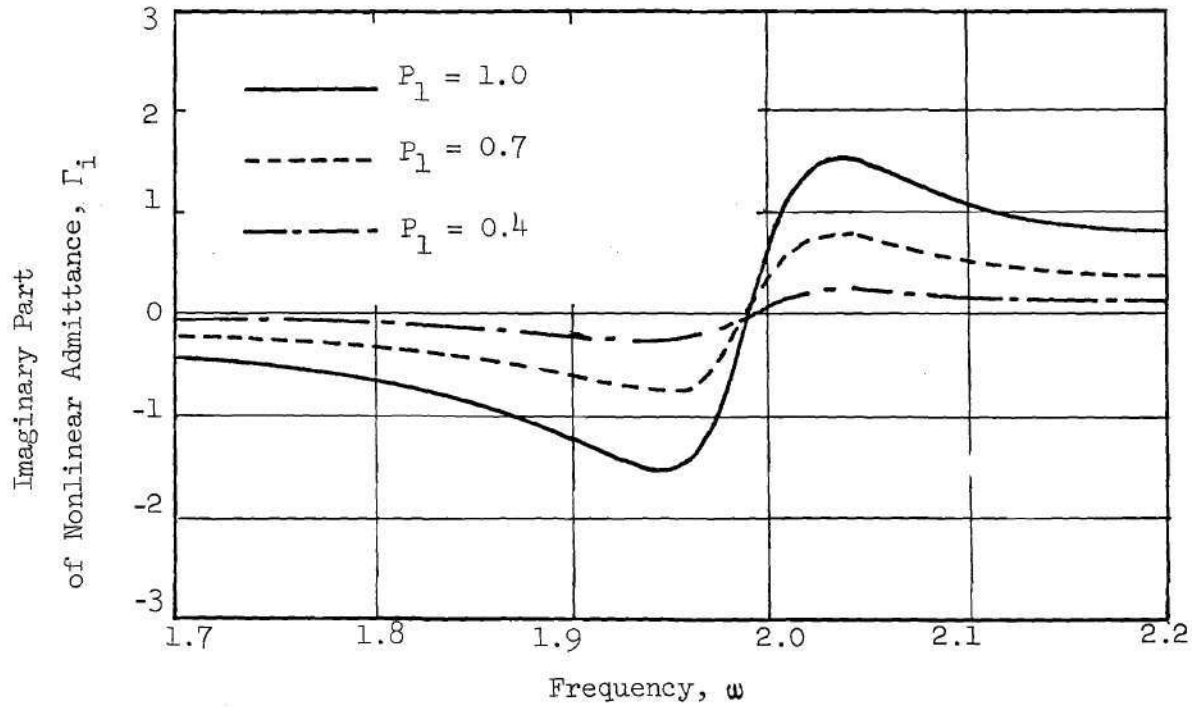

Figure 7. Imaginary Part of the Nonlinear Admittance for the 2T Mode ($\theta_1 = 20^\circ$, $r_{cc} = 1.0$, $r_{ct} = 0.9234$, $M_e = 0.2$)

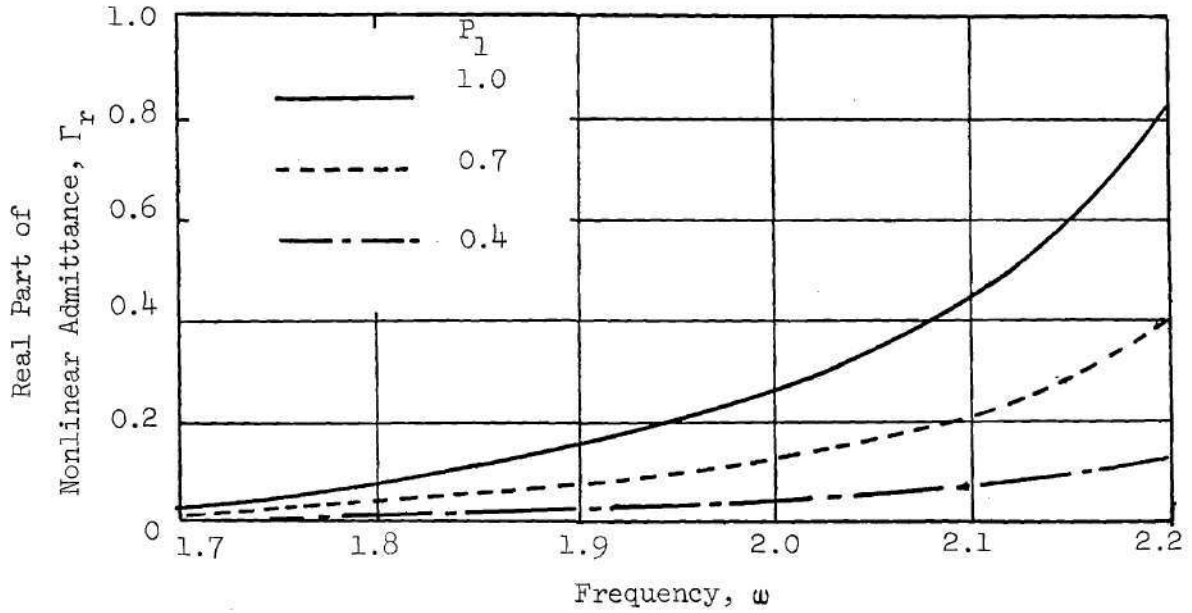

Figure 8. Real Part of the Nonlinear Admittance for the 1R Mode ($\theta_1 = 20^\circ$, $r_{cc} = 1.0$, $r_{ct} = 0.9234$, $M_e = 0.2$)

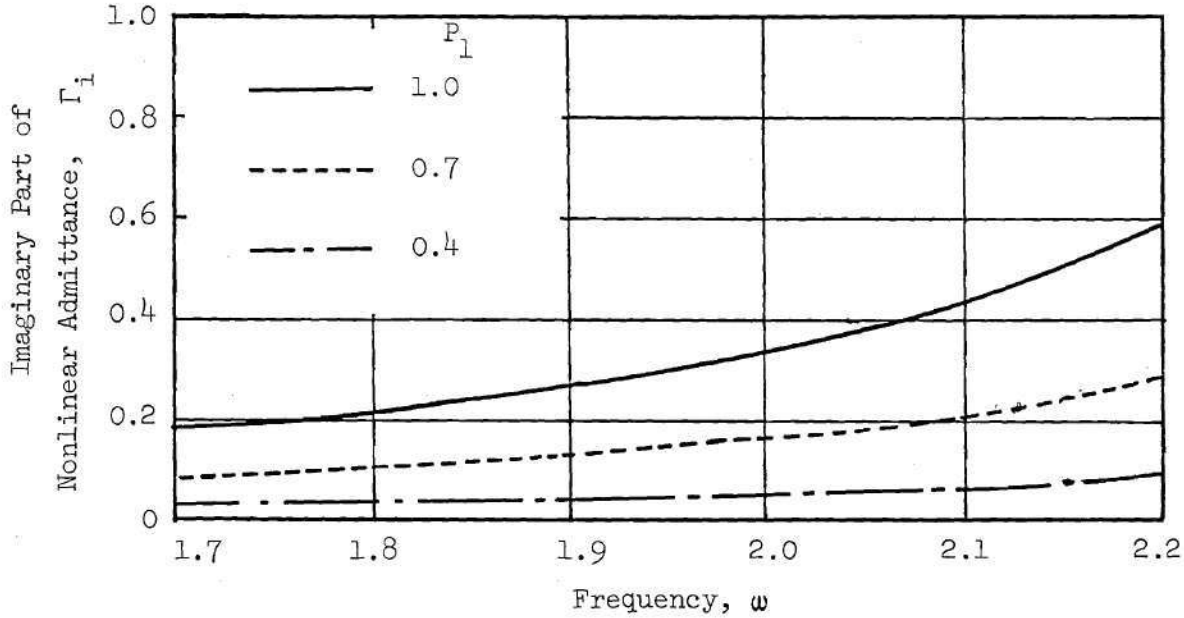

Figure 9. Imaginary Part of the Nonlinear Admittances for the 1R Mode ($\theta_1 = 20^\circ$, $r_{cc} = 1.0$, $r_{ct} = 0.9234$, $M_e = 0.2$)

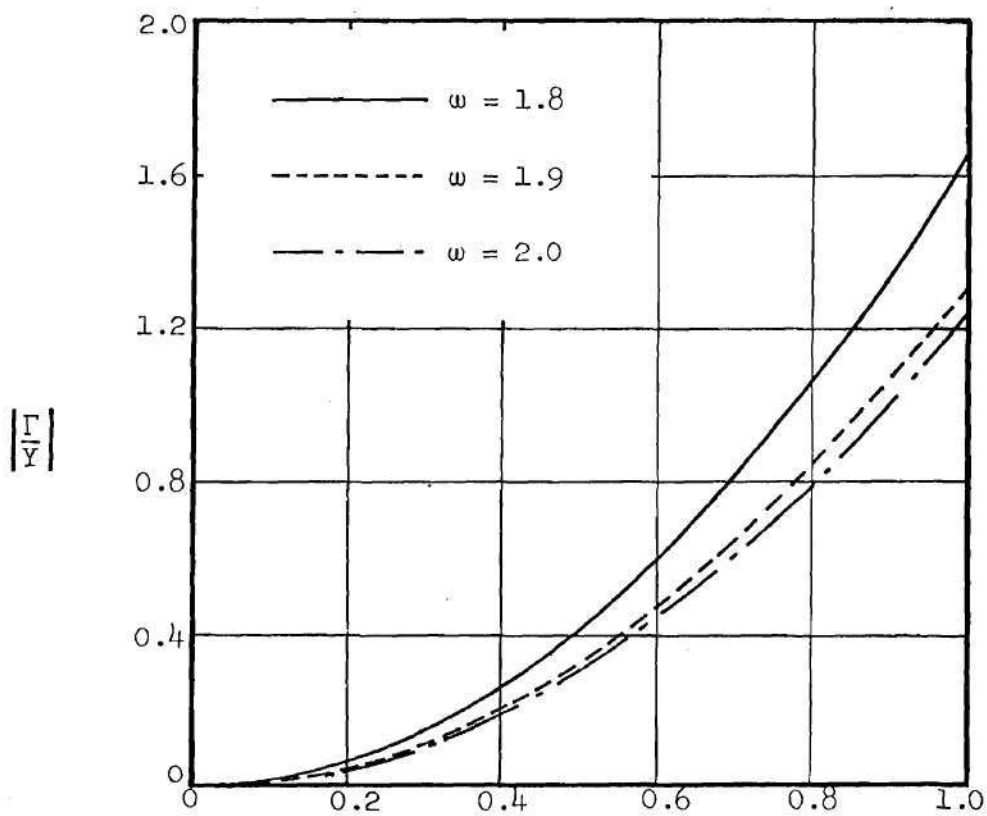

Figure 10. Relative Magnitudes of Linear and Nonlinear Admittances for 2T Mode. ($\theta_1 = 20^\circ$, $r_{cc} = 1.0$, $r_{ct} = 0.9234$, $M_e = 0.2$)

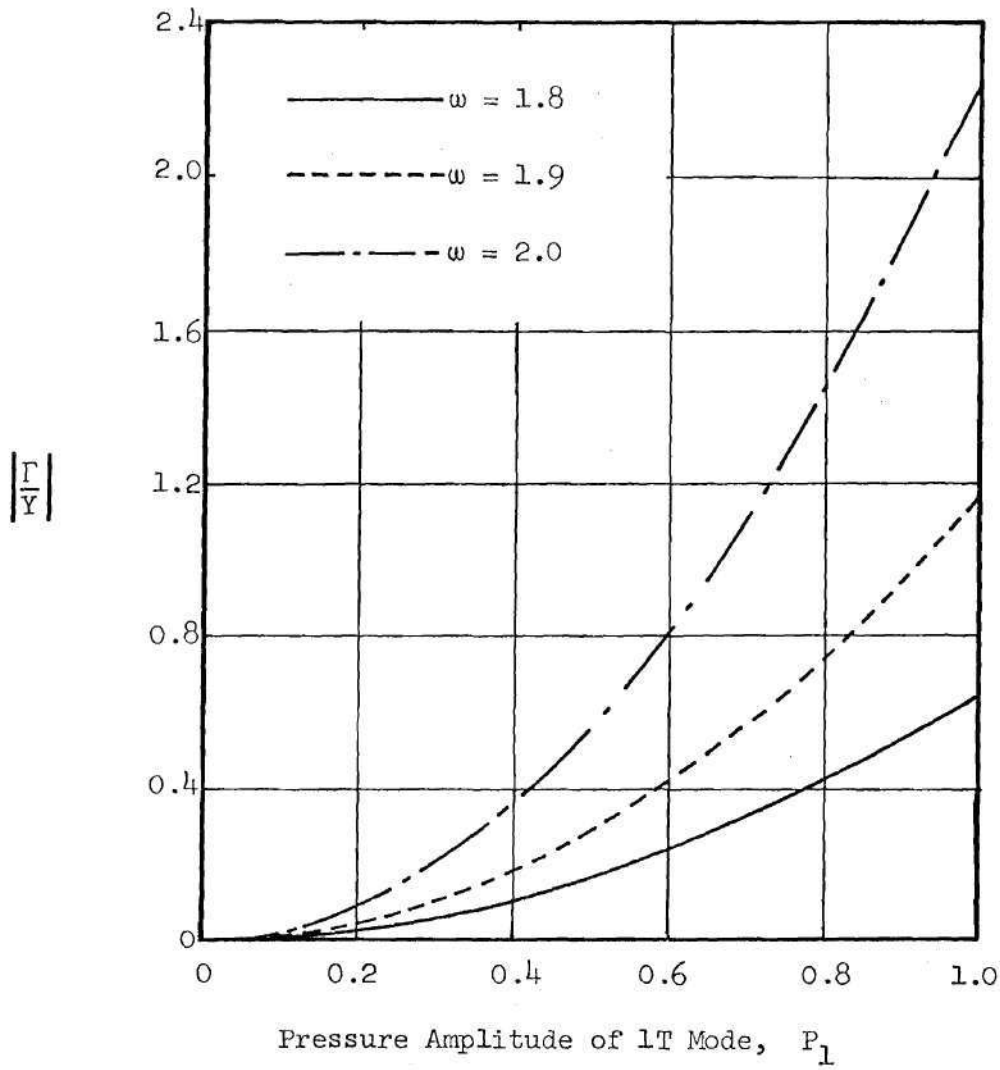

Figure 11. Relative Magnitudes of Linear and Nonlinear Admittances for 1R Mode ($\theta_1 = 20^\circ$, $r_{cc} = 1.0$, $r_{ct} = 0.9234$, $M_e = 0.2$)

the magnitude of the ratio of nonlinear admittance coefficient to the linear admittance coefficient for the 2T and 1R modes respectively. This ratio, $|\Gamma/Y|$, increases with increasing pressure amplitude. In the limiting case of $|P_1| = 0$, the nonlinear admittance coefficient is zero for any frequency, which is as expected.

Figures 12 and 13 show the influence of entrance Mach number M_e on the nonlinear nozzle admittance coefficients for 2T and 1R modes respectively. Here the relative magnitudes of the linear and nonlinear admittances (i.e., $|\Gamma/Y|$) are plotted as a function of amplitude of the 1T mode. In each case there is a significant decrease in $|\Gamma/Y|$ with increasing Mach number.

The effect of nozzle half-angle on $|\Gamma/Y|$ for the 2T mode is shown in Figure 14. It is readily seen that for θ_1 between 15 and 45 degrees there is only a slight effect of nozzle half-angle on the relative magnitudes of the linear and nonlinear admittances. However, it should be noted that both the linear and nonlinear theories are restricted to slowly convergent nozzles (i.e., small θ_1). Similar results were also obtained for the 1R mode and they are presented in Figure 15.

The influence of the radius of curvature at the throat of the nozzle on the quantity, $|\Gamma/Y|$, for the 2T and 1R modes is shown in Figures 16 and 17 respectively. It is observed that a change in the radius of curvature of the nozzle at the throat has an insignificant effect on the relative magnitudes of the linear and nonlinear admittances. On the other hand, any change in the radius of curvature of the nozzle

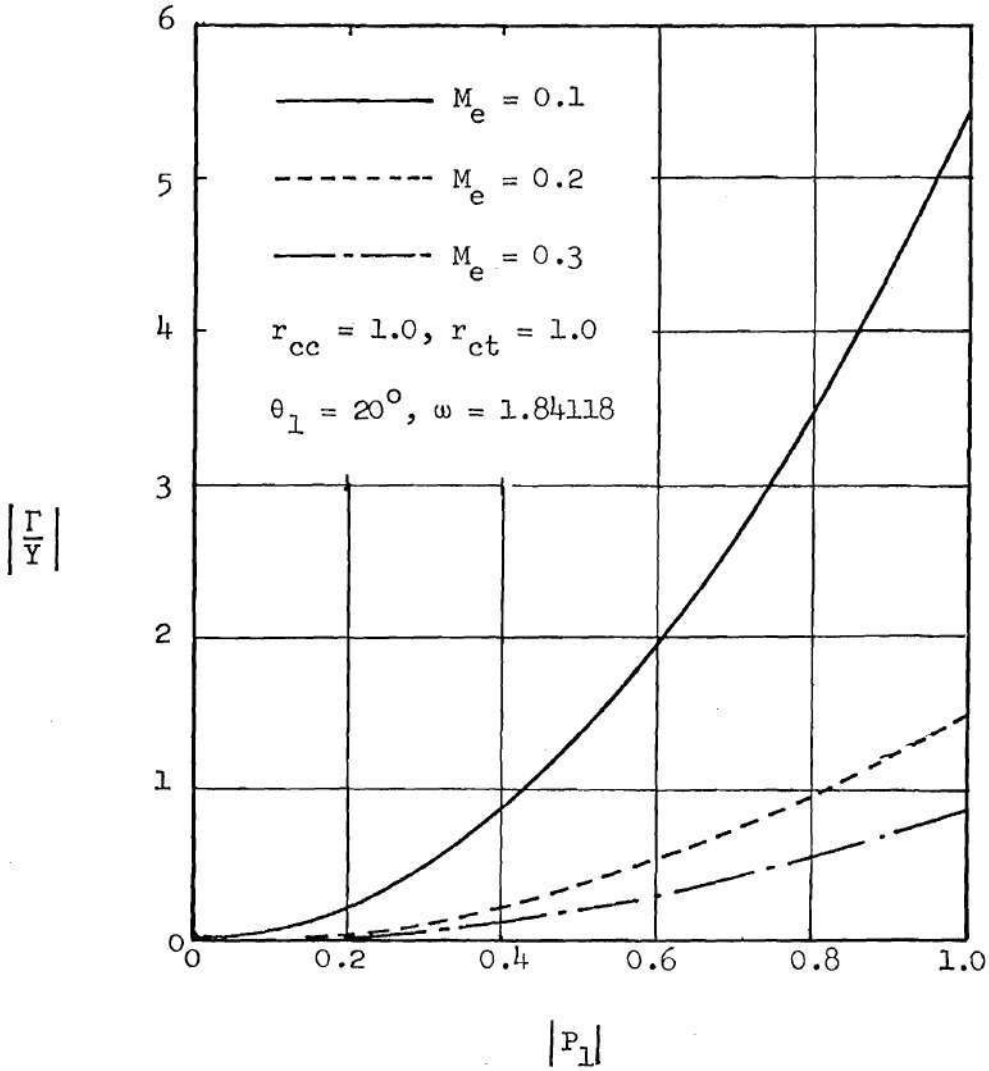

Figure 12. Effect of Entrance Mach Number on the Relative Magnitudes of Linear and Nonlinear Admittances for 2T Mode.

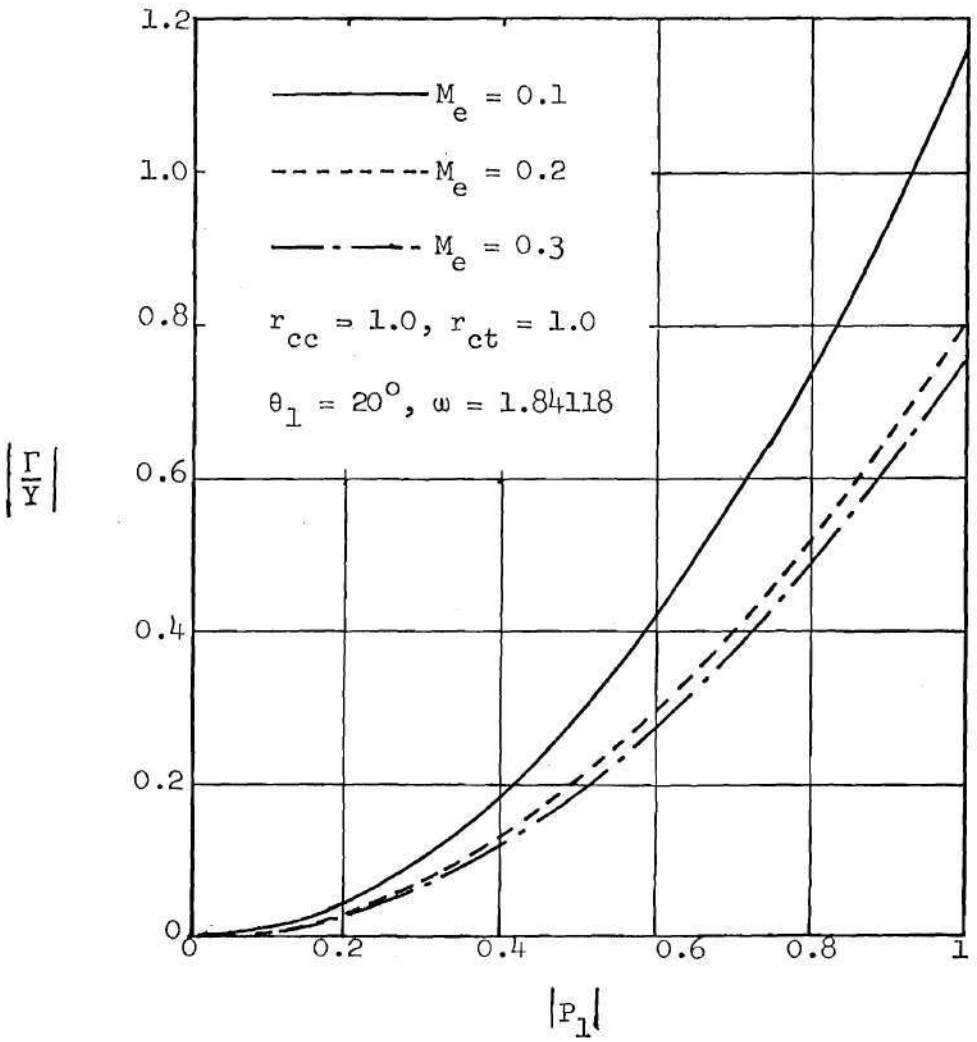

Figure 13. Effect of Entrance Mach Number on the Relative Magnitudes of Linear and Nonlinear Admittances for 1R Mode.

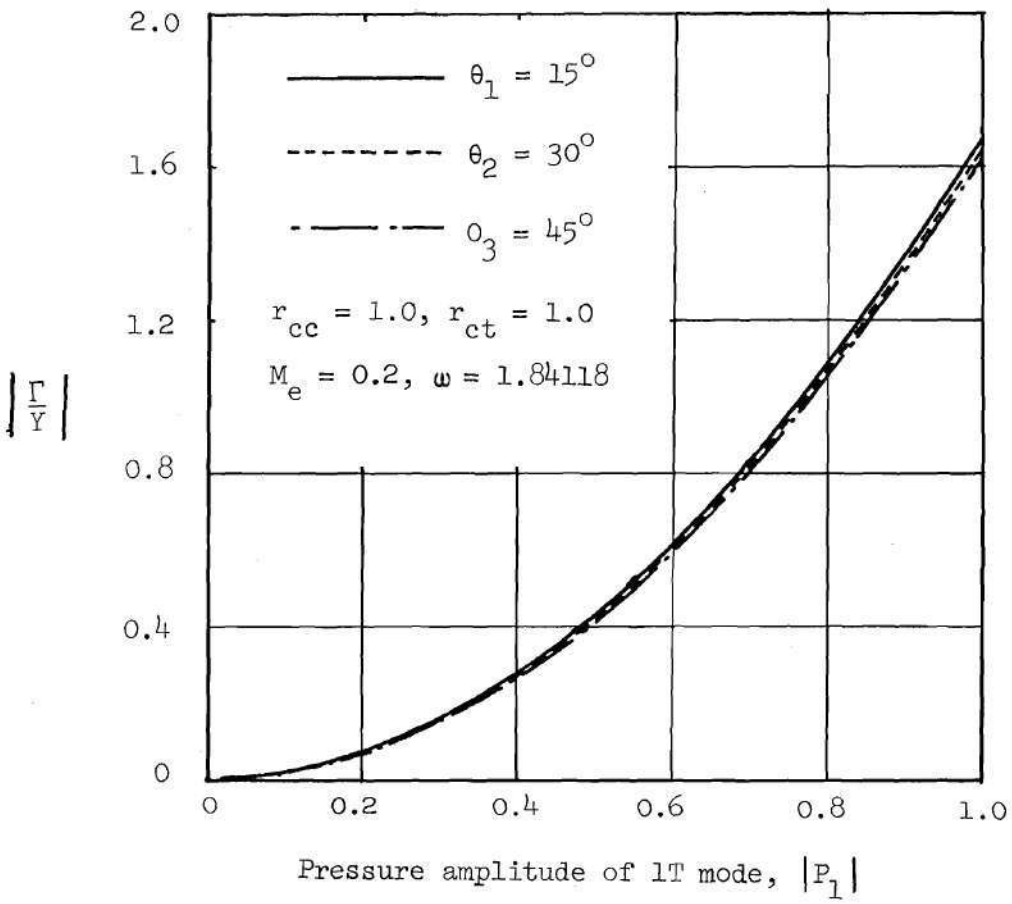

Figure 14. Effect of Nozzle Half-angle on the Relative Magnitudes of Linear and Nonlinear Admittances for the 2T Mode.

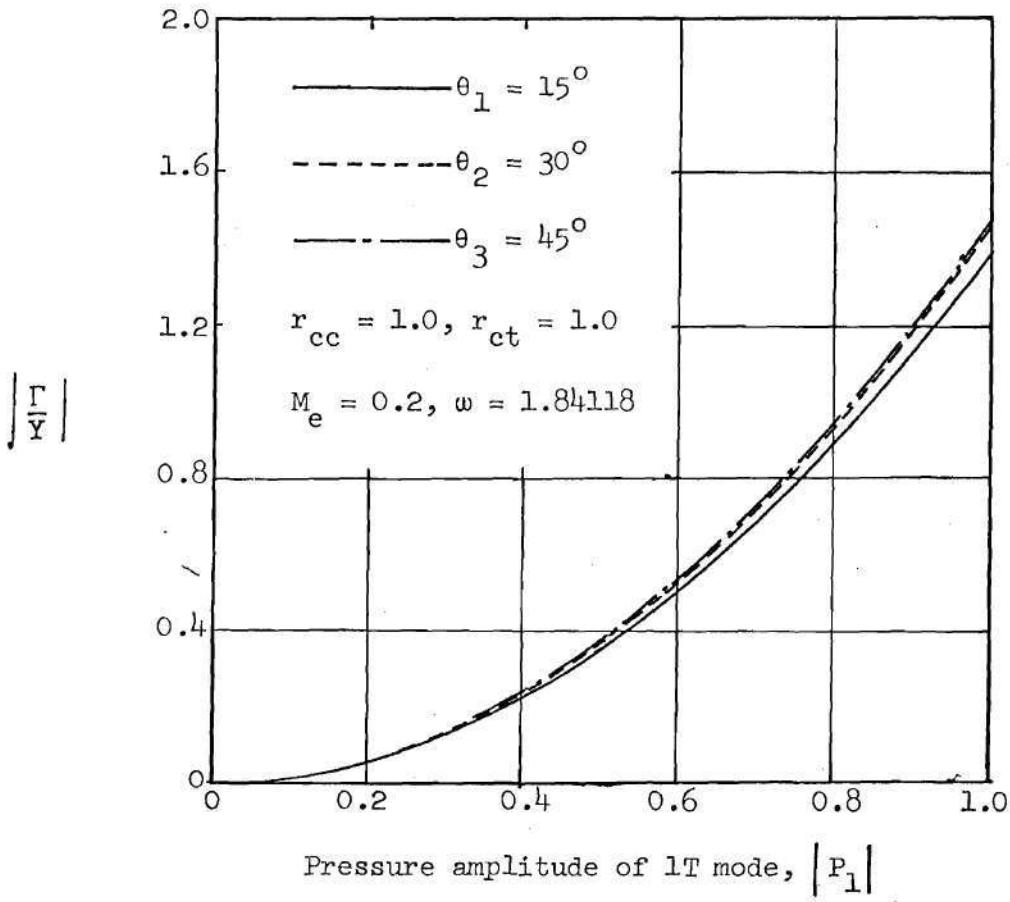

Figure 15. Effect of Nozzle Half-angle on the Relative Magnitudes of Linear and Nonlinear Admittances for the 1R Mode.

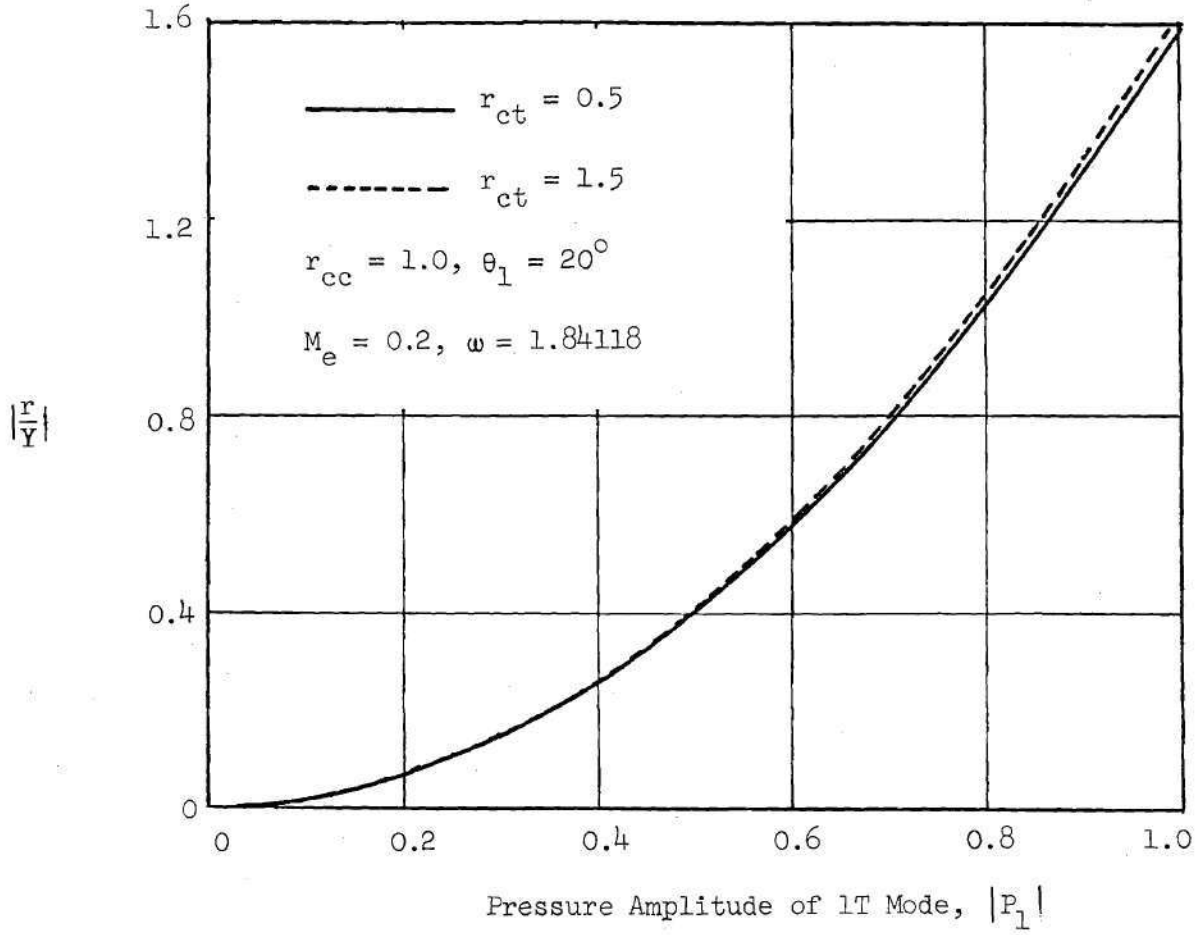

Figure 16. Effect of Radius of Curvature of the Nozzle at the Throat on the Relative Magnitudes of Linear and Nonlinear Admittances for the 2T Mode.

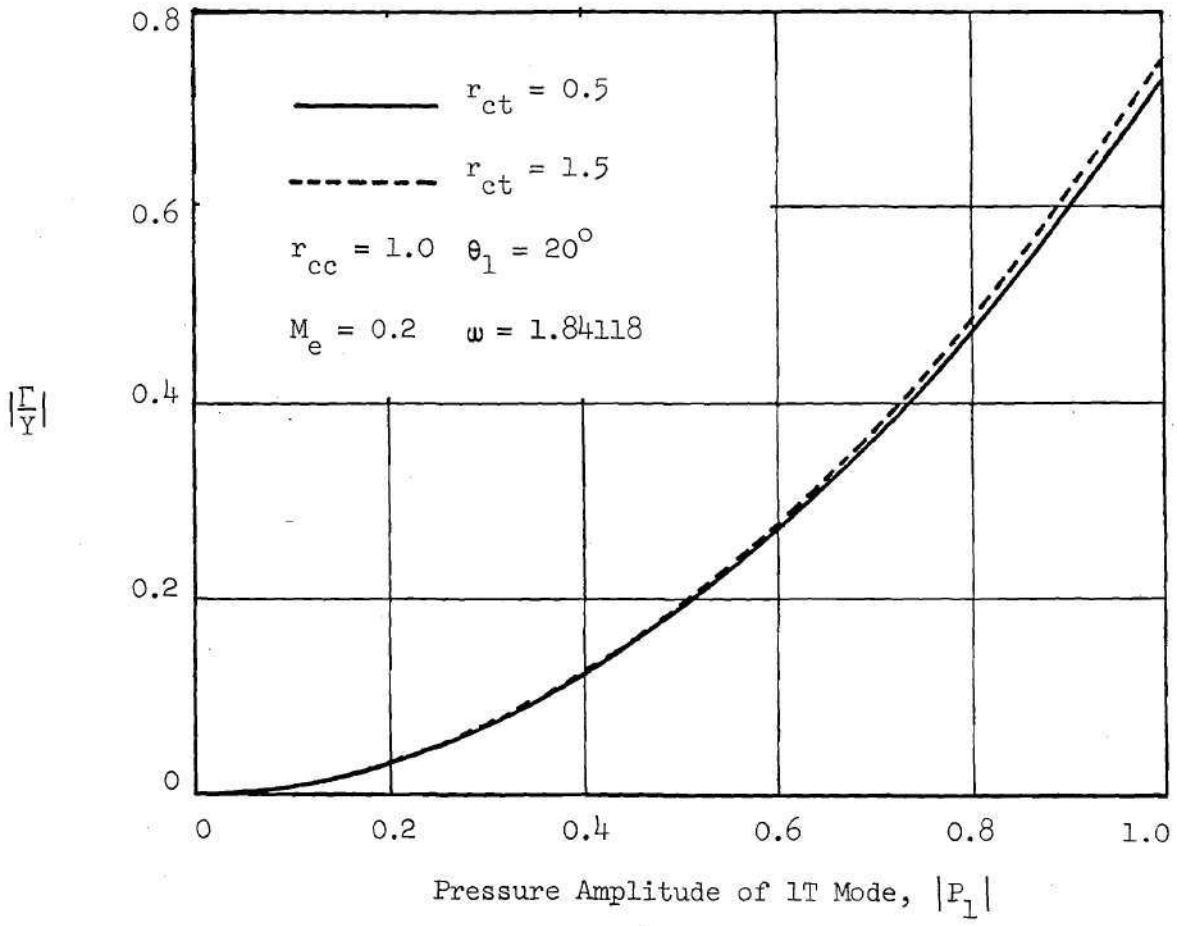

Figure 17. Effect of Radius of Curvature of the Nozzle at the Throat on the Relative Magnitudes of Linear and Nonlinear Admittances for the 1R Mode.

at the entrance section has considerable effect on the relative magnitudes of the linear and nonlinear admittances. This can be observed in Figures 18 and 19.

In summary, the results obtained in this study indicate that the magnitude of the nonlinear admittance coefficient is significantly large, especially at high pressure amplitudes. This points to a need for investigation of combustion instability in rocket motors with the inclusion of nozzle nonlinearities, in order to determine their effect on the instability.

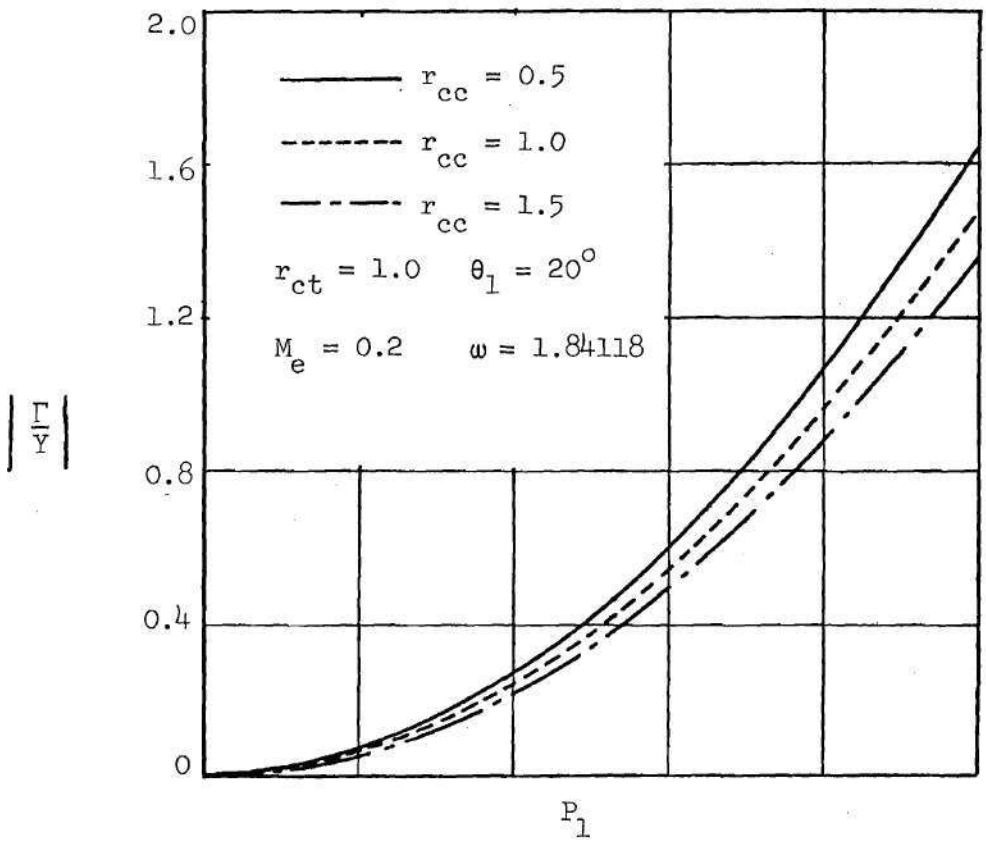

Figure 18. Effect of Radius of Curvature of the Nozzle at the Entrance on the Relative Magnitudes of Linear and Nonlinear Admittances for the 2T Mode.

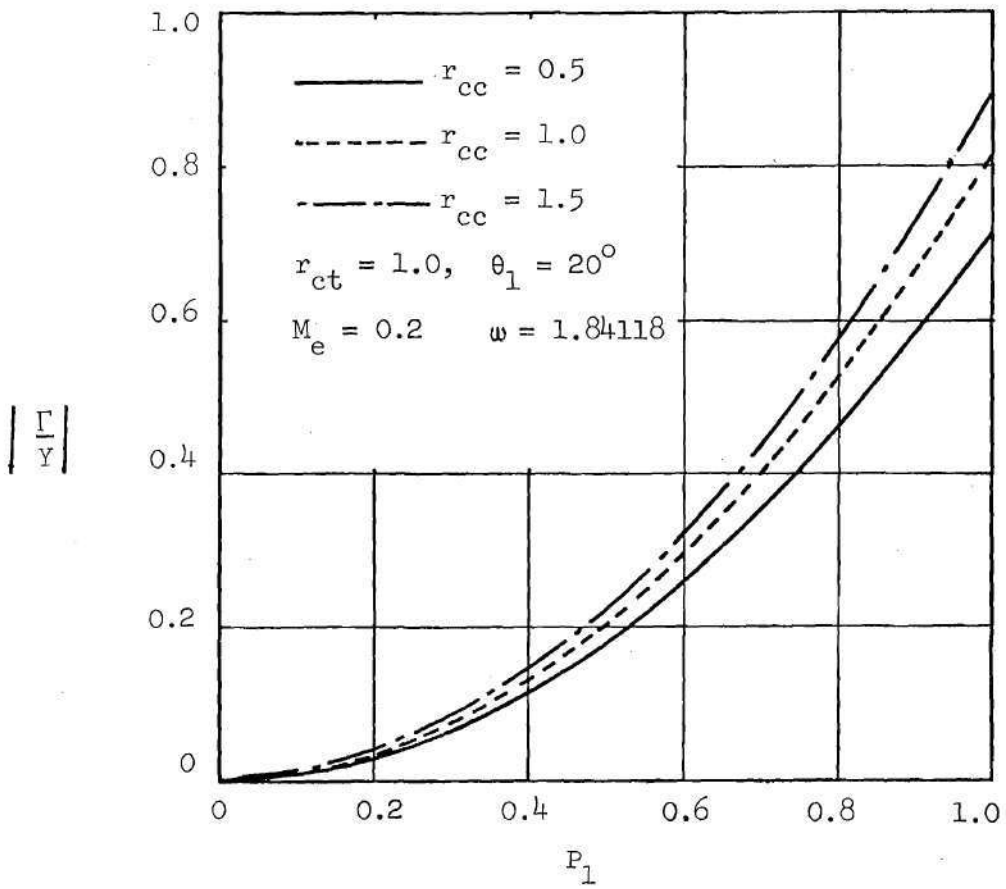

Figure 19. Effect of Radius of Curvature of the Nozzle at the Entrance on the Relative Magnitudes of Linear and Nonlinear Admittances for the 1R Mode.

CHAPTER IV

APPLICATION OF THE NOZZLE THEORY TO COMBUSTION INSTABILITY ANALYSIS

Introduction

This chapter describes the application of the nozzle theory developed in the preceding sections to the analysis of combustion instability in liquid propellant rocket motors. The rocket engine to be analyzed is described in Figure 1. The combustor is cylindrical with uniform injection of propellants at one end and a slowly converging nozzle at the other end. At the entrance to the nozzle, a nozzle admittance relation must be satisfied. As mentioned in Chapter I, previous combustion instability analysis[11] used a linear nozzle admittance relation. Now, the instability analysis will be carried out using the nonlinear nozzle admittance relation developed in Chapter II and the results thus obtained will be compared with those obtained using a linear nozzle admittance relation.

In the next section, a brief description of the analysis of oscillatory flow in the combustion chamber is presented. Since the present analysis is similar to the three-dimensional, second-order, potential theory developed by Powell and Zinn[11], the description given here is kept concise; details can be obtained from Reference 11. Furthermore, Reference 11 is followed closely in the initial part of this description, before the present modifications are incorporated.

Combustion Chamber Analysis

To keep the problem as simple as possible, yet still physically meaningful, the following assumptions are made. The gas phase in the combustor is assumed to consist of a single constituent which is thermally and calorically perfect. Transport phenomena, such as diffusion, viscosity, and heat conduction are neglected. It is assumed that the mean flow Mach number is small and that the waves have moderate amplitudes. The presence of burning propellant drops is represented by a distribution of unsteady mass sources[2].

Under these assumptions, one obtains the following nonlinear partial differential equation that describes the behavior of the velocity potential, Φ', of the combustor disturbance, correct to second order[11]:

$$\nabla^2\Phi' - \Phi'_{tt} = 2\bar{\underset{\rightarrow}{V}} \cdot \nabla\Phi'_t + \gamma(\nabla\cdot\bar{\underset{\rightarrow}{V}})\Phi'_t + 2\nabla\Phi \cdot \nabla\Phi'_t + (\gamma-1)\Phi'_t\nabla^2\Phi + W'_m \qquad (4\text{-}1)$$

The unsteady combustion process is represented by mass sources distributed throughout the volume of the chamber, and the response of the mass sources to pressure oscillations is assumed to be described by Crocco's pressure sensitive time lag hypothesis[2]. The mass source perturbation, W'_m, is then given by[9]

$$W'_m = -\gamma n \frac{d\bar{u}}{dz}\left[\Phi'_t(r, \theta, z, t) - \Phi'_t(r, \theta, z, t - \bar{\tau})\right] \qquad (4\text{-}2)$$

where n is the pressure "interaction index" that describes the sensitivity of the combustion process to pressure oscillations, and $\bar{\tau}$, commonly referred to as the sensitive time lag, is the part of the

total combustion time lag during which the combustion process is sensitive to pressure oscillations.

Substituting Eq. (4-2) into Eq. (4-1) and expressing the resulting equation in a cylindrical coordinate system yields the following wave equation:

$$E(\Phi') = \Phi_{rr} + \frac{1}{r}\Phi'_r + \frac{1}{r^2} + \Phi'_{zz} - \Phi'_{tt}$$

$$- 2\Phi'_r\Phi'_{rt} - \frac{2}{r^2}\Phi'_\theta\Phi'_{\theta t} - 2\Phi'_z\Phi'_{zt}$$

$$- (\gamma - 1)\,\Phi'_t\,(\Phi'_{rr} + \frac{1}{r}\Phi'_r + \frac{1}{r^2}\Phi'_{\theta\theta} + \Phi'_{zz})$$

$$- 2\bar{u}\Phi'_{zt} - \gamma\Phi'_t\frac{d\bar{u}}{dz}$$

$$+ \gamma n \frac{d\bar{u}}{dz}\left[\Phi'_t(r, \theta, z, t) - \Phi'_t(r, \theta, z, t - \bar{\tau})\right] = 0 \qquad (4\text{-}3)$$

In addition to satisfying Eq. (4-3), the desired solutions must satisfy rigid wall boundary conditions at the injector end of the chamber and at the chamber walls, while a nozzle admittance condition must be satisfied at the nozzle entrance. These boundary conditions are given (in a cylindrical coordinate system) by

$$\Phi'_r = 0 \text{ at } r = 1 \qquad (4\text{-}4)$$

$$\Phi'_z = 0 \text{ at } z = 0 \qquad (4\text{-}5)$$

While in previous combustion instability analysis[11], the nozzle boundary

condition that was used was

$$B(\Phi') \equiv \frac{\partial \Phi'_p}{\partial z} + \gamma Y \frac{\partial \Phi'_p}{\partial t} = 0 \tag{4-6}$$

in the present analysis, Eq. (2-36) is used as the nozzle boundary condition; that is, at $z = z_e$,

$$B(\Phi') \equiv \frac{\partial \Phi'_p}{\partial z} + \gamma Y_p \frac{\partial \Phi'_p}{\partial t} + \bar{u}\,\bar{c}^{-2}\,\Theta_p(\theta)\,\Psi_p(\psi)\,e^{iK_p\omega t}\,\Gamma_p = 0 \tag{4-7}$$

As in previous combustion instability analyses,[7,8,9,10,11] the Galerkin method is used in the solution of this nonlinear wave equation. This method has been introduced in Chapter II and the application here follows along similar lines.

As a first step in the application of the Galerkin method, the velocity potential, Φ', is expanded in terms of the natural acoustic modes of the chamber with unknown time-dependent amplitudes. Thus, the approximating series expansion $\tilde{\Phi}'$ is given by

$$\tilde{\Phi}' = \sum_{p=1}^{N} B_p(t)\,\Theta_p(\theta)\,R_p(r)\,Z_p(z) \tag{4-8}$$

where

$$\Theta_p(\theta) = \cos m\theta \tag{4-9}$$

$$R_p(r) = J_m(S_{mn}r) \tag{4-10}$$

$$Z_p(z) = \cosh\,(ib_p z) \tag{4-11}$$

Here, m and n are respectively the tangential and radial mode numbers, as in the nozzle analysis. For each value of the index p, there are corresponding mode numbers m and n. The complex constants b_p are the axial acoustic eigenvalues for a chamber with a solid wall boundary condition at the injector end and a linear nozzle admittance condition at the other end[11]. Each term in the above expansion exactly satisfies the boundary conditions given by Eqs. (4-4) and (4-5). The functions $B_p(t)$ are the unknown time-dependent amplitudes that will be determined by the application of the Galerkin orthogonality condition.

The approximating series expansion for Φ', given above, is similar to the approximating series expansion used in the nozzle analysis but there is one important difference. While in the nozzle analysis the unknown amplitudes are functions of the axial variable φ, the unknown amplitudes in the combustor analysis are functions of time. The primary objective in combustor stability analysis is to predict the growth of a disturbance with time starting at time t = 0; hence the time-dependence of Φ' is left to be determined from the solution. The simple geometry of the combustor enables one to form a good approximation for the spatial dependence of Φ' in the combustor, by expanding in terms of the natural acoustic modes. On the other hand, for a nozzle with an arbitrary converging geometry, the axial dependence of Φ' cannot be easily described. Hence, the time dependence of the solution is assumed to be sinusoidal, which is the case under limit-cycle conditions, and the Galerkin method is employed to determine the axial variation of the various terms in the series solution.

To determine $B_p(t)$, the assumed series expansion $\tilde{\Phi}'$ is substituted

into the wave equation, Eq. (4-3), to form the equation residual $E(\tilde{\Phi}')$. Similarly, the substitution of the series expansion into the nozzle boundary condition, Eq. (4-7) yields the boundary residual $B(\tilde{\Phi}')$. The residuals $E(\tilde{\Phi}')$ and $B(\tilde{\Phi}')$ are required to satisfy the Modified Galerkin Orthogonality Condition[9],

$$\int_0^{z_e}\int_0^{2\pi}\int_0^{1} E(\tilde{\Phi}')\, Z^*_j(z)\, \Theta_j(\theta)\, R_j(r)\, r\,dr\,d\theta\,dz$$

$$-\int_0^{2\pi}\int_0^{1} B(\tilde{\Phi}')\, Z^*_j(z_e)\, \Theta_j(\theta)\, R_j(r)\, r\,dr\,d\theta = 0$$

$$j = 1, 2, \ldots N \qquad (4\text{-}12)$$

Evaluating the spatial integrals in Eq. (4-12) yields the following system of N complex ordinary differential equations to be solved for the unknown complex amplitude functions, $B_p(t)$:

$$\sum_{p=1}^{N} \left\{ C_0(j,p) \frac{d^2B_p}{dt^2} + C_1(j,p)B_p(t) + \left[C_2(j,p) - nC_3(j,p) \right] \frac{dB_p}{dt} \right.$$

$$\left. + nC_3(j,p) \frac{d[B_p(t-\bar{\tau})]}{dt} + C_4(j,p)\, e^{iK_p\omega t} \right\}$$

$$+ \sum_{p=1}^{N}\sum_{q=1}^{N} \left\{ D_1(j,p,q)\, B_p \frac{dB_q}{dt} + D_2(j,p,q)\, B_p \frac{dB^*_q}{dt} \right.$$

$$\left. + D_3(k,p,q)\, B^*_p \frac{dB_q}{dt} + D_4(j,p,q)\, B^*_p \frac{dB^*_q}{dt} \right\} = 0$$

$$j = 1, 2, \ldots N \qquad (4\text{-}13)$$

Equation (4-13) is the same as Eq. (12) of Reference 11 except for the additional term $C_4(j,p)\, e^{iK_p \omega t}$. This term arises from the presence of nozzle nonlinearities: Use of Eq. (4-6) as the nozzle boundary condition results in an equation without this additional term and the resulting equation is the same as Eq. (12) of Reference 11. The coefficient $C_4(j,p)$ is given by

$$C_4(j,p) = \bar{u}_e\, \bar{c}_e^{\,2}\, \Gamma_p\, Z^*_j(z_e) \int_0^{2\pi} \Theta_p(\theta)\, \Theta_j(\theta)\, d\theta \int_0^1 R_p(r)\, R_j(r)\, dr \qquad (4\text{-}14)$$

where $\bar{u}_e$ and $\bar{c}_e$ are respectively the steady-state velocity and speed of sound at the nozzle entrance. The other coefficients appearing in Eq. (4-13) are the same as those in Reference 11 and details of these can be found there. All of these coefficients are determined by evaluating the various integrals of hyperbolic, trigonometric, and Bessel functions that arise from the spatial integrations indicated in the Galerkin orthogonality conditions.

The time-dependent behavior of an engine following the introduction of a disturbance is determined by specifying the form of the initial disturbance and then following the subsequent behavior of the individual modes by numerically integrating Eq. (4-13). Once the time-dependence of the individual modes is known, the velocity potential, $\tilde{\Phi}'$, is calculated from Eq. (4-8). The pressure perturbation at any location within the chamber is related to $\tilde{\Phi}'$ by the following second-order momentum equation[17]:

$$p' = -\gamma\left[\tilde{\Phi}'_t + \bar{u}\,\tilde{\Phi}'_z + \tfrac{1}{2}\left(\tilde{\Phi}'^2_r + \frac{1}{r^2}\,\tilde{\Phi}'^2_\theta + \tilde{\Phi}'^2_z\right) - \tfrac{1}{2}\,\tilde{\Phi}'^2_t\right] \qquad (4\text{-}15)$$

Solution Procedure

Equation (4-13) is a system of N ordinary differential equations that can be solved for the N complex time-dependent functions, $B_p(t)$. Solution of this coupled system enables one to predict the growth of an initial disturbance, starting from time t = 0. A fourth-order Runge-Kutta scheme[11] is employed for the numerical integration of this system of equations. In the present calculations a three-mode series expansion consisting of the first tangential, second tangential and first radial modes is used. To start the numerical integration of the system of equations given by Eq. (4-13), it is necessary to specify the nature of the initial disturbance: that is, the amplitudes $B_p(t)$ at time t = 0. Initial values of the amplitude of each mode can be independently specified. In the numerical computations that have been performed, the initial disturbance is assumed to be in the 1T mode only and is assumed to be sinusoidal in time.

It is obvious that the oscillatory flows in the combustor and nozzle are mutually dependent on each other and must be treated as such. This mutual dependence is evident in the solution procedure: the combustion chamber analysis requires the knowledge of nozzle admittances but these nozzle admittances are functions of the frequency of the oscillation and pressure amplitude, which can be obtained only after the combustion chamber analysis has been performed.

Since the frequency of oscillation and amplitudes of the various modes in the combustor, upon which the nonlinear nozzle admittances depend, are not known a priori, an iterative solution technique is used. In this procedure, the linear nozzle admittances for each of the combustor modes for the nozzle under consideration are first calculated. Next, the combustion chamber analysis is carried out using these linear nozzle admittances and the limit-cycle frequency and pressure amplitude of the 1T mode at the nozzle entrance are determined. This information is then used in the nozzle analysis to determine the nonlinear nozzle admittances (Γ_p, $p = 2, 3$) which are then used in the chamber analysis to calculate new limit-cycle frequencies and limit-cycle pressure amplitude. If the limit-cycle amplitude obtained with the nonlinear nozzle boundary condition is significantly different from the limit-cycle amplitude obtained with the linear nozzle admittances, new values of the non-linear admittances are calculated and the process is repeated until the change in limit-cycle amplitude is sufficiently small.

In addition to the nozzle admittance values, the following parameters are necessary inputs to the combustion chamber analysis: (1) the time lag, $\bar{\tau}$, (2) the interaction index, n, (3) the steady state Mach number at the nozzle entrance, M_e, and (4) the chamber length-to-diameter ratio, L/D. For a given combustor-nozzle configuration (i.e., given M_e and L/D), the combination of n and $\bar{\tau}$ determines whether or not the engine is linearly stable. To attain the limit cycles, it is necessary to operate the engine in the linearly unstable range of n and $\bar{\tau}$; operation in the linearly stable range results in the damping out of any disturbance. Hence it is necessary to calculate the linear

stability characteristics of the combustion chamber under consideration. The linear stability analysis that was developed in Reference 11 is used for these calculations and to obtain the neutral stability curve. A typical neutral stability curve is shown in Figure 20. Similar curves are obtained for each motor.

Combustion instability calculations have been made for different values of the following parameters: (1) the time lag $\bar{\tau}$, (2) the interaction index, n, (3) the steady state Mach number at the nozzle entrance, M_e, and (4) the chamber length-to-diameter ratio, L/D. In each case, solutions have been obtained with and without the inclusion of nozzle nonlinearities. These results are presented and discussed in the next chapter.

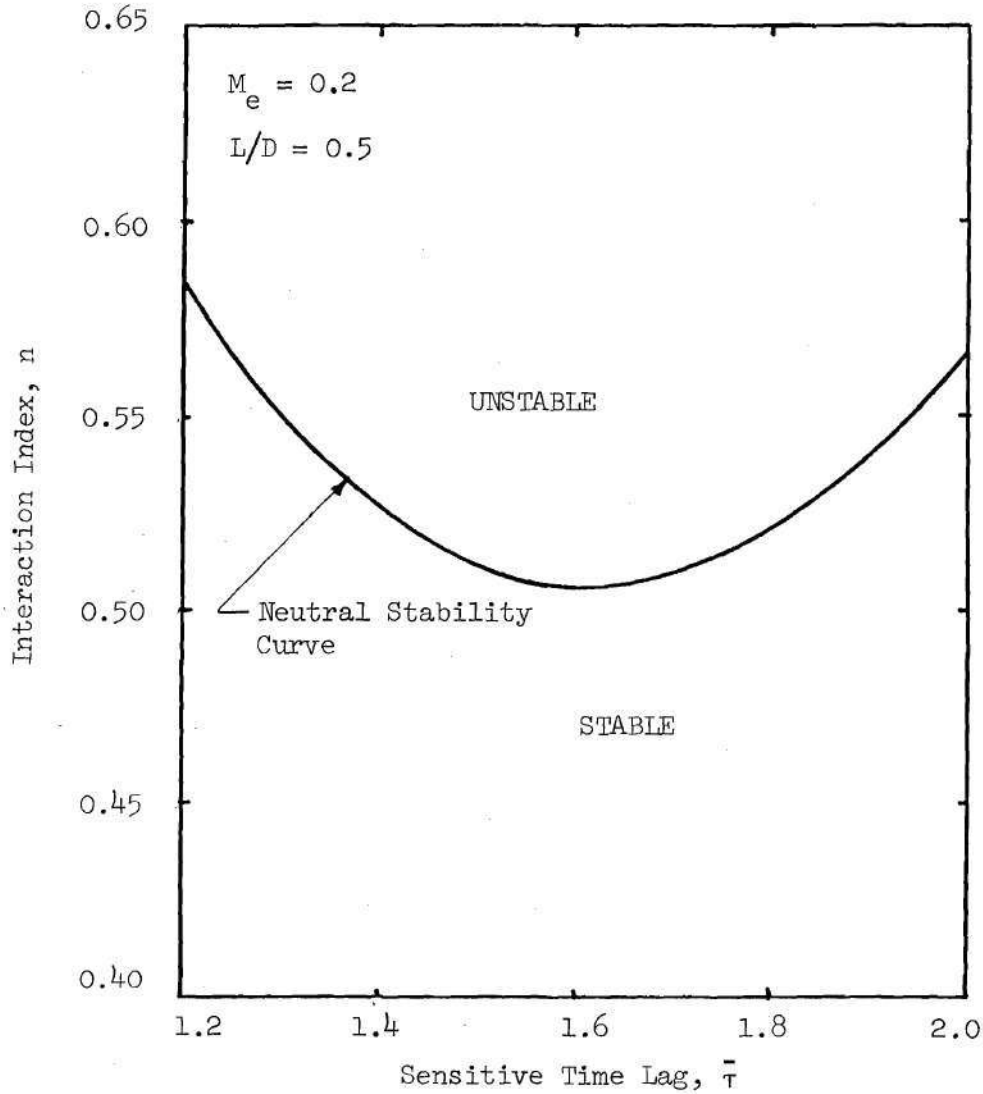

Figure 20. Linear Stability Limits

CHAPTER V

RESULTS AND DISCUSSION

All the combustors that have been analyzed are attached to nozzles with the following specifications: radius of nozzle at the combustion chamber, $r_{cc} = 1.0$; radius of nozzle at the throat, $r_{ct} = 1.0$; and nozzle half-angle, $\theta_1 = 20^{\circ}$. As shown in Chapter III, the nozzle parameters do not have a significant effect on the relative magnitudes of nonlinear and linear admittances. Since the main objective of this thesis is the determination of the effect of nozzle nonlinearities upon the behavior of unstable combustors, it is considered sufficient to examine combustors with this typical nozzle. A value of 1.2 is assumed for the specific heat ratio, γ.

Figure 21 shows the time history of the nozzle pressure peaks, with and without the inclusion of the nozzle nonlinearities. The exit Mach number of the combustor is 0.2 and length-to-diameter ratio is 0.5, with $n = 0.52$ and $\bar{\tau} = 1.6$. The indicated pressure peaks are zero-to-peak values. It is seen that the inclusion of nozzle nonlinearities has negligible effect on the development of pressure oscillations in the chamber. The limiting amplitudes are also observed to be almost exactly the same. This fact is further illustrated in Figures 22 to 28. Also, the frequency of oscillations are seen to remain unchanged. The wave forms are nearly sinusoidal, indicating a very weak effect of the flow nonlinearities. Corresponding to a $\bar{\tau}$ value of 1.6, the value

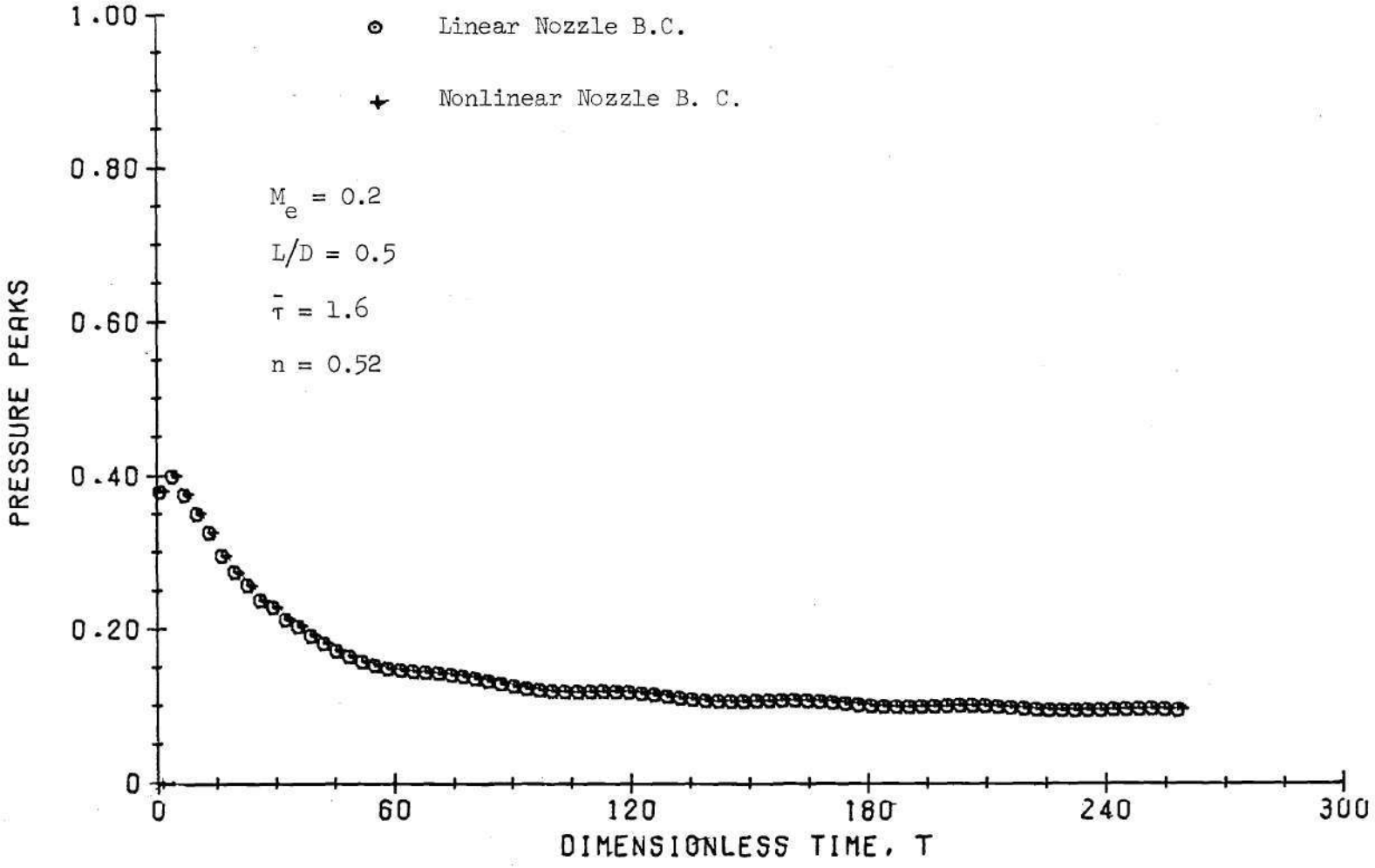

Figure 21. Time History of the Pressure Peaks at the Nozzle Entrance for a Mildly Unstable Motor

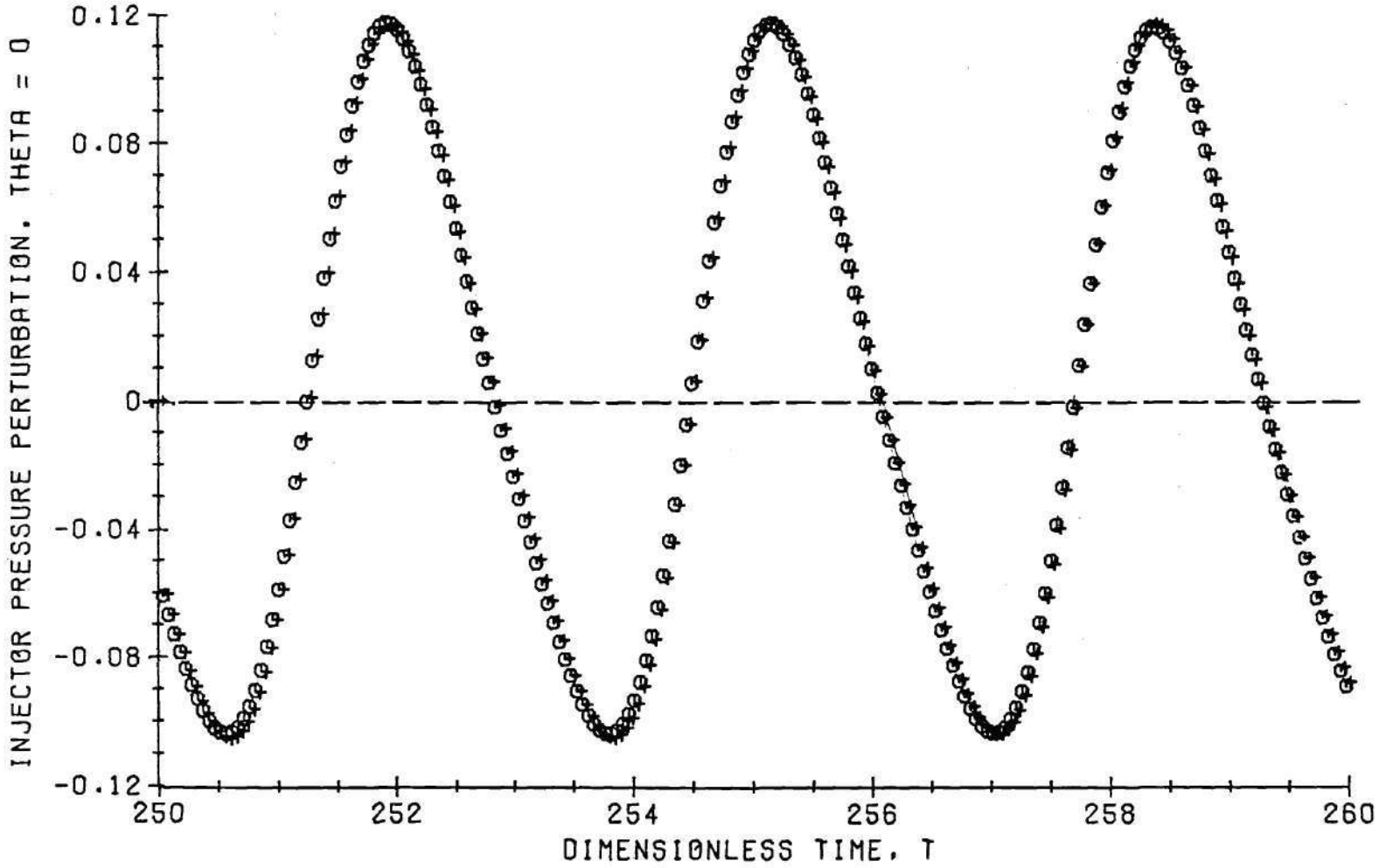

Figure 22. Limiting Injector Pressure Wave Forms at $\theta = 0$ for a Mildly Unstable Motor ($M_e = 0.2$, $L/D = 0.5$, $\bar{\tau} = 1.6$, $n = 0.52$).

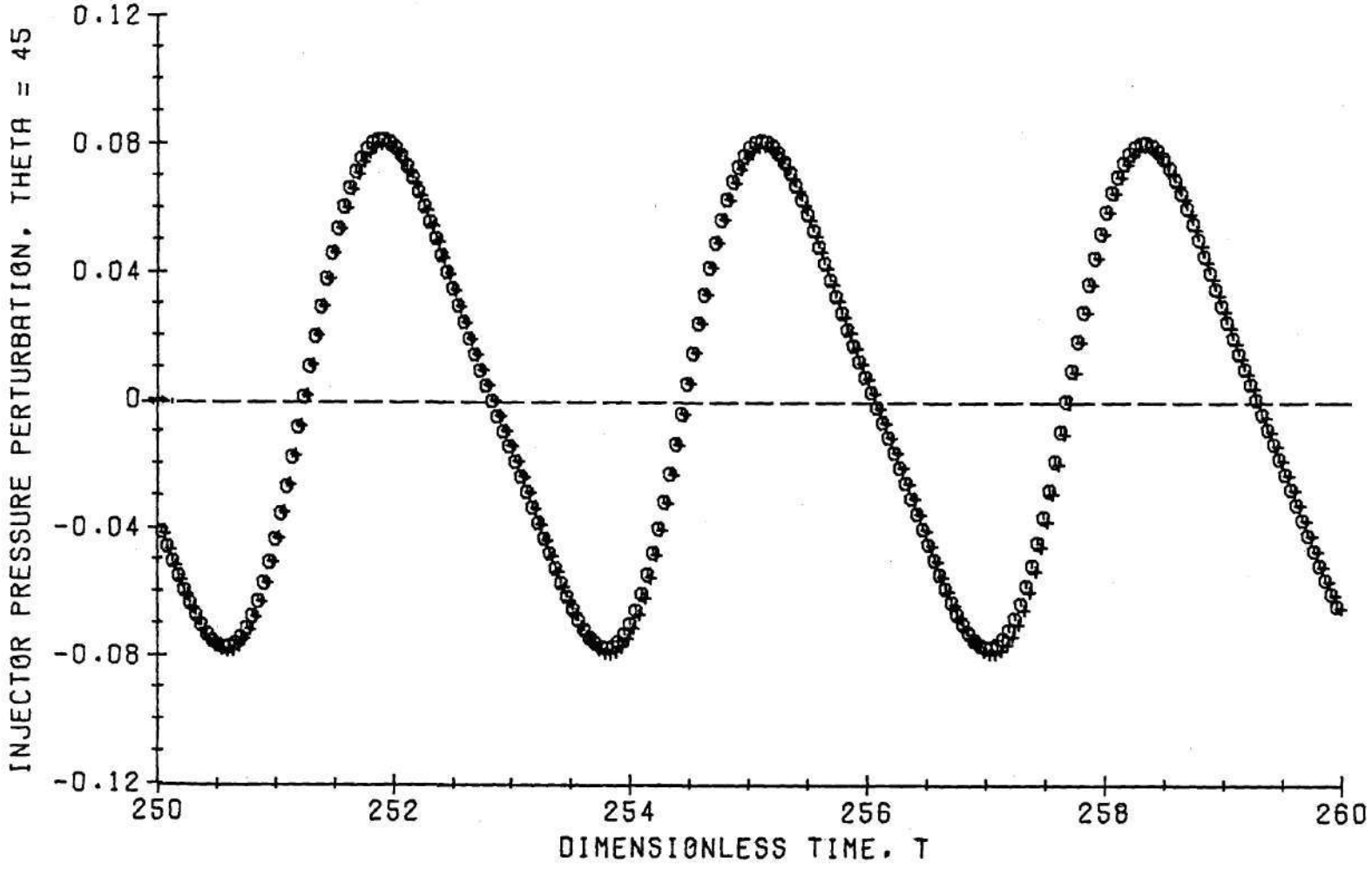

Figure 23. Limiting Injector Pressure Wave Forms at $\theta = 45^{\circ}$ for a Mildly Unstable Motor ($M_e = 0.2$, $L/D = 0.5$, $\bar{\tau} = 1.6$, $n = 0.52$).

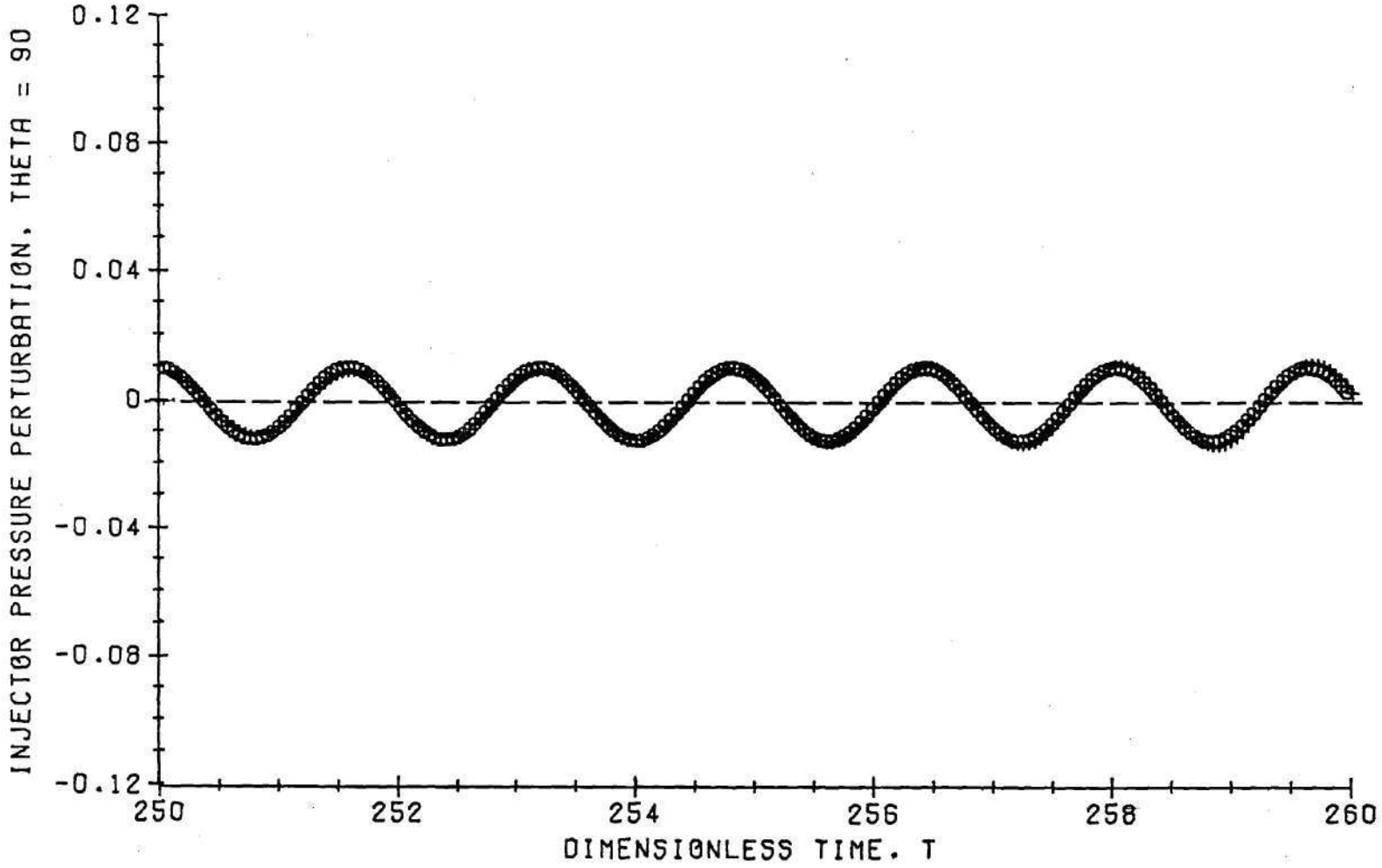

Figure 24. Limiting Injector Pressure Wave Forms at $\theta = 90^{\circ}$ for a Mildly Unstable Motor ($M_e = 0.2$, $L/D = 0.5$, $\bar{\tau} = 1.6$, $n = 0.52$).

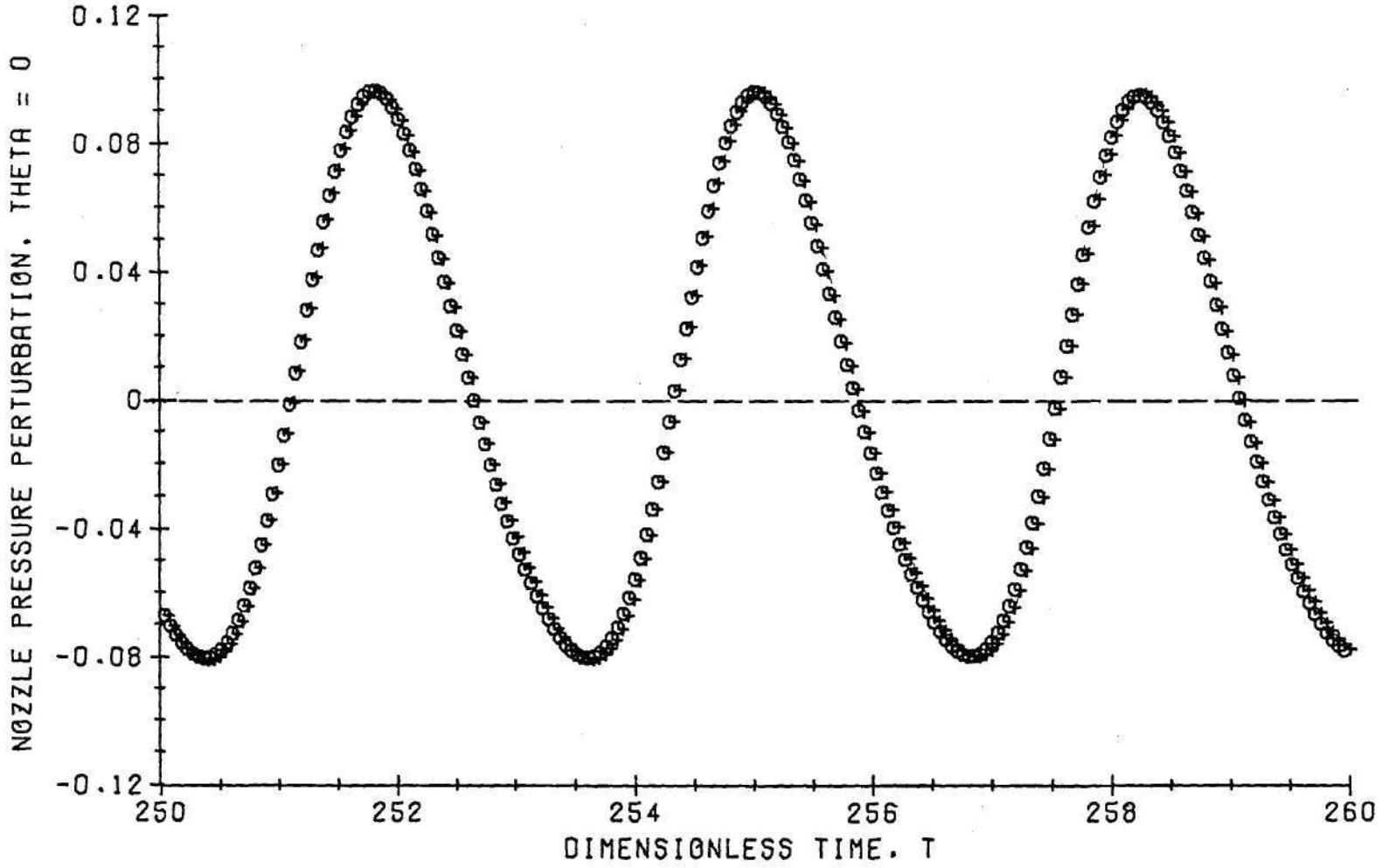

Figure 25. Limiting Pressure Wave Forms at the Nozzle Entrance for a Mildly Unstable Motor (M_e = 0.2, L/D = 0.5, $\bar{\tau}$ = 1.6, n = 0.52).

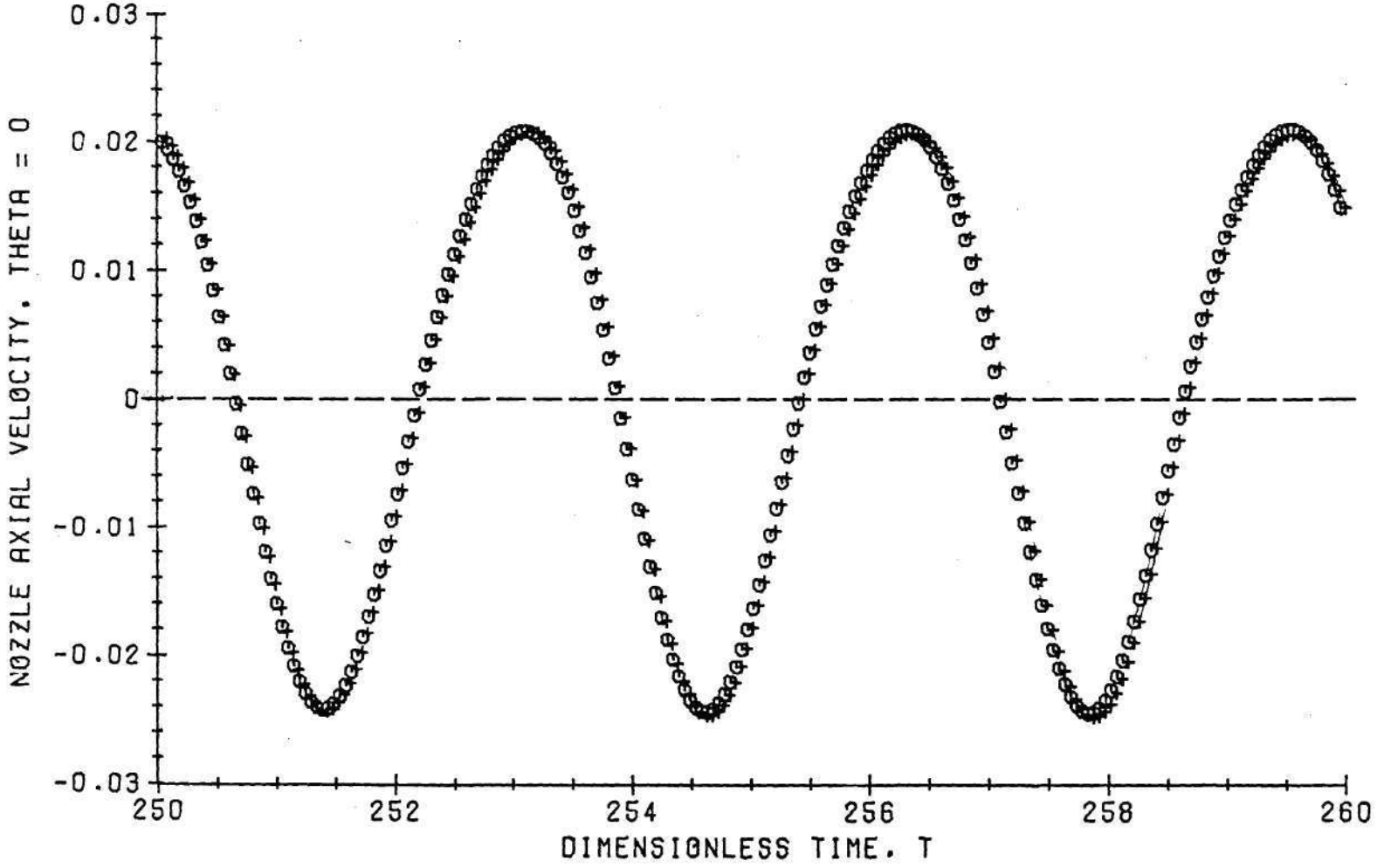

Figure 26. Limiting Axial Velocity Wave Forms at the Nozzle Entrance for a Mildly Unstable Motor (M_e = 0.2, L/D = 0.5, $\bar{\tau}$ = 1.6, n = 0.52).

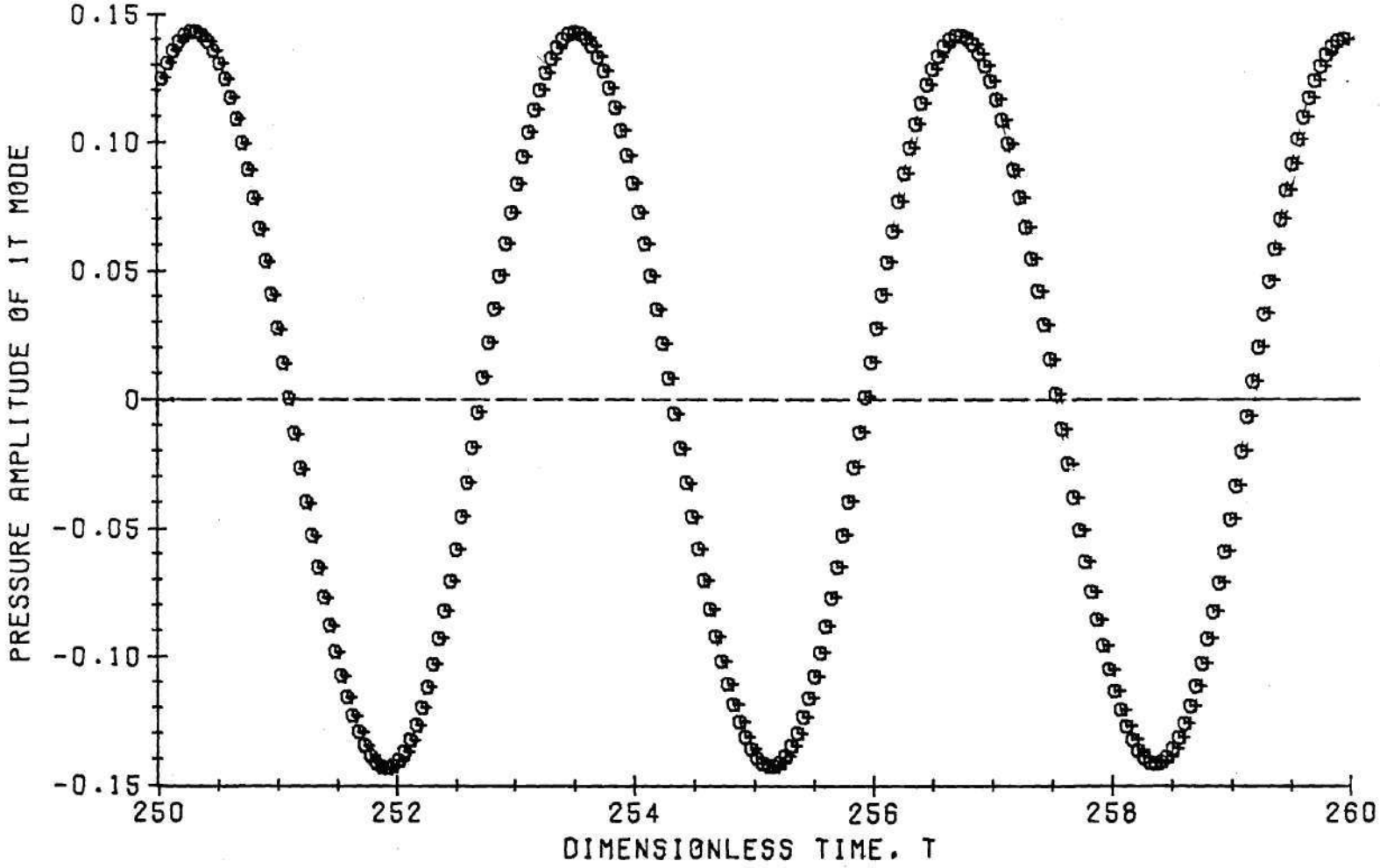

Figure 27. Limiting Pressure Amplitude Wave Forms for a Mildly Unstable Motor (M_e = 0.2, L/D = 0.5, $\bar{\tau}$ = 1.6, n = 0.52).

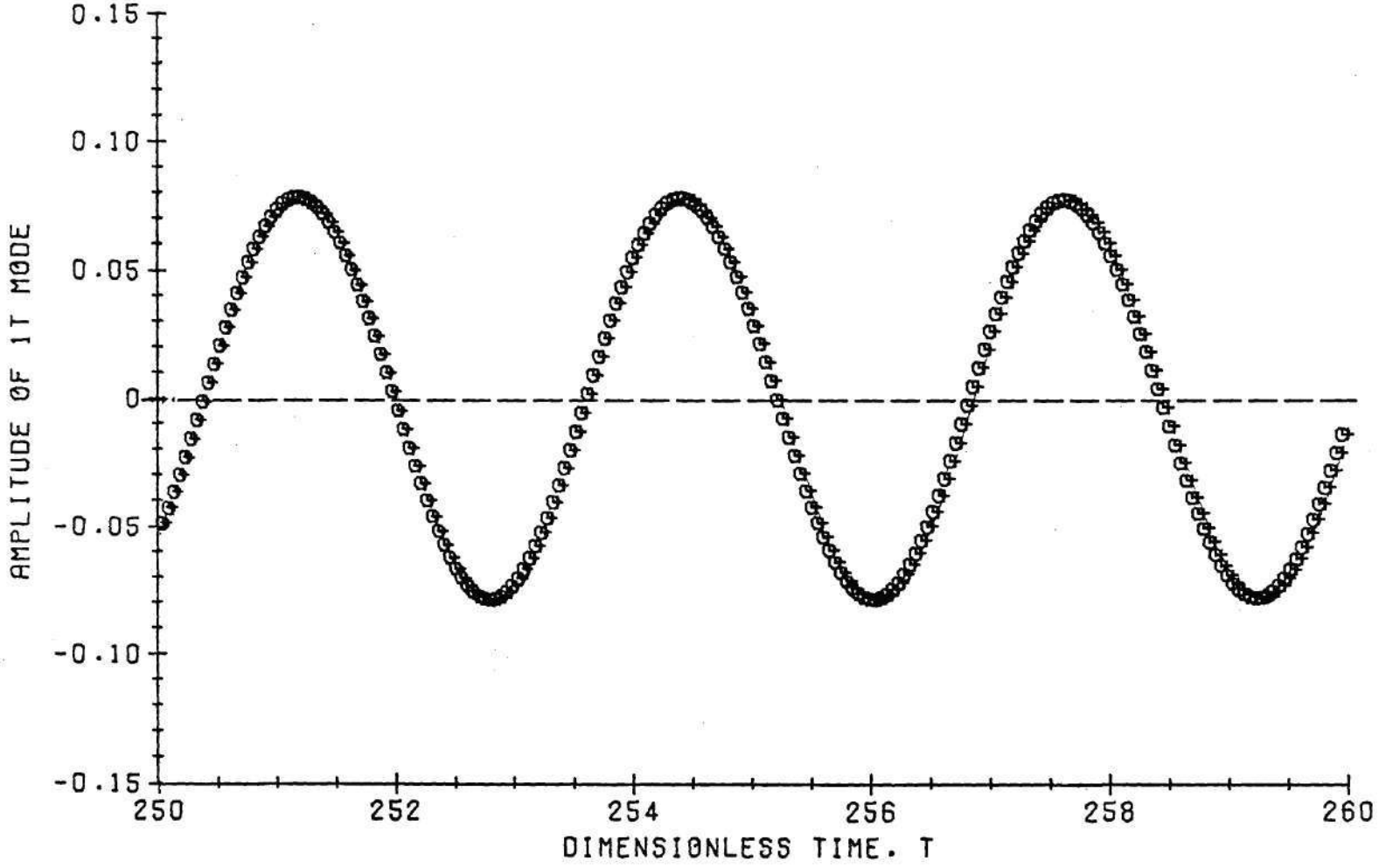

Figure 28. Limiting 1T Mode Amplitude Wave Forms for a Mildly Unstable Motor (M_e = 0.2, L/D = 0.5, $\bar{\tau}$ = 1.6, n = 0.52).

of interaction index for neutral stability is 0.50694. For the motor analyzed, n is 0.52, which is only slightly higher than the neutral stability value. Hence this combination of n and $\bar{\tau}$ results in only a slightly unstable motor. Consequently, the amplitude of the resulting pressure oscillations is rather low.

Figure 29 shows the time history of pressure peaks at the nozzle entrance for a highly unstable motor. Chamber exit Mach number, chamber length-to-diameter ratio and $\bar{\tau}$ are all the same as for the previous case but the interaction index, n = 0.7 resulting in a highly unstable motor. While the inclusion of the nozzle nonlinearities leads to a slightly different growth history of the pressure oscillation, there is very little difference in the limiting amplitude values. Figures 30 to 36 show the limiting wave forms of the injector and nozzle pressures. Inclusion of nozzle nonlinearities introduces a slight shift in phase but there is negligible change in peak-to-peak amplitude values. The limiting pressure wave forms are no longer sinusoidal. In contrast to the previous case, the distortion of the sinusoidal waveforms is a consequence of the strong mode coupling. Large values of limiting pressure amplitudes are attained and there is pronounced effect of flow nonlinearities. Still, the nozzle nonlinearities are seen to exert no significant effects.

In Figure 37, comparison of limit-cycle injector pressure perturbations are made for a few more values of the interaction index, with the other parameters being the same. As before, the use of a nonlinear nozzle admittance relation has no significant effect on the limiting injector pressure amplitude. The nozzle nonlinearities have

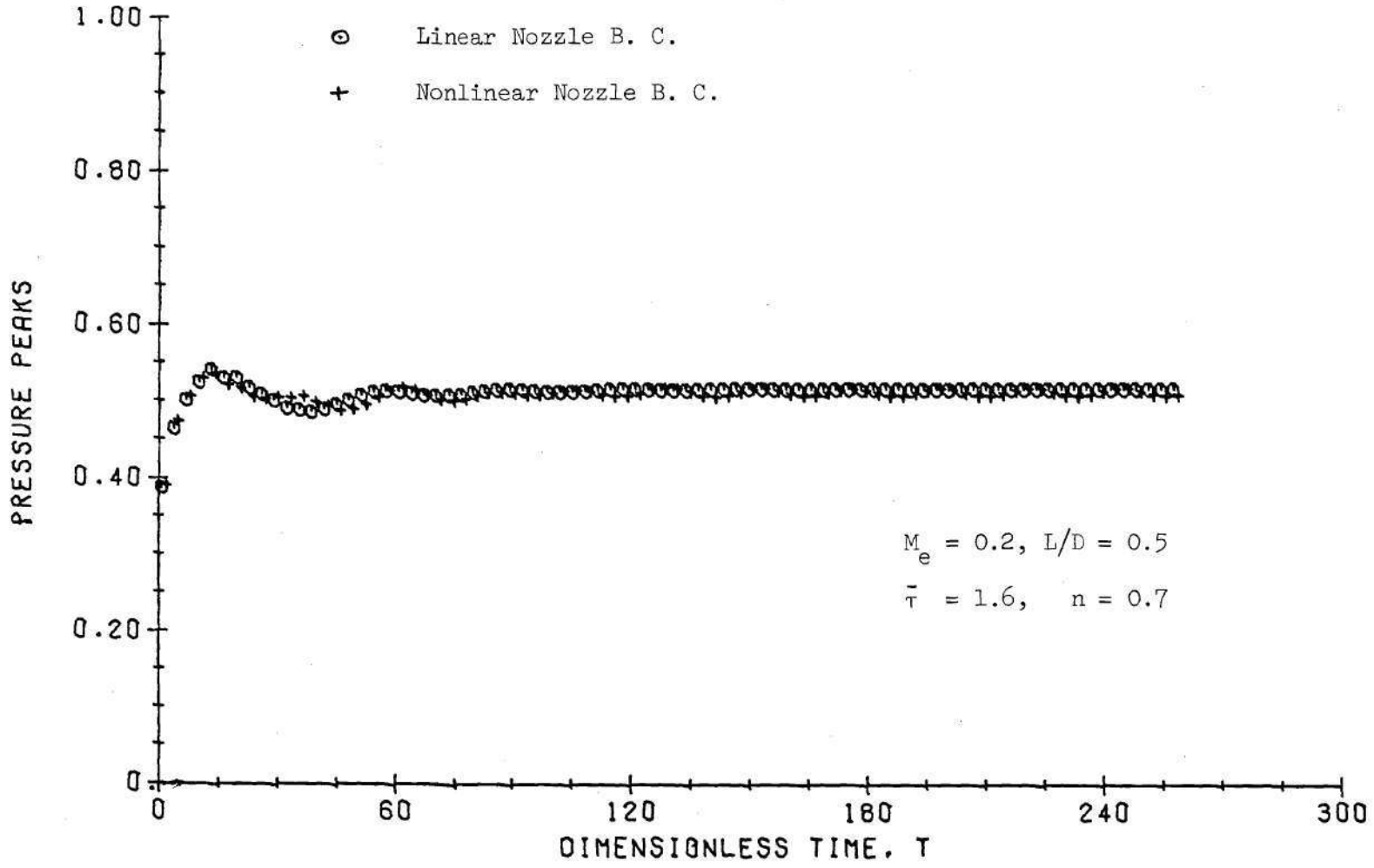

Figure 29. Time History of the Pressure Peaks at Nozzle Entrance for a Strongly Unstable Motor

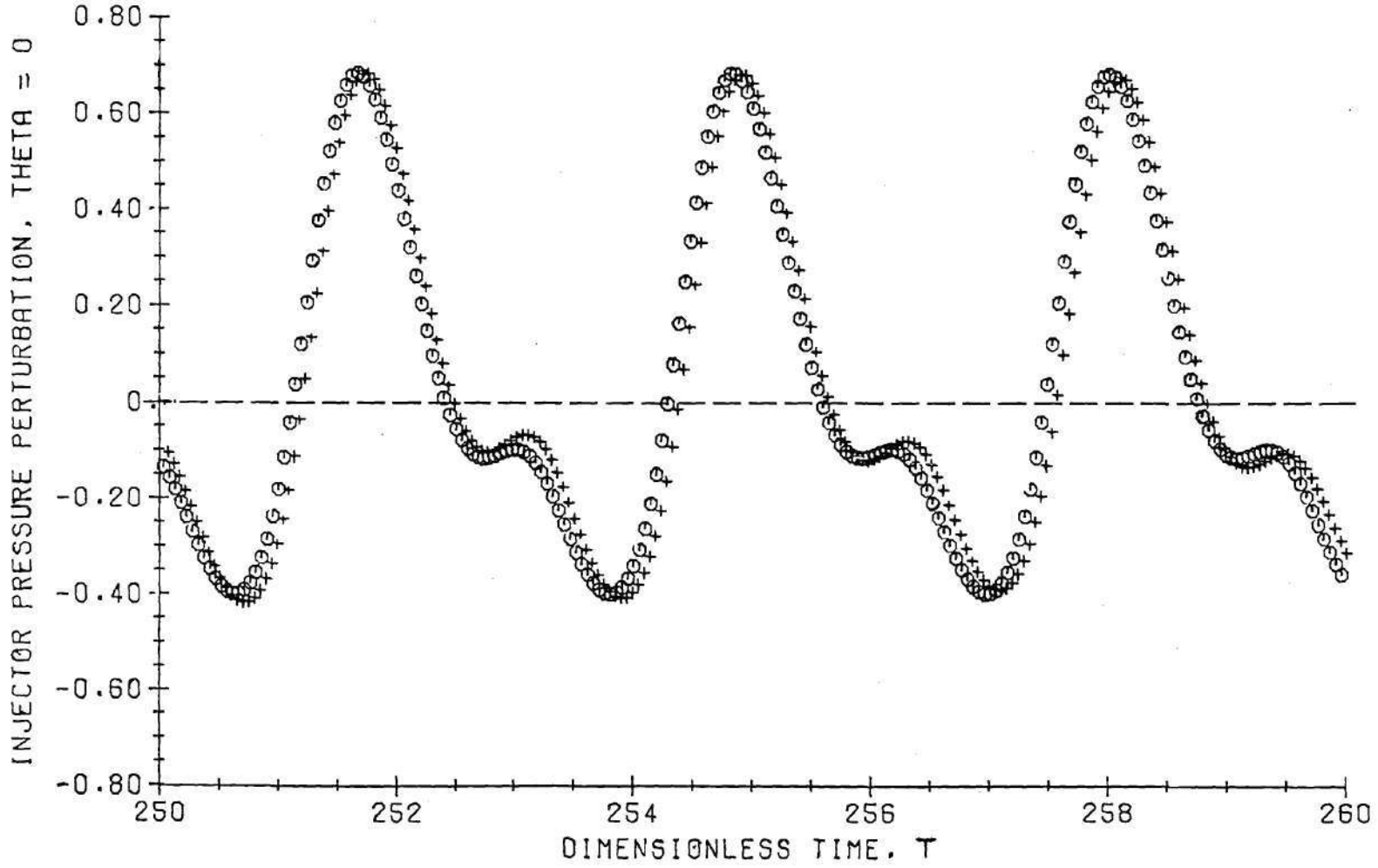

Figure 30. Limiting Injector Pressure Wave Forms at $\theta = 0^{\circ}$ for a Strongly Unstable Motor ($M_e = 0.2$, $L/D = 0.5$, $\bar{\tau} = 1.6$, $n = 0.7$).

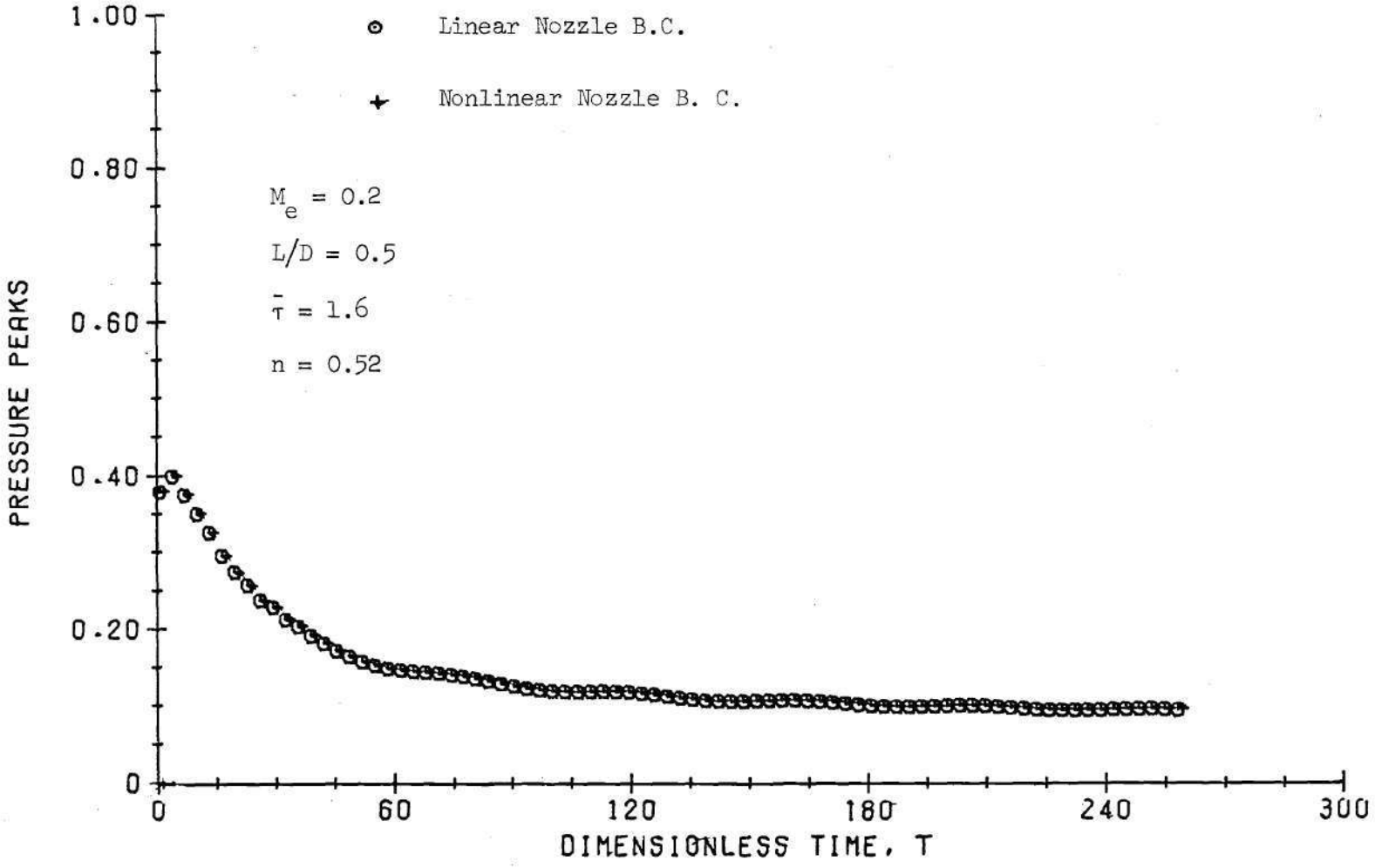

Figure 21. Time History of the Pressure Peaks at the Nozzle Entrance for a Mildly Unstable Motor

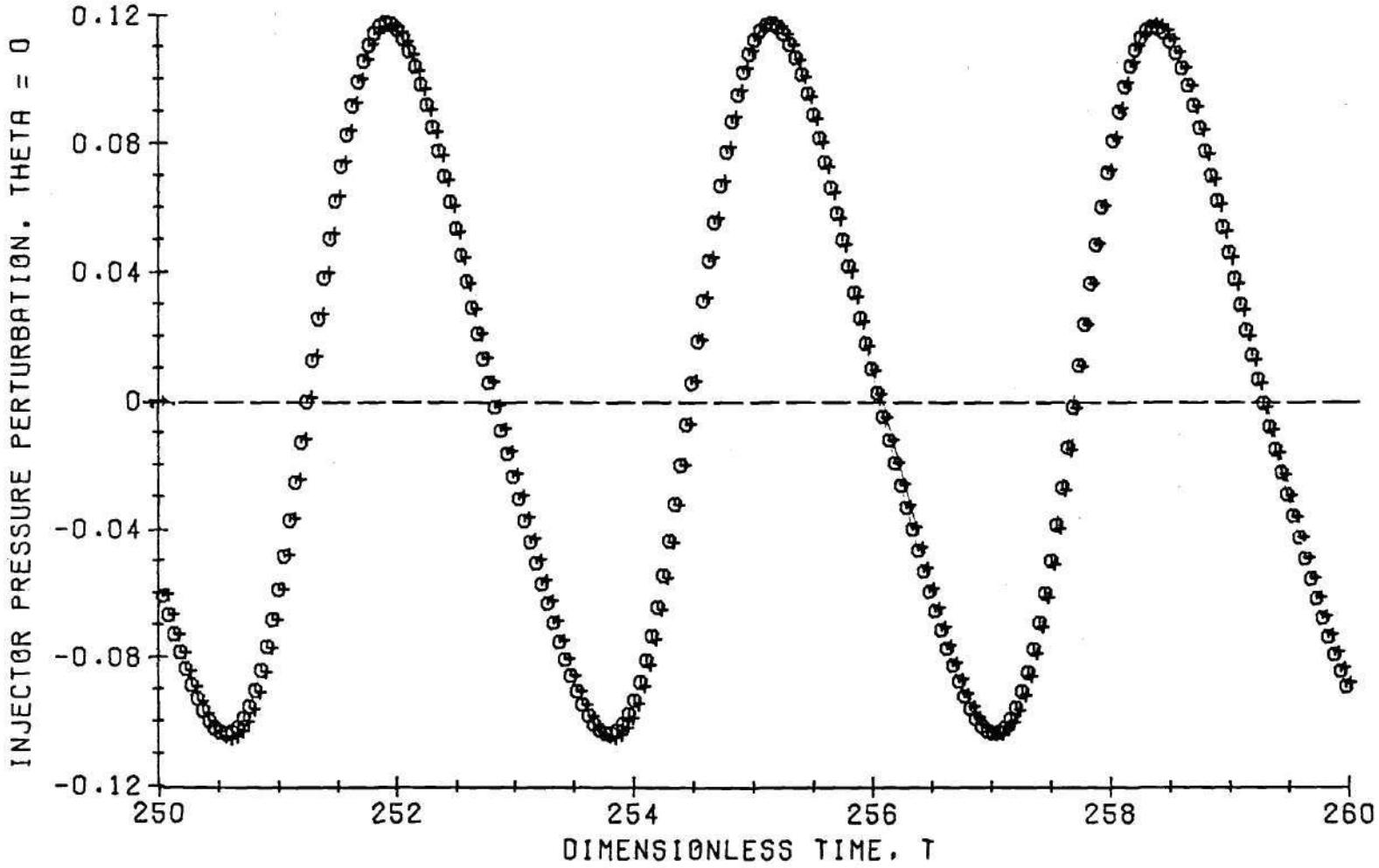

Figure 22. Limiting Injector Pressure Wave Forms at $\theta = 0$ for a Mildly Unstable Motor ($M_e = 0.2$, $L/D = 0.5$, $\bar{\tau} = 1.6$, $n = 0.52$).

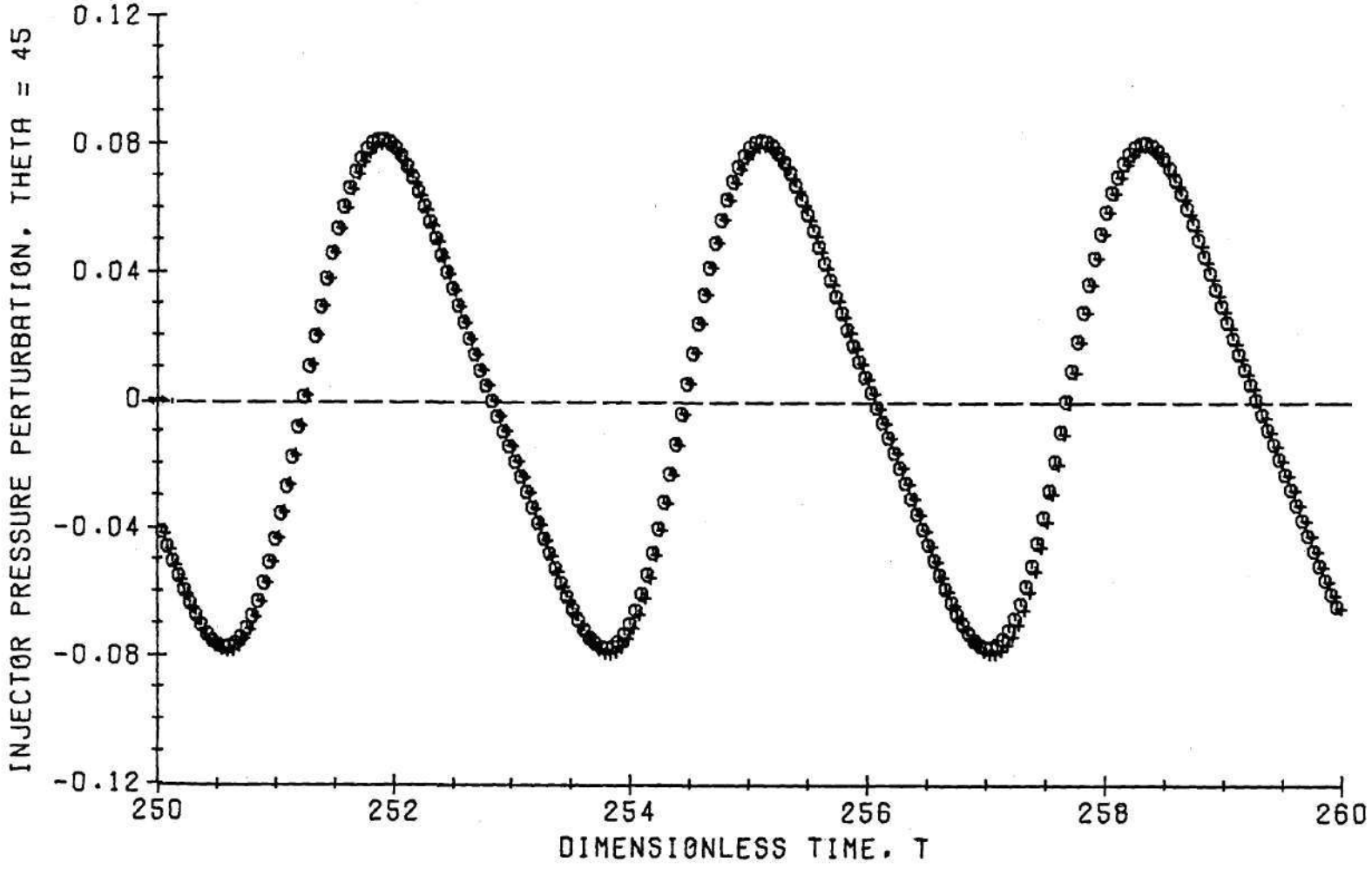

Figure 23. Limiting Injector Pressure Wave Forms at $\theta = 45^{\circ}$ for a Mildly Unstable Motor ($M_e = 0.2$, $L/D = 0.5$, $\bar{\tau} = 1.6$, $n = 0.52$).

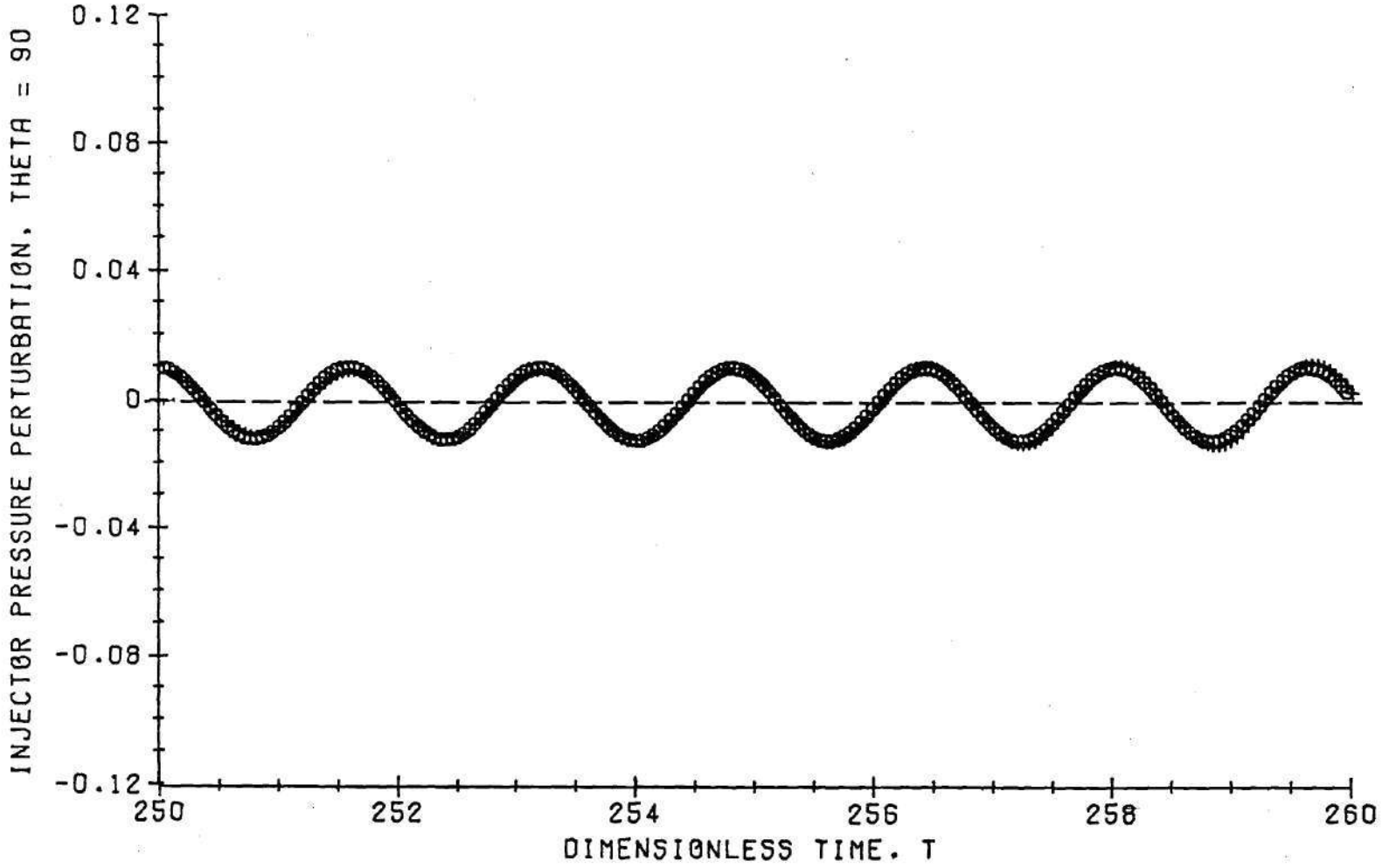

Figure 24. Limiting Injector Pressure Wave Forms at $\theta = 90^{\circ}$ for a Mildly Unstable Motor ($M_e = 0.2$, $L/D = 0.5$, $\bar{\tau} = 1.6$, $n = 0.52$).

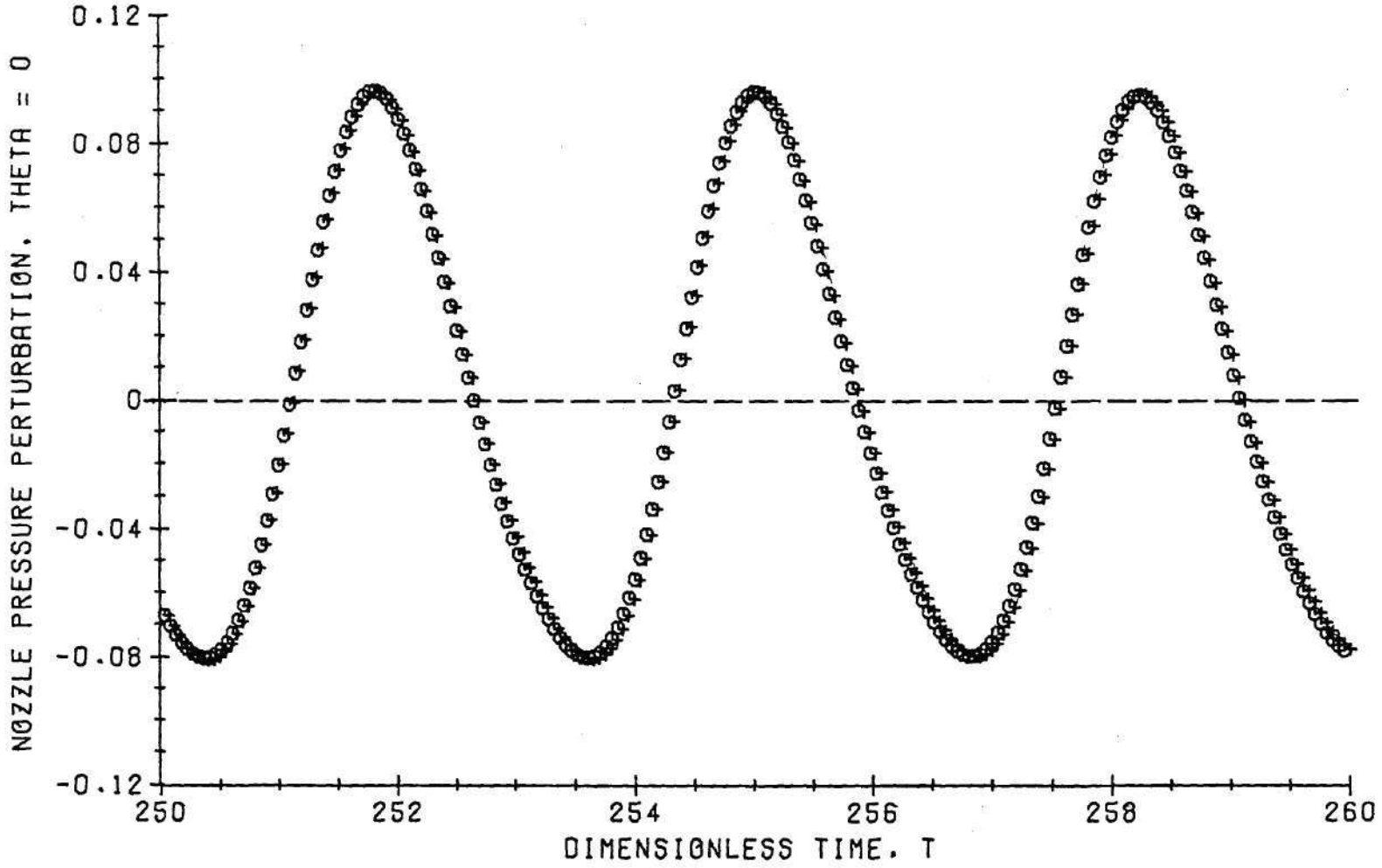

Figure 25. Limiting Pressure Wave Forms at the Nozzle Entrance for a Mildly Unstable Motor (M_e = 0.2, L/D = 0.5, $\bar{\tau}$ = 1.6, n = 0.52).

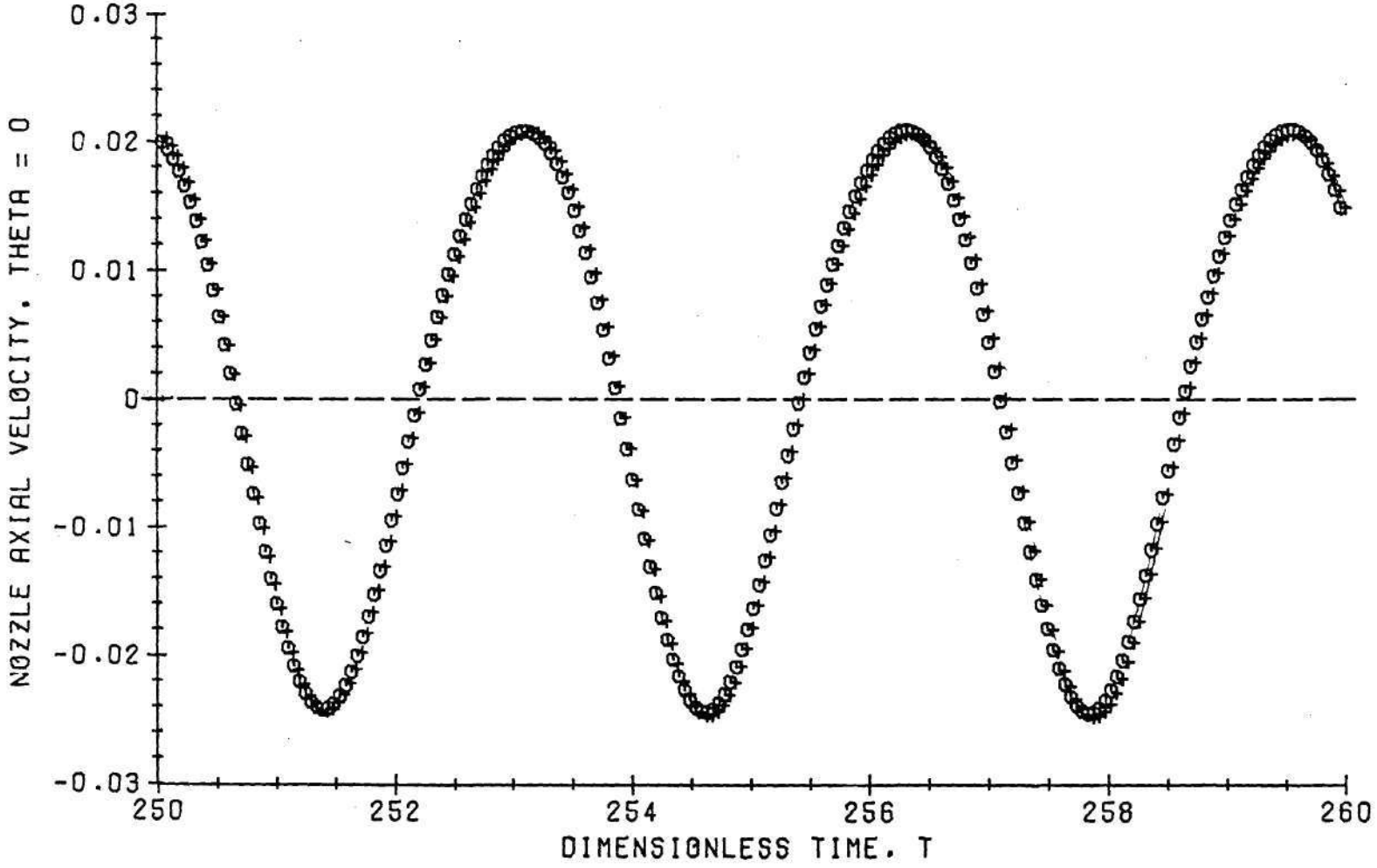

Figure 26. Limiting Axial Velocity Wave Forms at the Nozzle Entrance for a Mildly Unstable Motor (M_e = 0.2, L/D = 0.5, $\bar{\tau}$ = 1.6, n = 0.52).

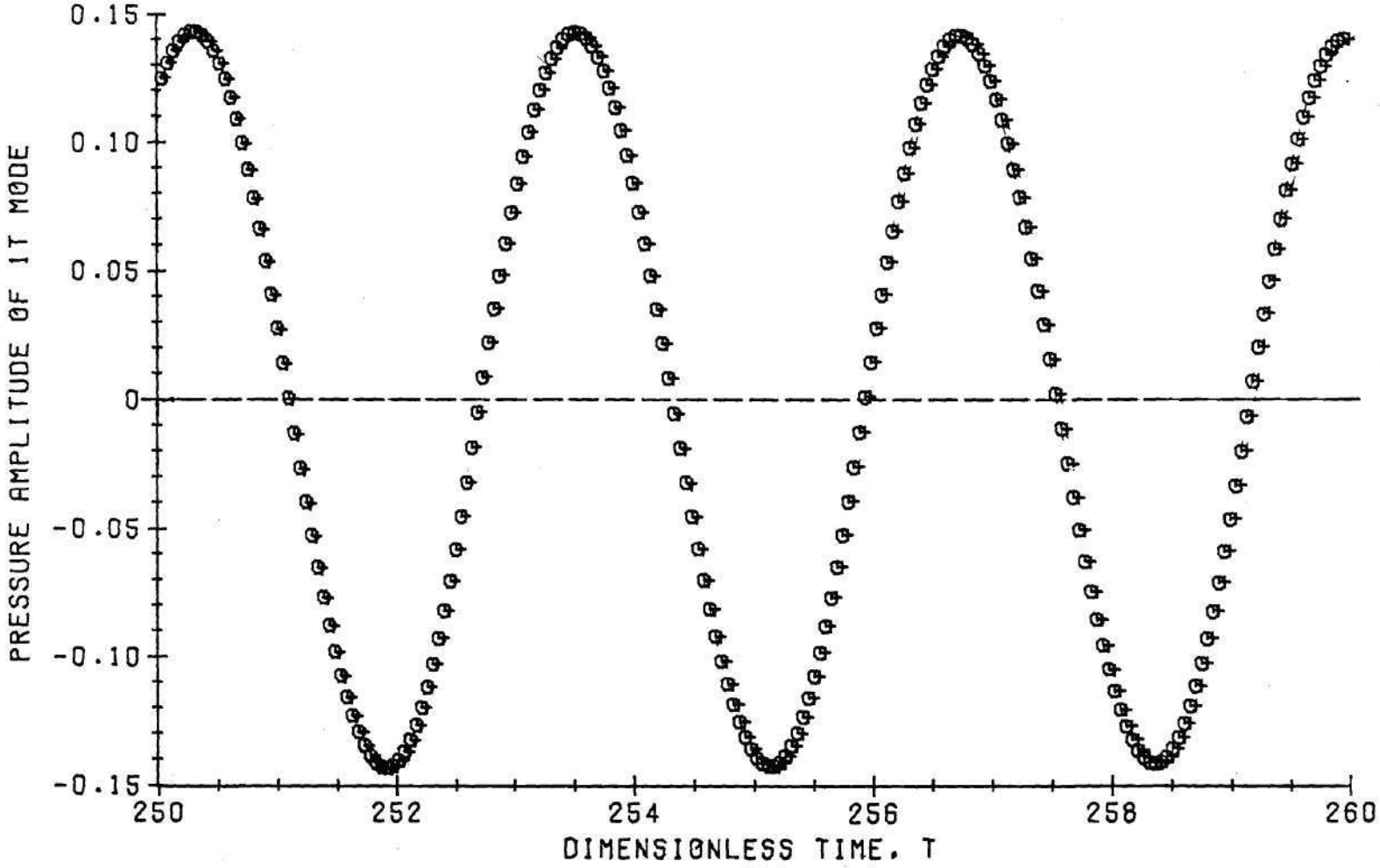

Figure 27. Limiting Pressure Amplitude Wave Forms for a Mildly Unstable Motor (M_e = 0.2, L/D = 0.5, $\bar{\tau}$ = 1.6, n = 0.52).

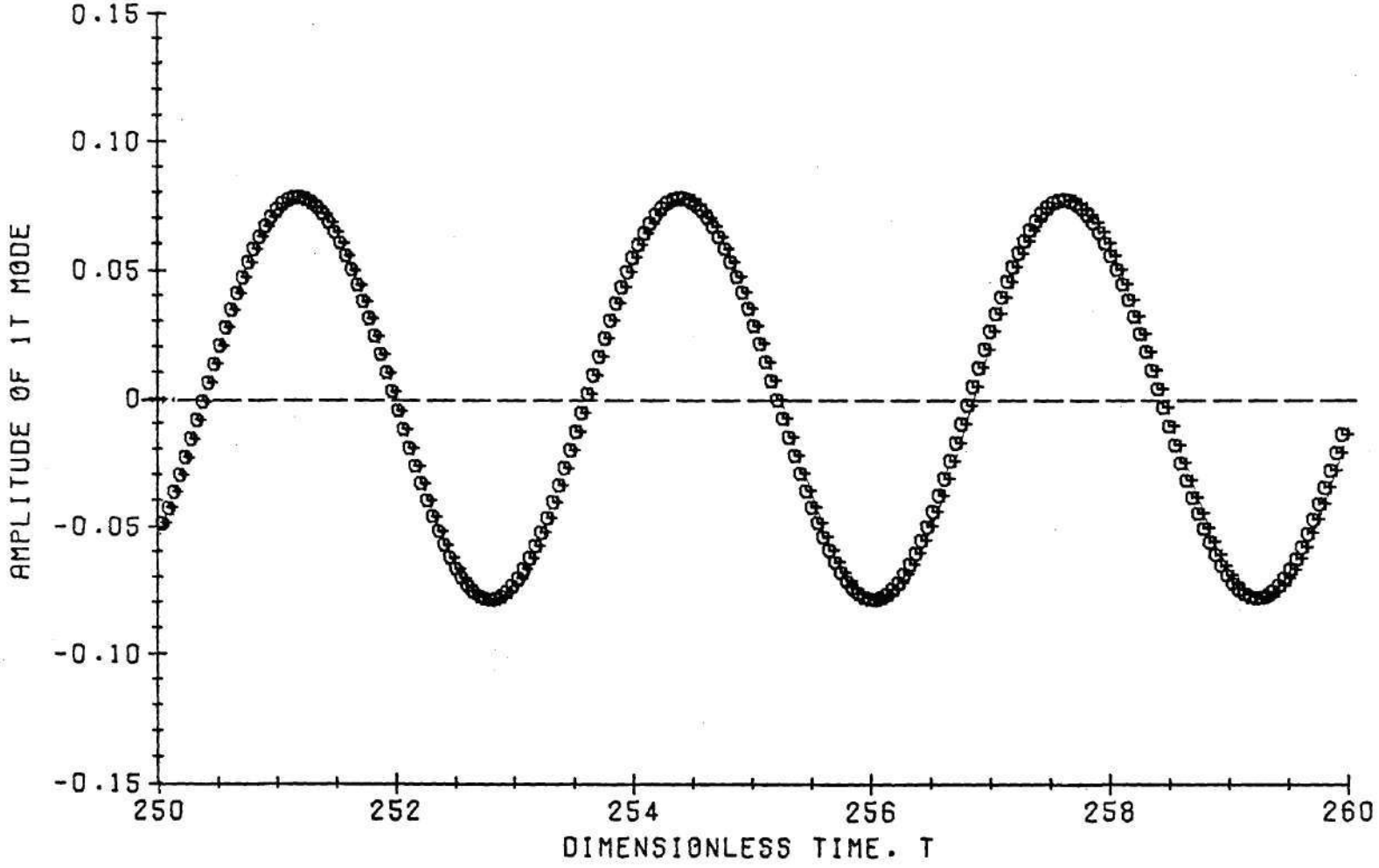

Figure 28. Limiting 1T Mode Amplitude Wave Forms for a Mildly Unstable Motor (M_e = 0.2, L/D = 0.5, $\bar{\tau}$ = 1.6, n = 0.52).

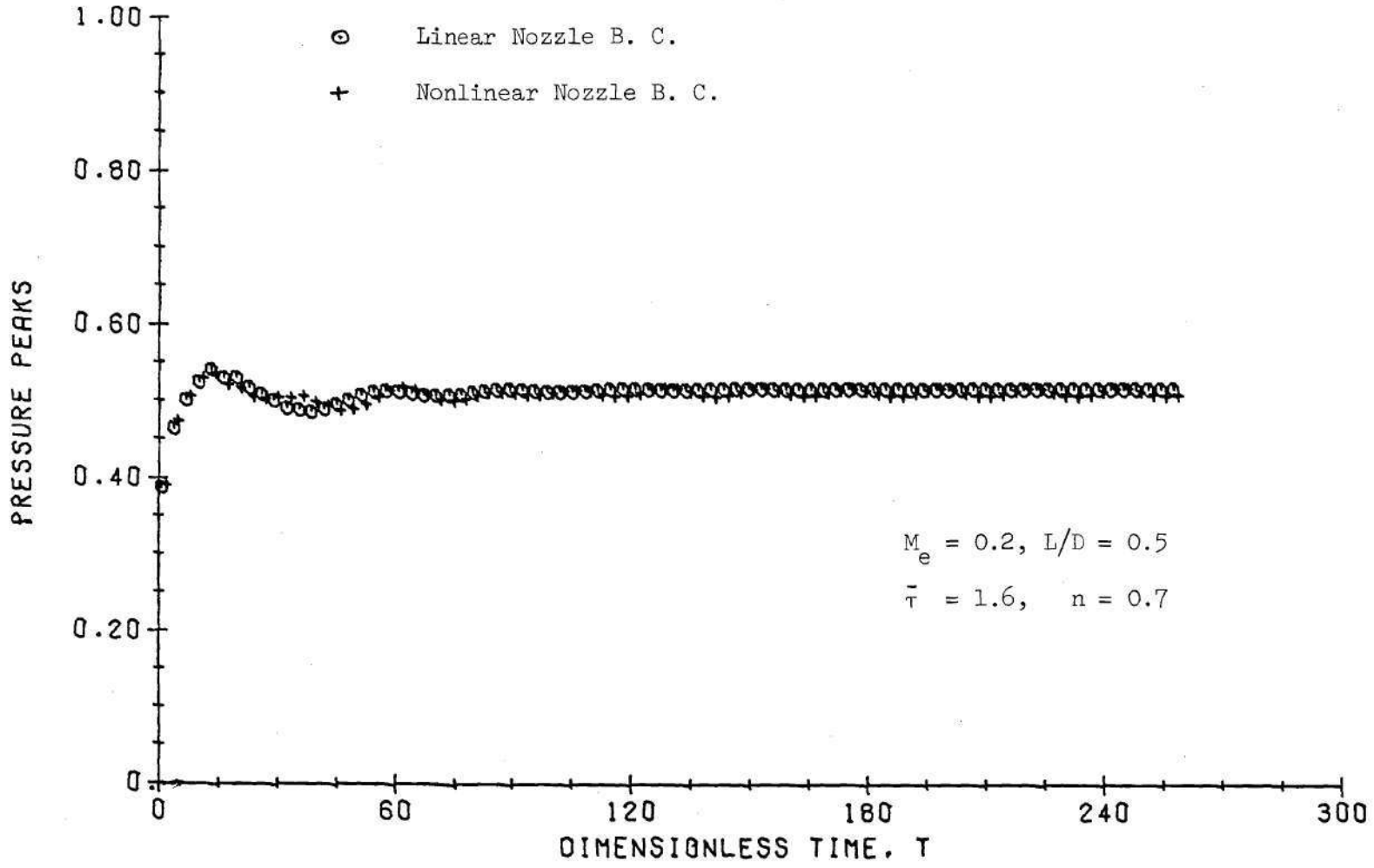

Figure 29. Time History of the Pressure Peaks at Nozzle Entrance for a Strongly Unstable Motor

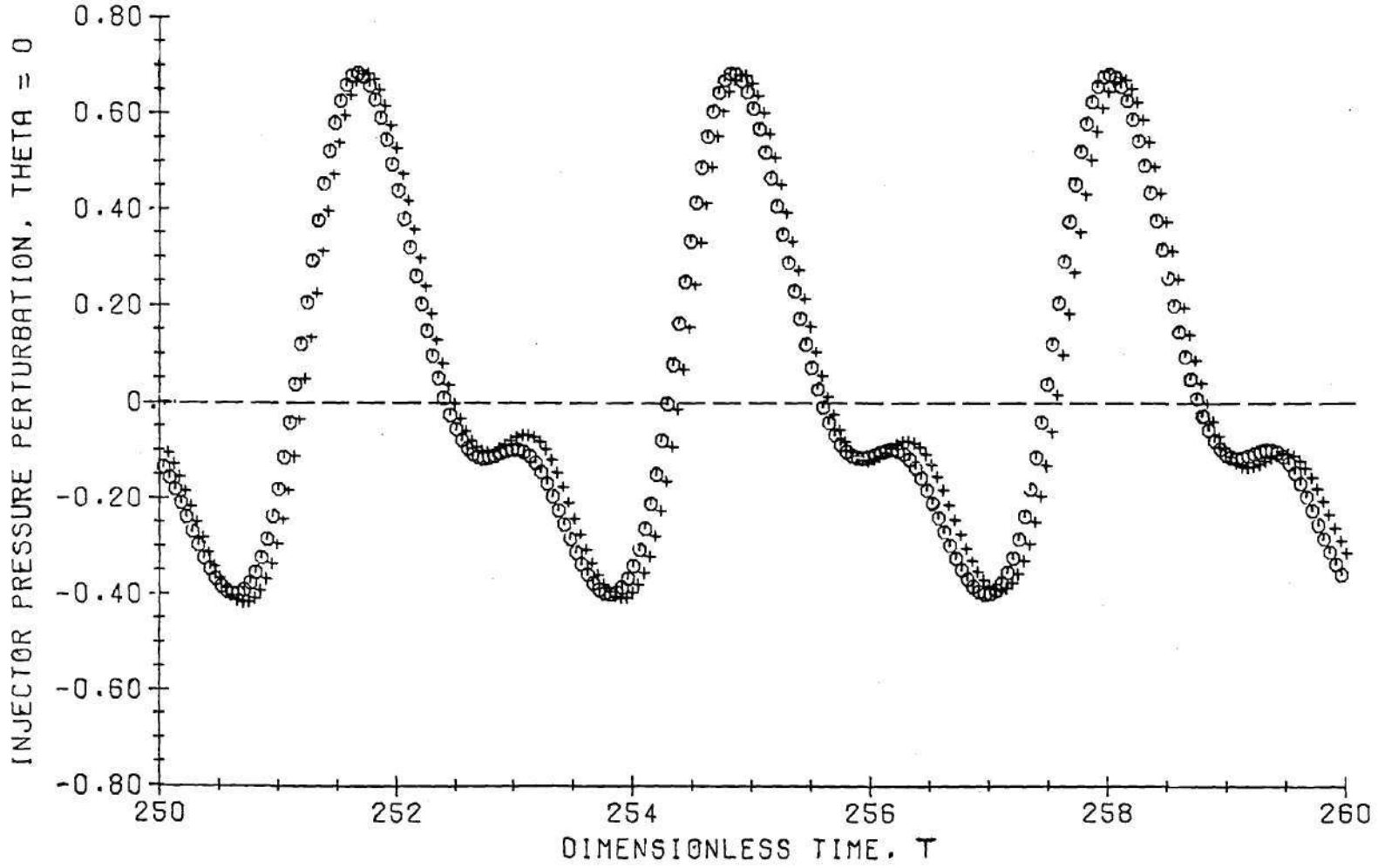

Figure 30. Limiting Injector Pressure Wave Forms at $\theta = 0^{\circ}$ for a Strongly Unstable Motor ($M_e = 0.2$, $L/D = 0.5$, $\bar{\tau} = 1.6$, $n = 0.7$).

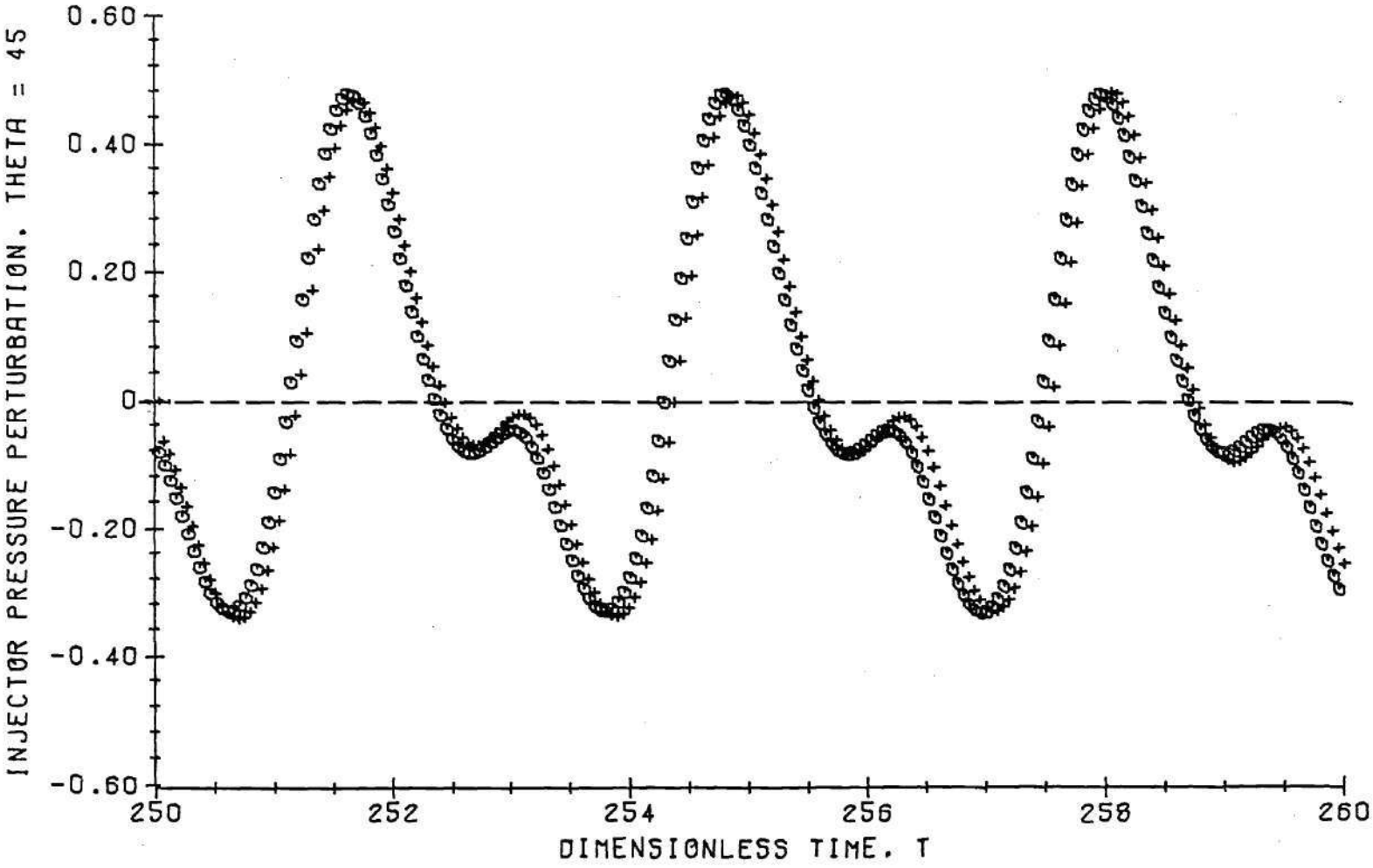

Figure 31. Limiting Injector Pressure Wave Forms at $\theta = 45^{\circ}$ for a Strongly Unstable Motor ($M_e = 0.2$, $L/D = 0.5$, $\bar{\tau} = 1.6$, $n = 0.7$).

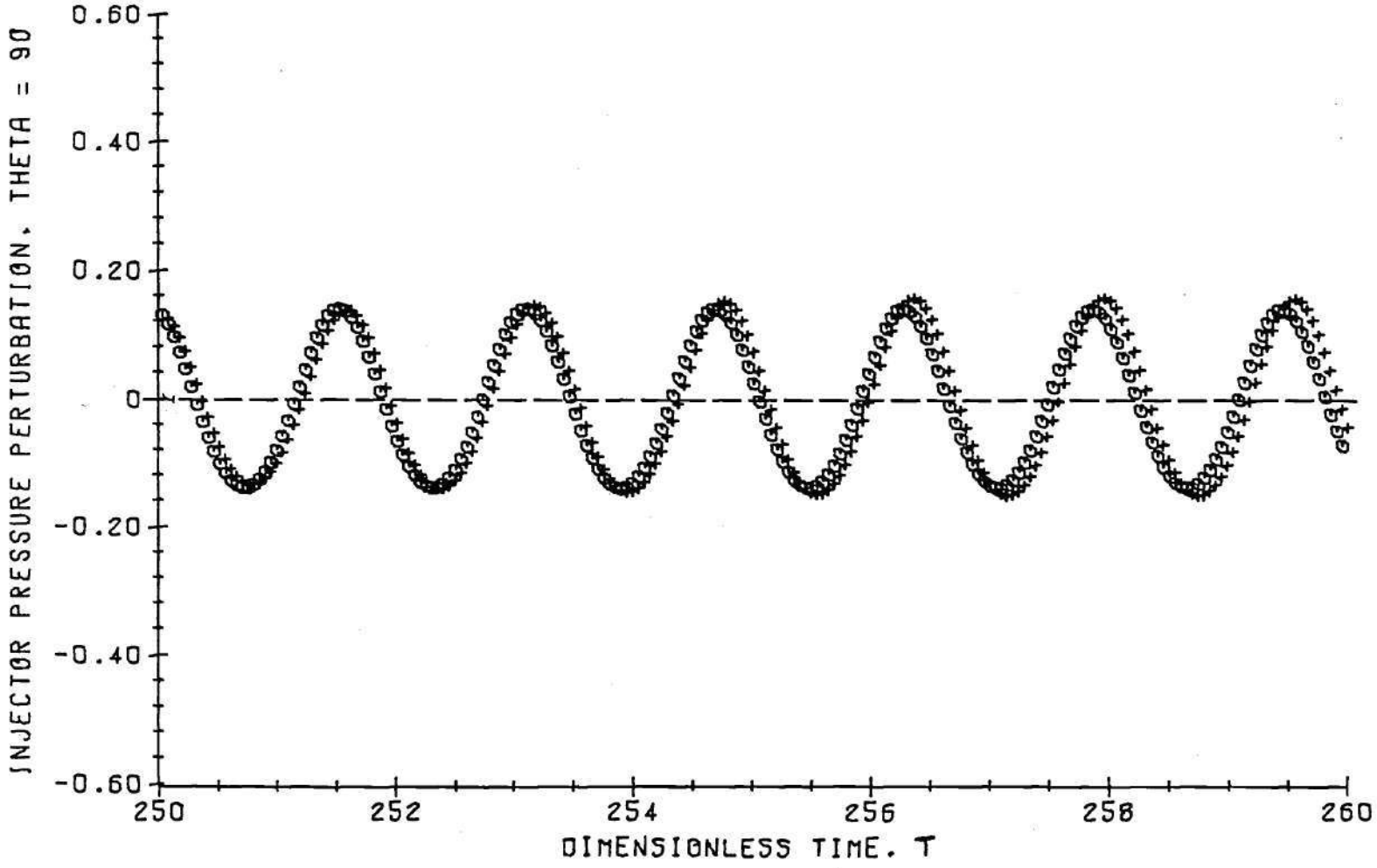

Figure 32. Limiting Injector Pressure Wave Forms at $\theta = 90^{\circ}$ for a Strongly Unstable Motor ($M_e = 0.2$, $L/D = 0.5$, $\bar{\tau} = 1.6$, $n = 0.7$).

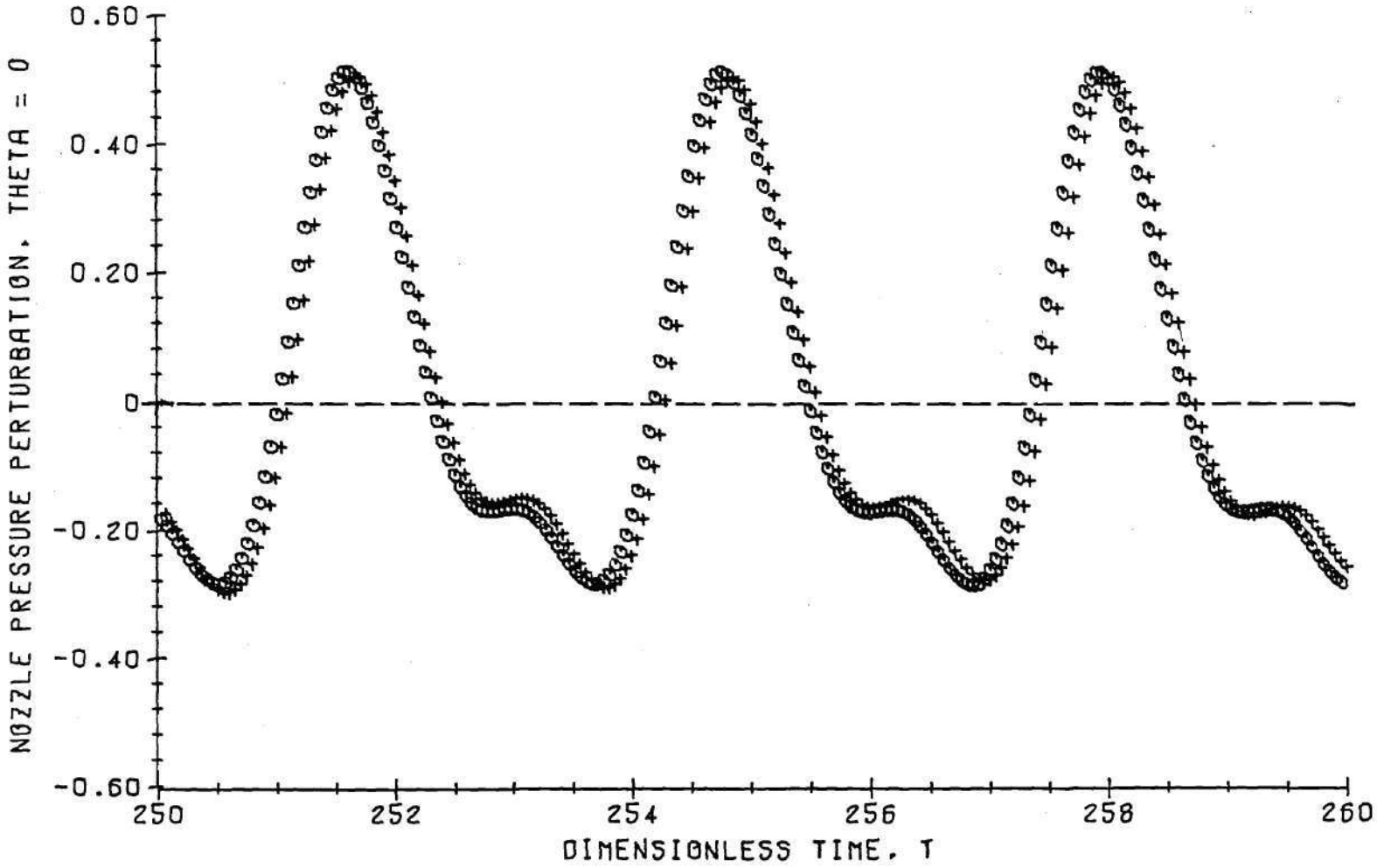

Figure 33. Limiting Pressure Wave Forms at the Nozzle Entrance for a Strongly Unstable Motor (M_e = 0.2, L/D = 0.5, $\bar{\tau}$ = 1.6, n = 0.7).

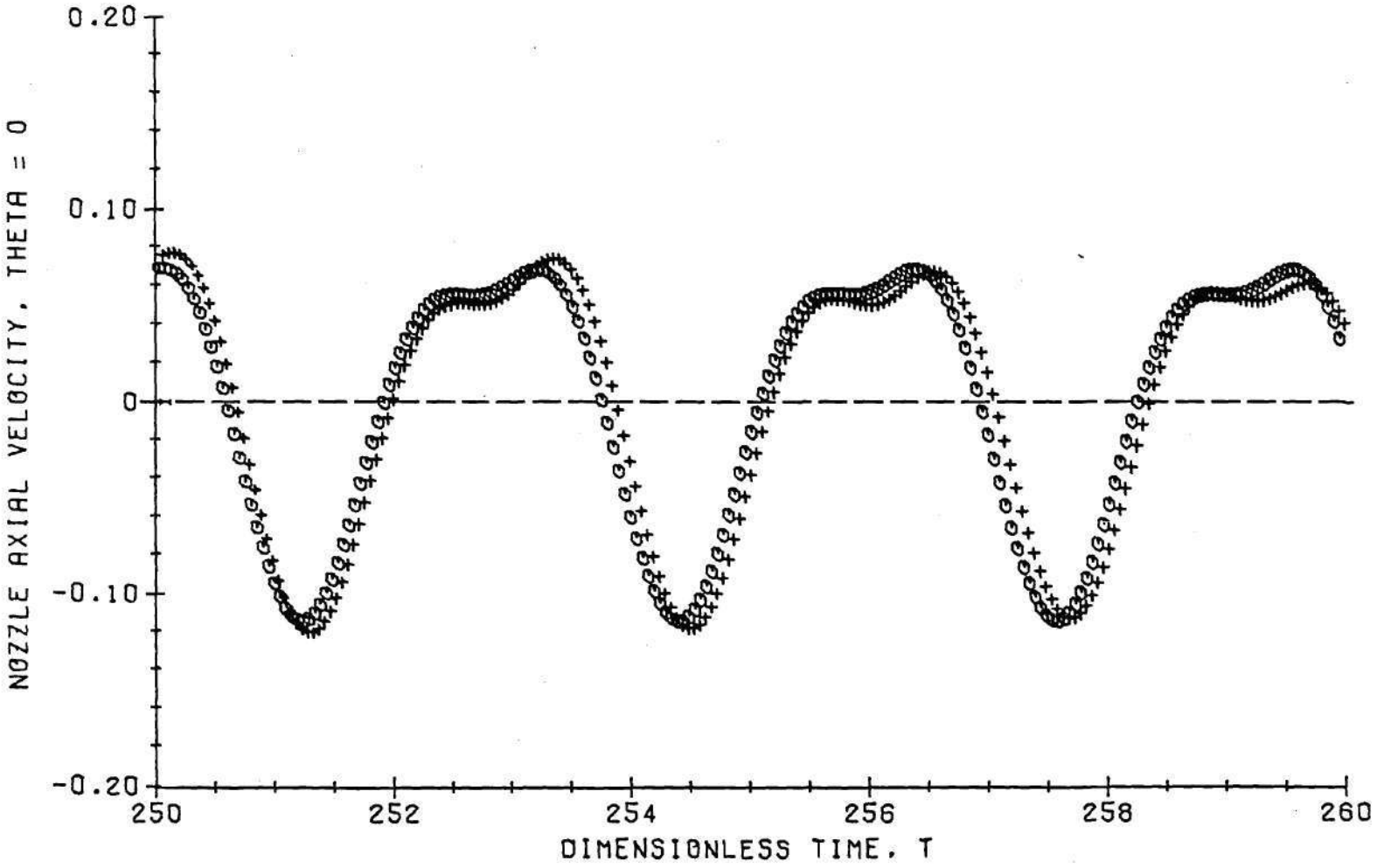

Figure 34. Limiting Axial Velocity Wave Forms at the Nozzle Entrance for a Strongly Unstable Motor (M_e = 0.2, L/D = 0.5, $\bar{\tau}$ = 1.6, n = 0.7).

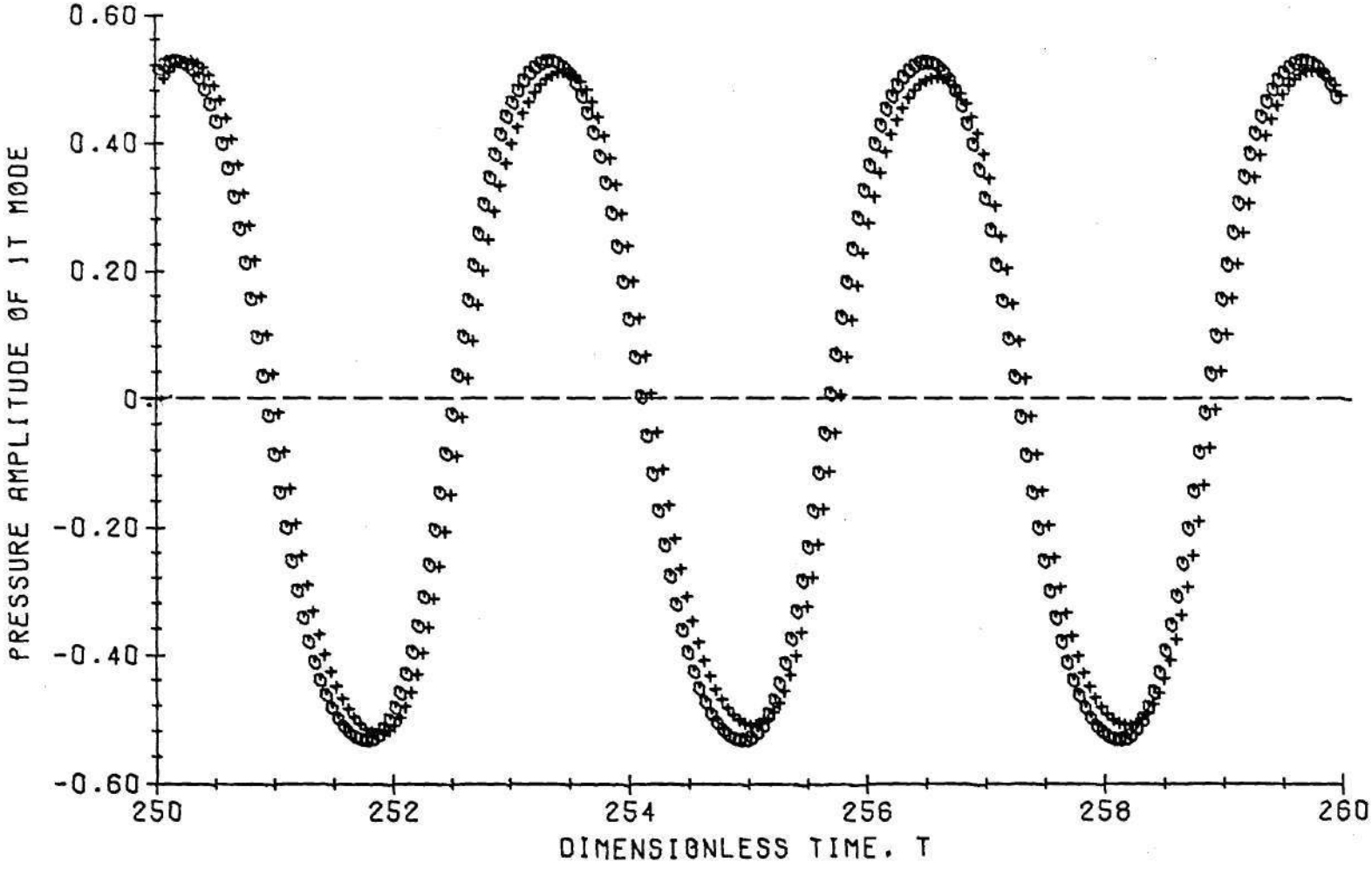

Figure 35. Limiting 1T Pressure Amplitude Wave Forms for a Strongly Unstable Motor (M_e = 0.2, L/D = 0.5, $\bar{\tau}$ = 1.6, n = 0.7).

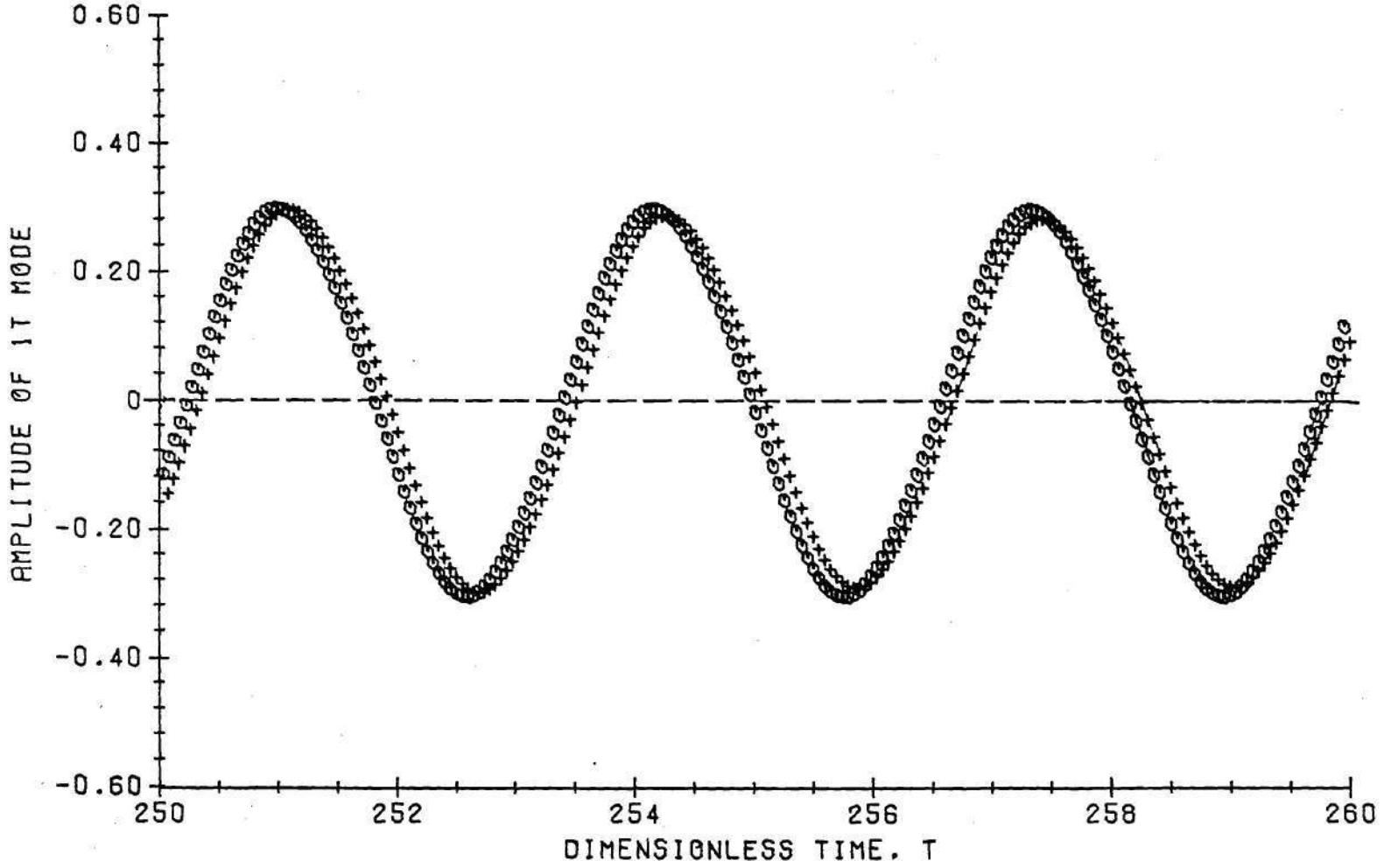

Figure 36. Limiting 1T Amplitude Wave Forms for a Strongly Unstable Motor (M_e = 0.2, L/D = 0.5, $\bar{\tau}$ = 1.6, n = 0.7).

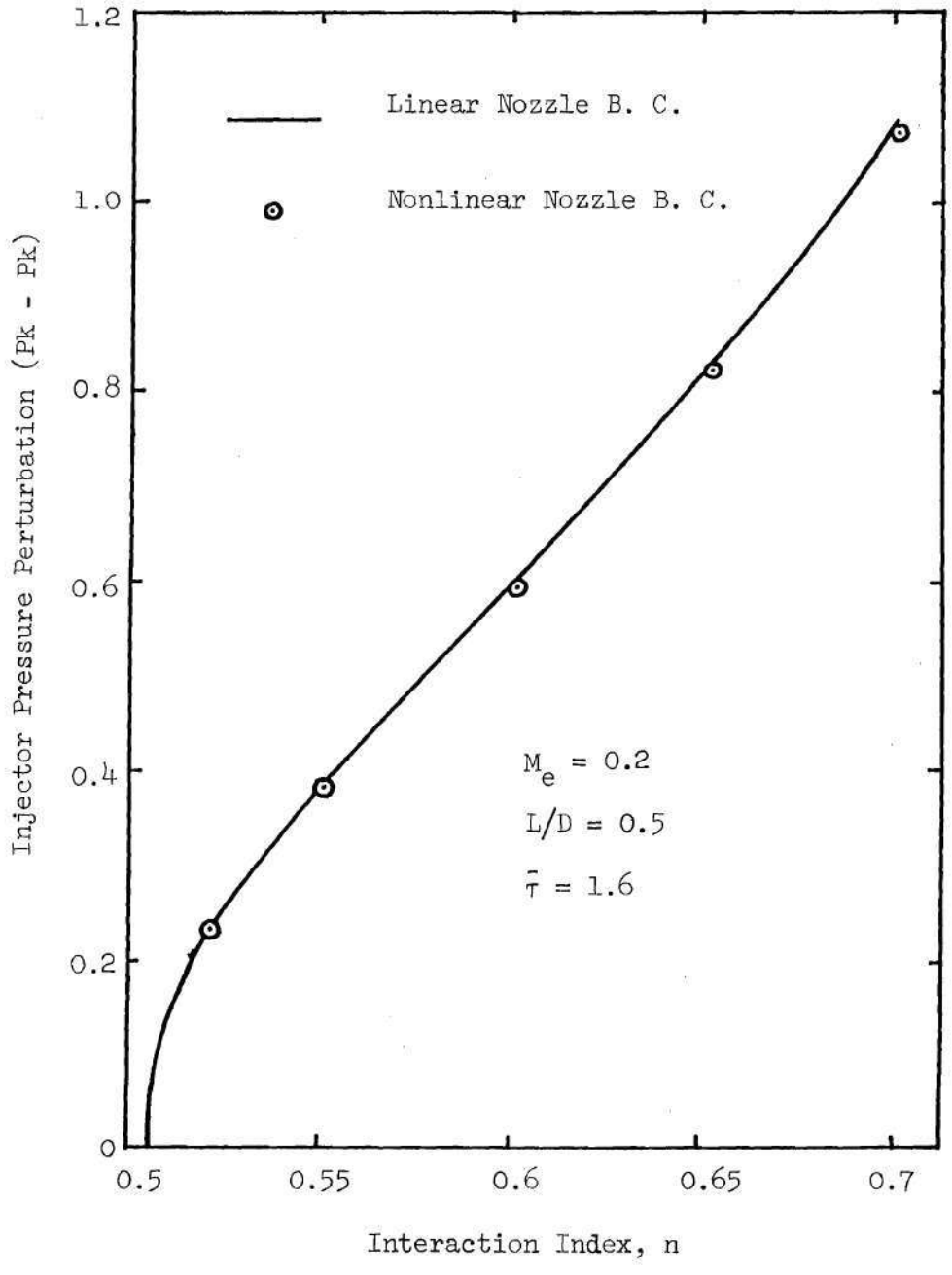

Figure 37. Comparison of Limit-Cycle Injector Pressure Perturbation for Different Values of n.

negligible effect on limiting nozzle pressure and axial velocity perturbations, as evident from Figures 38 and 39.

All of the above calculations were performed with $\bar{\tau} = 1.6$. Figures 40 and 41 show the results obtained using different values of $\bar{\tau}$ for the same combustor-nozzle configuration. In all of these cases, the interaction index n is so chosen that the displacement above the neutral stability limit, δn, is the same. Comparison of the limiting pressure amplitudes shows that once again the nozzle nonlinearities do not have any significant effect on the limiting amplitude values.

Calculations have also been performed for combustors with different exit Mach numbers. These results are plotted in Figure 42. A value of 1.6 is used for $\bar{\tau}$, with constant displacement above the neutral stability limit. Limiting amplitudes obtained using nonlinear nozzle boundary condition agree closely with those obtained using linear nozzle boundary condition.

Figure 43 shows a comparison of the limiting pressure amplitudes, with and without the inclusion of nozzle nonlinearities, for combustion chambers of different lengths. Again, the nozzle nonlinearities appear to have no significant effect.

Thus, all of the results presented here indicate that the inclusion of the nozzle nonlinearities does not have any significant effect on the limit-cycle behavior of the motor. The reason for this appears reasonably clear. The effect of nozzle nonlinearities is felt mainly in the 2T and 1R mode amplitudes. But, since the amplitudes of the 2T and 1R modes are considerably less than the amplitude of the 1T mode, the changes in their amplitudes due to the nozzle nonlinearities

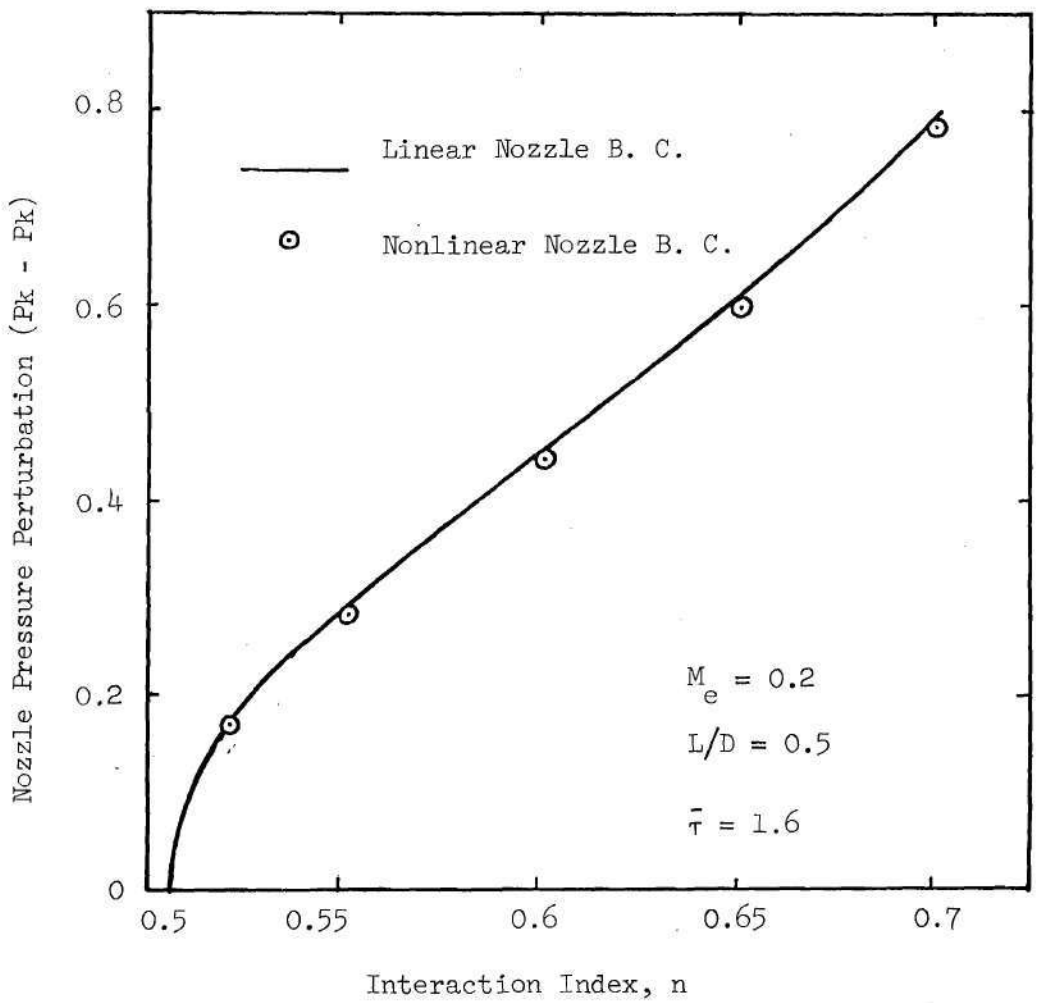

Figure 38. Comparison of Limit-cycle Pressure Perturbation at the Nozzle Entrance for Different Values of n.

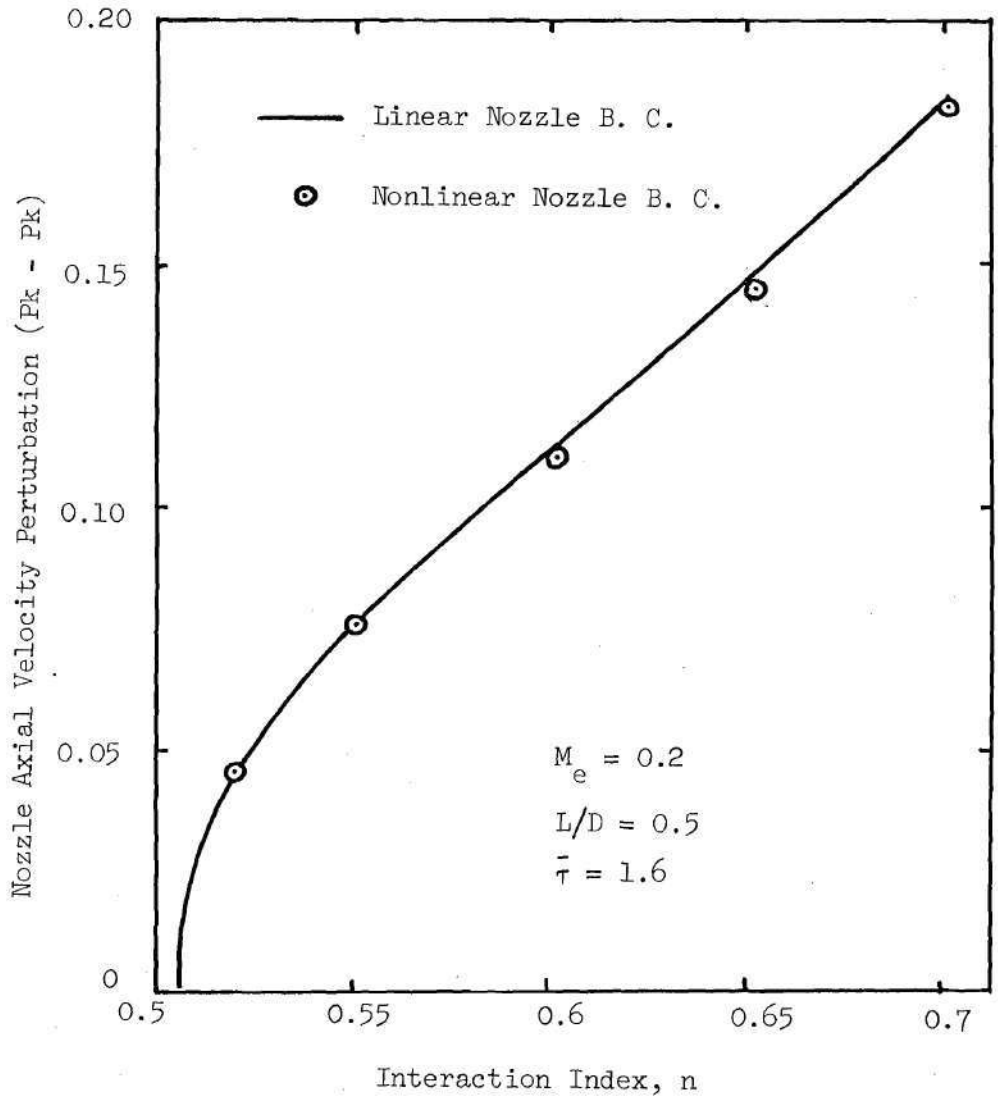

Figure 39. Comparison of Limit-cycle Axial Velocity Perturbation at the Nozzle Entrance for Different Values of n.

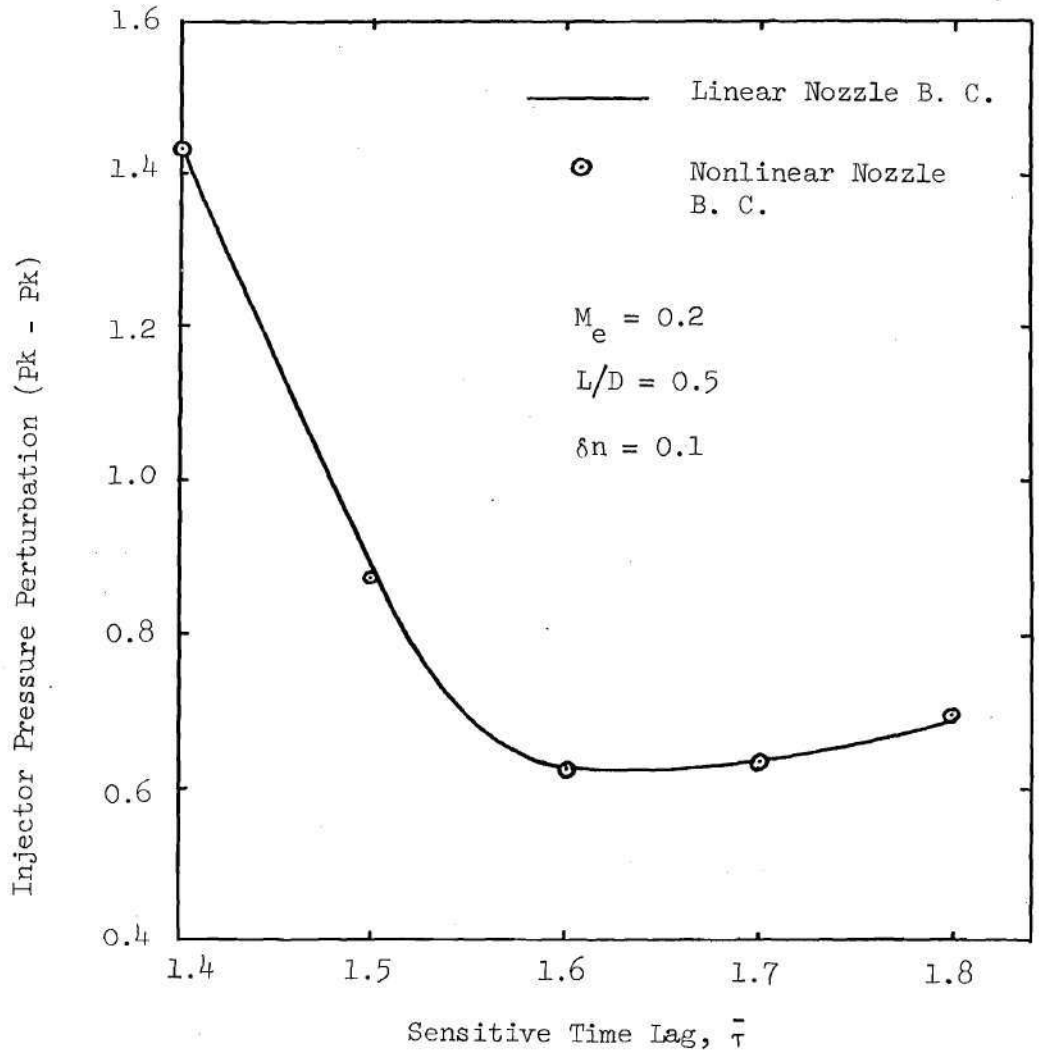

Figure 40. Comparison of Limit-cycle Injector Pressure Perturbation for Different Values of $\bar{\tau}$.

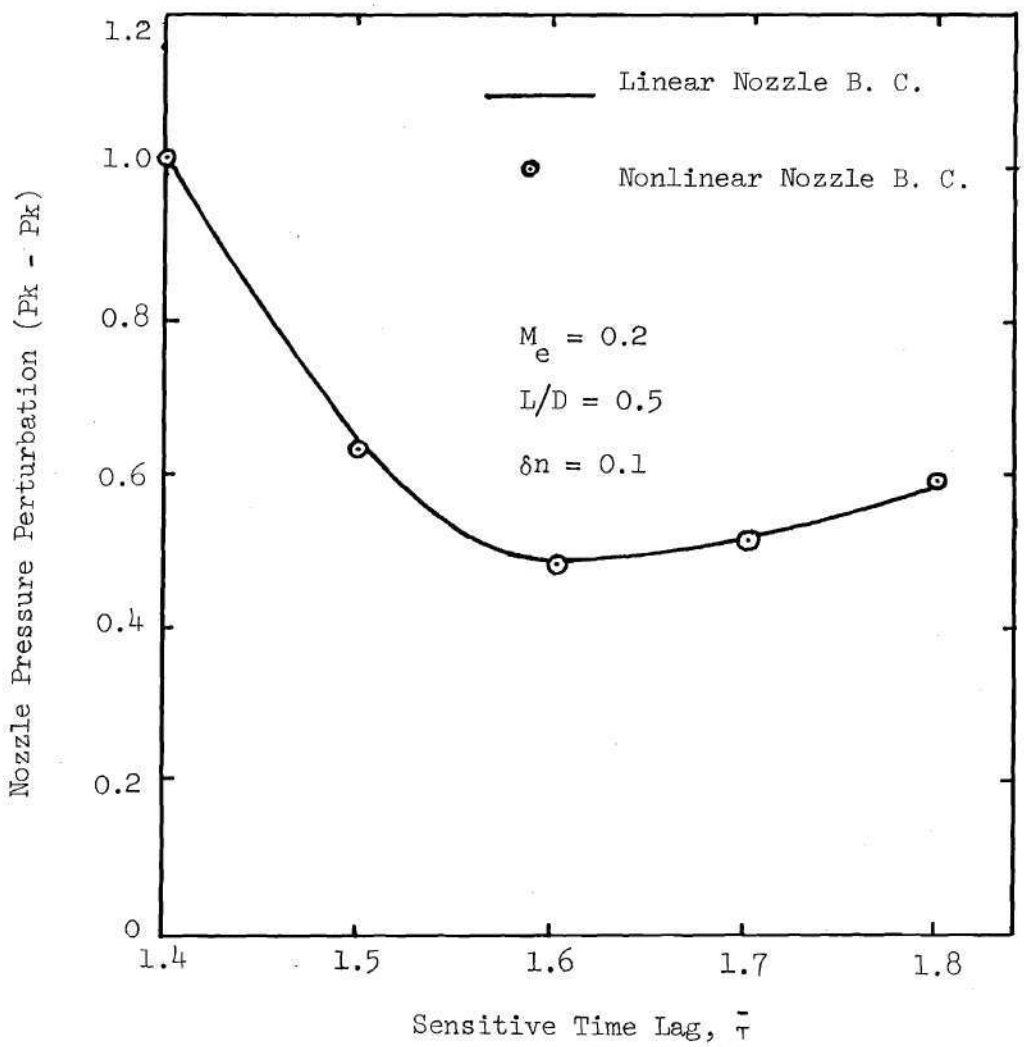

Figure 41. Comparison of Limit-cycle Pressure Perturbation at the Nozzle Entrance for Different Values of $\bar{\tau}$.

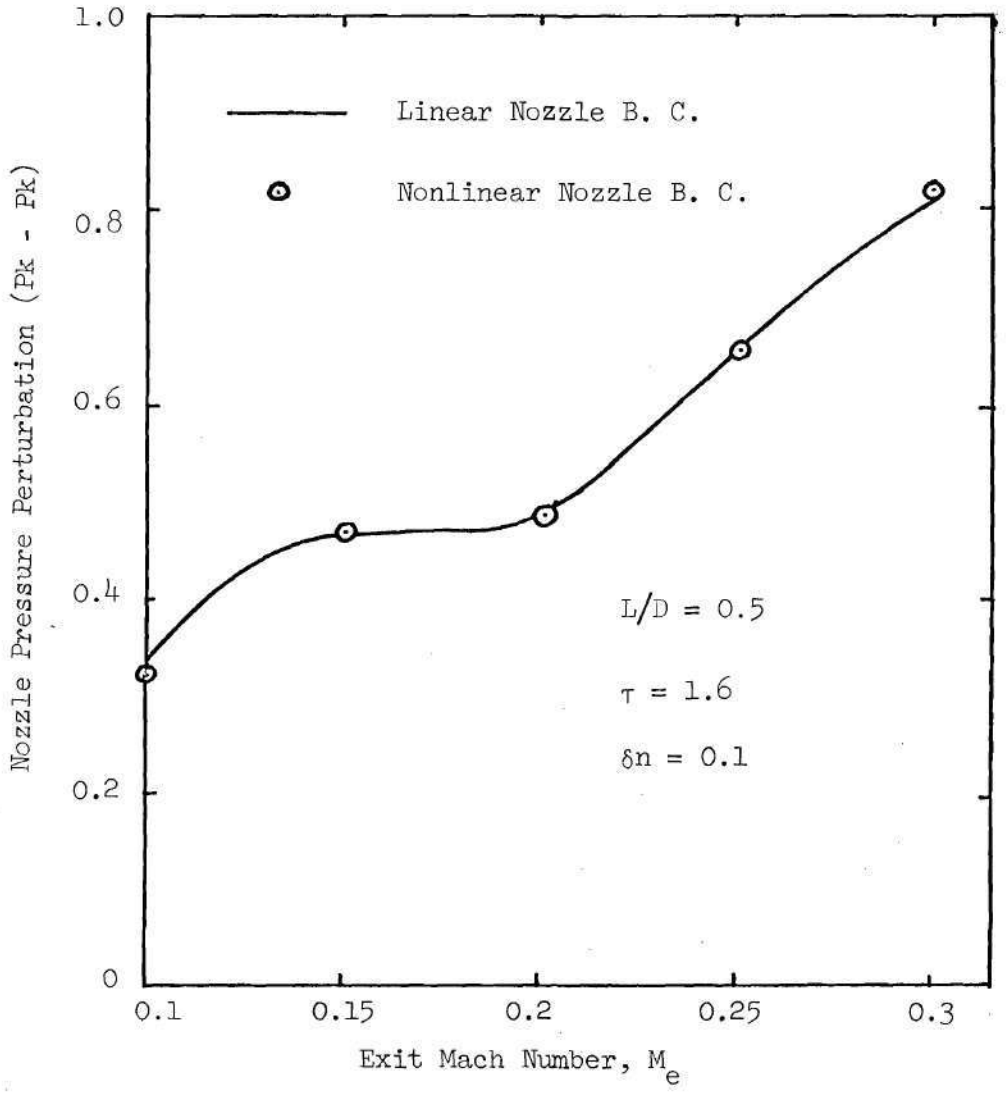

Figure 42. Comparison of Limit-cycle Pressure Perturbation at the Nozzle Entrance for Different Values of Exit Mach Number.

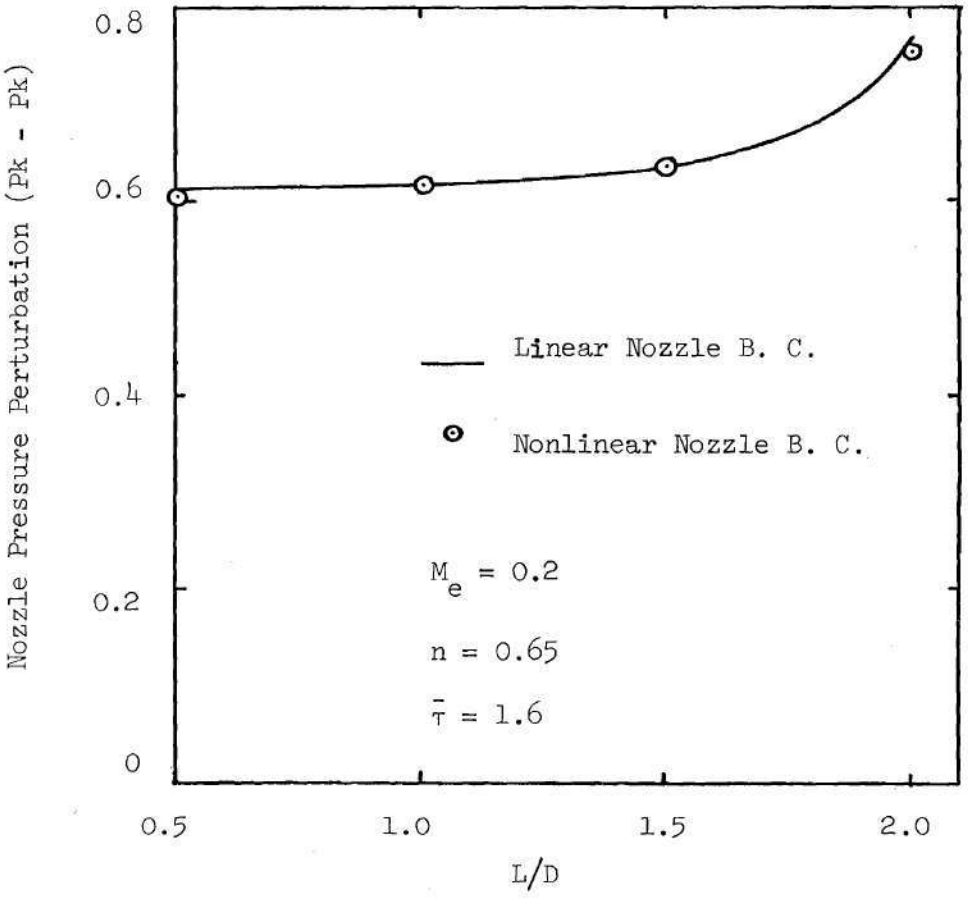

Figure 43. Comparison of Limit-cycle Pressure Perturbation at the Nozzle Entrance for Different Values of Chamber Length-to-diameter Ratio.

do not significantly alter the motor conditions. Thus the fact that the amplitudes of the 2T and 1R modes are much less than the amplitude of the 1T mode accounts for the weak effect of the nozzle nonlinearities.

CHAPTER VI

CONCLUDING REMARKS

Oscillatory flow in the subsonic portion of an axisymmetric nozzle operating in the supercritical range has been studied using the Galerkin method. A three-dimensional nonlinear nozzle admittance relation has been developed and nozzle responses have been calculated for different nozzles. The combustion instability theory developed by Powell and Zinn (Ref. 11) has been modified to include the effect of nozzle nonlinearities. Using a three-mode series consisting of the first tangential, the second tangential and the first radial modes, combustion instability calculations have been performed for different values of motor and combustion parameters. In each case, under the assumption of moderate amplitude instability, computations have been made, with and without the inclusion of nozzle nonlinearities. The results show that the presence of nozzle nonlinearities has no significant effect on the limiting amplitude, frequency and pressure wave forms. This result can be attributed to the fact that the amplitudes of the 2T and 1R modes are considerably less than the amplitude of the 1T mode for the combustion instability theory which was used.

Hence, in nonlinear stability calculations of liquid rocket motors, the effect of nozzle nonlinearities can be safely neglected and the linear nozzle boundary condition can be used to describe the flow conditions at the nozzle entrance.

APPENDIX A

DERIVATION OF THE NOZZLE POTENTIAL EQUATION

It is shown in this appendix how the continuity and momentum equations for the oscillatory flow in the nozzle can be combined with the aid of the isentropic relation to yield a single equation describing the behavior of the velocity potential, Φ, in the nozzle.

Consider the momentum equation, i.e., Eq. (2-2). Under the assumption of irrotational flow

$$\nabla \times \underset{\rightarrow}{V} = 0 \tag{A-1}$$

Equation (2-2) simplifies to

$$\frac{\partial \underset{\rightarrow}{V}}{\partial t} + \tfrac{1}{2} \nabla(V^2) = - \frac{\nabla p}{\gamma \rho} \tag{A-2}$$

Introducing the velocity potential defined by Eq. (2-5) into Eq. (A-2) and interchanging the order of differentiation with respect to time and space gives

$$\nabla \Phi_t + \nabla(V^2/2) + \frac{\nabla p}{\gamma \rho} = 0 \tag{A-3}$$

Using the isentropic relation

$$\frac{p}{\rho^{\gamma}} = \text{constant} \tag{A-4}$$

it can be easily shown that

$$\frac{\nabla p}{\rho} = \frac{\gamma}{\gamma-1} \nabla(p/\rho) \tag{A-5}$$

Substituting Eq. (A-5) in Eq. (A-3) gives

$$\nabla \left[\Phi_t + \frac{V^2}{2} + \frac{1}{\gamma-1} \frac{p}{\rho} \right] = 0 \tag{A-6}$$

Integrating,

$$\Phi_t + \frac{V^2}{2} + \frac{1}{\gamma-1} \frac{p}{\rho} = \frac{1}{\gamma-1} \tag{A-7}$$

where the constant of integration has been determined by considering the stagnation conditions.

In Eq. (A-7), multiplying throughout by ρ and differentiating with respect to t gives

$$\frac{p}{\rho} \frac{\rho_t}{\rho} + \Phi_{tt} + \frac{1}{2} \frac{\partial V^2}{\partial t} = 0 \tag{A-8}$$

From the continuity equation (i.e., Eq. (2-1)),

$$\frac{\rho_t}{\rho} = - \nabla^2 \Phi - \nabla \Phi \cdot \frac{\nabla \rho}{\rho} \tag{A-9}$$

Using Eq. (A-4), it can be shown that

$$\frac{\nabla \rho}{\rho} = \frac{1}{\gamma} \frac{\nabla p}{p}$$

and hence Eq. (A-9) becomes

$$- \frac{p}{\rho} \nabla^2 \Phi - \nabla \Phi \cdot \frac{\nabla p}{\gamma \rho} + \Phi_{tt} + \frac{1}{2} \frac{\partial V^2}{\partial t} = 0 \tag{A-10}$$

Finally, eliminating p and ρ in Eq. (A-10) by using Eqs. (A-3) and (A-7) gives

$$\nabla^2\Phi - \Phi_{tt} = 2\nabla\Phi \cdot \nabla\Phi_t + (\gamma-1)\,\Phi_t\,\nabla^2\Phi$$

$$+ \frac{\gamma-1}{2}\,(\nabla\Phi \cdot \nabla\Phi)\,\nabla^2\Phi + \frac{1}{2}\,\nabla\Phi \cdot \nabla(\nabla\Phi \cdot \nabla\Phi) \qquad \text{(A-11)}$$

which is the nozzle potential equation.

APPENDIX B

ANALYTICAL EXPRESSIONS FOR THE COEFFICIENTS

The analytical expressions for the coefficients appearing in Eq. (2-22) contain certain integrals involving trigonometric and Bessel functions. A list of these integrals is first given below. In these integrals, the functions $\Theta_p(\theta)$ and $R_p(r)$ are defined by

$$\Theta_p(\theta) = \cos(m\theta)$$

$$R_p(r) = J_m(S_p r)$$

where m is the tangential mode number for the p^{th} mode.

The integrals involving trigonometric functions are

$$\alpha_1(p, q, j) = \int_0^{2\pi} \Theta_p(\theta)\, \Theta_q(\theta)\, \Theta_j(\theta)\, d\theta$$

$$\alpha_2(p, q, j) = \int_0^{2\pi} \Theta_p'(\theta)\, \Theta_q'(\theta)\, \Theta_j(\theta)\, d\theta$$

$$\alpha_3(p, q, j) = \int_0^{2\pi} \Theta_p''(\theta)\, \Theta_q(\theta)\, \Theta_j(\theta)\, d\theta$$

$$\alpha_4(p, j) = \int_0^{2\pi} \Theta_p(\theta)\, \Theta_j(\theta)\, d\theta$$

$$\alpha_5(p, j) = \int_0^{2\pi} \Theta_p''(\theta)\, \Theta_j(\theta)\, d\theta$$

The integrals involving Bessel functions are

$$\beta_1(p, q, j) = \int_0^1 R_p(r)\, R_q(r)\, R_j(r)\, dr$$

$$\beta_2(p, q, j) = \int_0^1 R_p(r)\, R_q(r)\, R_j(r)\, \frac{1}{r}\, dr$$

$$\beta_3(p, q, j) = \int_0^1 R_p'(r)\, R_q'(r)\, R_j(r)\, rdr$$

$$\beta_4(p, q, j) = \int_0^1 R_p''(r)\, R_q(r)\, R_j(r)\, rdr$$

$$\beta_5(p, q, j) = \int_0^1 R_p'(r)\, R_q(r)\, R_j(r)\, dr$$

$$\beta_6(p, j) = \int_0^1 R_p(r)\, R_j(r)\, rdr$$

$$\beta_7(p, j) = \int_0^1 R_p'(r)\, R_j(r)\, dr$$

$$\beta_8(p, j) = \int_0^1 R_p''(r)\, R_j(r)\, rdr$$

$$\beta_9(p, j) = \int_0^1 R_p(r)\, R_j(r)\, \frac{1}{r}\, dr$$

While all those integrals that involve trigonometric functions can be

evaluated analytically, closed-form analytical solutions do not exist for all the integrals involving Bessel functions; hence, these must be computed numerically.

For convenience in presenting the analytical expressions for the coefficients, let

$$\delta_1(p, q, j) = 0 \quad \text{if} \quad (K_p + K_q) \neq K_j$$

$$= 0 \quad \text{if} \quad K_p + K_q = K_j$$

$$\delta_2(p, j) = 0 \quad \text{if} \quad K_p \neq K_j$$

$$= 1 \quad \text{if} \quad K_p = K_j$$

The coefficients that appear in Eq. (2-22) can now be written down in terms of the above integrals as follows:

$$C_1(\varphi, p, j) = \frac{2r_w^2 f_1(\varphi)}{\omega} \delta_2(p, j) \alpha_4(p, j) \beta_6(p, j)$$

$$C_2(\varphi, p, j) = - 2r_w^2 K_p \delta_2(p, j) \alpha_4(p, j) \beta_6(p, j)$$

$$\left\{ \frac{r_w^2}{K_p \omega} f_2(\varphi) + 2i \right\}$$

$$C_3(\varphi, p, j) = \frac{2f_3(\varphi)}{\omega \bar{\rho} \bar{u}} \delta_2(p, j) \alpha_4(p, j) \left\{ \beta_7(p, j) + \beta_8(p, j) \right\}$$

$$+ \frac{2f_3(\varphi)}{\omega \bar{\rho} \bar{u}} \delta_2(p, j) \alpha_5(p, j) \beta_9(p, j)$$

$$+ 2 K_p r_w^2 \delta_2(p, j) \alpha_4(p, j) \beta_6(p, j)$$

$$\left\{ \frac{K_p \omega}{\bar{u}^2} + i f_4(\varphi) \right\}$$

$$D_1(\varphi, p, q, j) = - \frac{(1+i)(\gamma-1) r_w^2 K_q}{2} \delta_1(p, q, j) \alpha_1(p, q, j) \beta_1(p, q, j)$$

$$D_2(\varphi, p, q, j) = - \frac{(1-i)(\gamma+1) r_w^2 \bar{u}^2}{2\omega} \delta_1(p, q, j) \alpha_1(p, q, j) \beta_1(p, q, j)$$

$$D_3(\varphi, p, q, j) = - K_q r_w^2 \delta_1(p, q, j) \alpha_1(p, q, j) \beta_1(p, q, j)$$

$$\left\{ (1+i) + \frac{(1-i) f_5(\varphi)}{2K_q \omega} \right\}$$

$$D_4(\varphi, p, q, j) = \frac{(1+i K_p r_w^2 f_4(\varphi)}{2} \delta_1(p, q, j) \alpha_1(p, q, j) \beta_1(p, q, j)$$

$$- \frac{(1-i)}{2\omega} \delta_1(p, q, j) \left\{ \alpha_1(p, q, j) \beta_3(p, q, j) \right.$$

$$+ \alpha_2(p, q, j) \beta_2(p, q, j) + (\gamma-1) \alpha_1(p, q, j) \beta_4(p, q, j)$$

$$+ (\gamma-1) \alpha_1(p, q, j) \beta_5(p, q, j)$$

$$\left. + (\gamma-1) \alpha_3(p, q, j) \beta_2(p, q, j) \right\}$$

$$D_5(\varphi, p, q, j) = - \delta_1(p, q, j) \left\{ \alpha_1(p, q, j) \beta_3(p, q, j) \right.$$

$$+ \alpha_2(p, q, j)\, \beta_2(p, q, j) \Big\} \Big\{ \frac{(1+i)\, K_q}{\bar{u}^2} + \frac{(1-i)\, f_6(\varphi)}{4\, \omega \bar{\rho} \bar{u}} \Big\}$$

$$- \frac{(\gamma-1)(1+i)\, K_q}{2\, \bar{u}^2}\, \delta_1(p, q, j) \Big\{ \alpha_1(p, q, j)\, \beta_4(p, q, j)$$

$$+ \alpha_1(p, q, j)\, \beta_5(p, q, j) + \alpha_3(p, q, j)\, \beta_2(p, q, j) \Big\}$$

REFERENCES

1. Tsien, H. S., "The Transfer Functions of Rocket Nozzles," American Rocket Society Journal, Vol. 22, 1952, pp. 139-143.

2. Crocco, L. and Cheng, S. I., Theory of Combustion Instability in Liquid Propellant Rocket Motors, Appendix B. AGARD Monograph No. 8, Butterworths, London, 1956.

3. Crocco, L. and Sirignano, W. A., "Behavior of Supercritical Nozzles Under Three Dimensional Oscillatory Conditions," Princeton University, Department of Aerospace and Mechanical Sciences, Report No. 790, April 1967.

4. Zinn, B. T., "A Theoretical Study of Nonlinear Transverse Combustion Instability in Liquid Propellant Rocket Motors," Princeton University, Department of Aerospace and Mechanical Sciences, Report No. 732, May 1966.

5. Zinn, B. T. and Crocco, L., "Periodic Finite-Amplitude Oscillations in Slowly Converging Nozzles," Astronautica Acta, Vol. 13, 1968, pp. 481-488.

6. Zinn, B. T. and Crocco, L., "The Nozzle Boundary Condition in the Nonlinear Rocket Instability Problem," Astronautica Acta, Vol. 13, 1968, pp. 489-496.

7. Lores, M. E. and Zinn, B. T., "The Prediction of Nonlinear Longitudinal Combustion Instability in Liquid Propellant Rockets," NASA CR-120904, April 1972.

8. Lores, M. E. and Zinn, B. T., "Nonlinear Longitudinal Combustion Instability in Rocket Motors," presented at the AIAA 11th Aerospace Sciences Meeting, January 1973.

9. Zinn, B. T. and Powell, E. A., "Nonlinear Combustion Instability in Liquid Propellant Rocket Engines," Proceedings of the 13th Symposium (International) on Combustion, The Combustion Institute, pp. 491-503.

10. Powell, E. A. and Zinn, B. T., "The Prediction of the Nonlinear Behavior of Unstable Liquid Rockets," NASA CR-72902, July 1971.

11. Powell, E. A. and Zinn, B. T., "The Prediction of Nonlinear Three-Dimensional Combustion Instability in Liquid Rockets with Conventional Nozzles," NASA CR-121279, October 1973.

12. Finlayson, B. A. and Scriven, L. E., "The Method of Weighted Residuals -- A Review," Applied Mechanics Reviews, Vol. 19, No. 9, September 1966, pp. 735-744.

13. Ames, W. F., Nonlinear Partial Differential Equations in Engineering, Academic Press, New York, 1965, pp. 243-262.

14. Bell, W. A. and Zinn, B. T., "The Prediction of Three-Dimensional Liquid-Propellant Rocket Nozzle Admittances," NASA CR-121129, February 1973.

15. Conte, S. D. and Carl de Boor, Elementary Numerical Analysis, McGraw-Hill Book Company, New York, 1972.

16. Abramowitz, M. and Stegun, Irene A., Handbook of Mathematical Functions, Dover Publications, Inc., New York, 1968.

17. Powell, E. A., "Nonlinear Combustion Instability in Liquid Propellant Rocket Engines," Ph.D. Thesis, Georgia Institute of Technology, GITAER 70-6 (September 1970).

VITA

Mysore Srikantiah Padmanabhan was born in September, 1948. He attended Gandhinagar High School in Bangalore, India.

Mr. Padmanabhan studied in the Bangalore University and in 1969, he received the Bachelor of Engineering degree in Mechanical Engineering. He continued his education at the Indian Institute of Science and in 1971, he received the Master of Engineering degree in Aeronautical Engineering. He entered Georgia Institute of Technology in September, 1971.

Mr. Padmanabhan is an associate member of the Society of Sigma Xi.